1-1-2018

Tau Aggregation, Conformational Selection, and Inhibition

Michael R. Holden
University of Denver

Tau Aggregation, Conformational Selection, and Inhibition

Abstract

Tau fibrils are a pathological hallmark of over 20 neurodegenerative disorders, including Alzheimer's disease. There currently is no cure for these diseases and treatments are limited. Once Tau fibrils form in the brain, they propagate down neuronal networks, and this spreading is linked to disease progression. Studying the behavior and structure of Tau monomer and Tau aggregates therefore may give insight into methods by which the spread of Tau fibrils can be inhibited. The structures of the Tau fibrils from different diseases are thought to vary, partially giving rise to the different disease phenotypes. Tau natively binds to microtubules by either three or four imperfect repeat regions, giving rise to the naming convention of 3R and 4R Tau. In solution, full-length Tau exists as a disordered monomer in dynamic conformational equilibrium. This solution-phase heterogeneity could, in part, explain conformational diversity of Tau fibrils.

A homogeneous set of Tau fibrils transitioned to a new heterogeneous population of conformers after multiple cycles of seeding. The original fibrils were formed under stirring conditions, which enhanced the fragile population. Under the quiescent growth conditions of multiple cycles of seeding, the faster growing populations became the dominant set of conformers. This explains how a new dominant fibril population can evolve from minor subpopulations. These findings demonstrate that changes in the selective pressures on Tau fibrils during fibril propagation could lead to the formation of polymorphs with differing clinical consequences.

Microtubule associated protein 2 (MAP2) is a neuronal homologue to Tau and performs similar functions in the cell. MAP2 has not been shown to be a major antigenic component of the neurofibrillary tangles associated with disease. However, this does not exclude their presence in small quantities. Microtubule binding repeat regions from 3R and 4R MAP2 slow nucleation and block seeded aggregation of 4R Tau protein. Also, as few as a single MAP2 molecule bind to and cap the 4R Tau fibril end. This could account for the inhibition via disruption of the ability of Tau to subsequently bind to the capped fibril end. MAP2 inhibition of Tau fibril formation and progression could be a natural modulator of the fibril spreading in the brain.

Document Type

Dissertation

Degree Name

Ph.D.

Department

Chemistry and Biochemistry

First Advisor

Martin Margittai, Ph.D.

Second Advisor

Michelle Knowles

Third Advisor

J. Alex Huffman

Keywords
Alzheimer's Disease, Fibril, MAP2, Microtubule associated protein 2, Tau

Subject Categories
Biochemistry | Cognitive Neuroscience

Tau Aggregation, Conformational Selection, and Inhibition

_____

A Dissertation

Presented to

the Faculty of Natural Sciences and Mathematics

University of Denver

_____

In Partial Fulfillment

of the Requirements for the Degree

Doctor of Philosophy

_____

by

Michael R. Holden

June 2018

Advisor: Dr. Martin Margittai

Author: Michael R. Holden
Title: Tau Aggregation, Conformational Selection, and Inhibition
Advisor: Dr. Martin Margittai
Degree Date: June 2018

Abstract

Tau fibrils are a pathological hallmark of over 20 neurodegenerative disorders, including Alzheimer's disease. There currently is no cure for these diseases and treatments are limited. Once Tau fibrils form in the brain, they propagate down neuronal networks, and this spreading is linked to disease progression. Studying the behavior and structure of Tau monomer and Tau aggregates therefore may give insight into methods by which the spread of Tau fibrils can be inhibited. The structures of the Tau fibrils from different diseases are thought to vary, partially giving rise to the different disease phenotypes. Tau natively binds to microtubules by either three or four imperfect repeat regions, giving rise to the naming convention of 3R and 4R Tau. In solution, full-length Tau exists as a disordered monomer in dynamic conformational equilibrium. This solution-phase heterogeneity could, in part, explain conformational diversity of Tau fibrils.

A homogeneous set of Tau fibrils transitioned to a new heterogeneous population of conformers after multiple cycles of seeding. The original fibrils were formed under stirring conditions, which enhanced the fragile population. Under the quiescent growth conditions of multiple cycles of seeding, the faster growing populations became the dominant set of conformers. This explains how a new

dominant fibril population can evolve from minor subpopulations. These findings demonstrate that changes in the selective pressures on Tau fibrils during fibril propagation could lead to the formation of polymorphs with differing clinical consequences.

Microtubule associated protein 2 (MAP2) is a neuronal homologue to Tau and performs similar functions in the cell. MAP2 has not been shown to be a major antigenic component of the neurofibrillary tangles associated with disease. However, this does not exclude their presence in small quantities. Microtubule binding repeat regions from 3R and 4R MAP2 slow nucleation and block seeded aggregation of 4R Tau protein. Also, as few as a single MAP2 molecule bind to and cap the 4R Tau fibril end. This could account for the inhibition via disruption of the ability of Tau to subsequently bind to the capped fibril end. MAP2 inhibition of Tau fibril formation and progression could be a natural modulator of the fibril spreading in the brain.

Acknowledgements

I'd like to extend sincere gratitude to many people for aiding or supporting me in my journey to this point. I must thank the University of Denver for extending me an invitation to join their graduate program and for funding various aspects of my work throughout my time here.

I would next like to graciously thank Dr. Martin Margittai first for offering me the opportunity to join his lab. Later, the countless hours of deep discussion and scientific analysis he shared with me shaped my abilities and elevated my critical thinking. His passion and undeniable work ethic has always impressed upon me a rigor, that without, I would not have become the scientist I currently am. I must also thank the many undergraduates who worked with me for constantly challenging me with questions, problems, and the need for new experimental designs or analysis. I'd also like to thank my committee and other faculty members for providing critical feedback during various stages of my PhD.

Last, I'd like to thank my family for always providing me with advice and support throughout my life, but especially my wife, Amanda, for always supporting me in my educational endeavors. My mother earns the most special mention. In her short life she instilled upon me a passion for learning and dedication to my education, which has brought me to this point.

Table of Contents

List of Figures

Abbreviations

3R	three Repeat
4R	four Repeat
Aβ	amyloid beta
ABEL	antibrownian electrokinetic
AD	Alzheimer's disease
AFM	atomic force microscopy
ANOVA	analysis of variance
BCA	bicinchoninic acid assay
BSE	bovine spongiform encephalopathy
CTE	chronic traumatic encephalopathy
CW	continuous wave
DEER	double electron-electron resonance
DMEM	Dulbeccco's modified Eagle media
DMSO	dimethylsulfoxide
DNA	deoxyribonucleic acid
DTT	dithiothreitol
EDTA	ethylenediaminetetraacetic acid
EPR	electron paramagnetic resonance
FBS	fetal bovine serum
FRET	Förster resonance energy transfer
GdmCl	guanidinium hydrochloride

HEK	human embryonic kidney
HEPES	(4-(2-hydroxyethyl)-1-piperazineethanesulfonic acid)
IDP	intrinsically disordered protein
IPTG	isopropyl β-D-1-thiogalactopyranoside
MAP	microtubule associated protein
MB	methylene blue
MTBR	microtubule binding repeat
MTG	microbial transglutaminase
MTSL	(S-(1-oxyl-2,2,5,5-tetramethyl-2,5-dihydro-1H-pyrrol-3-yl)methyl methanesulfonothioate)
NFT	neurofibrillary tangle
NMR	nuclear magnetic resonance
MEM	minimal essential media
PBS	phosphate buffered saline
PCR	polymerase chain reaction
PEG	polyethylene glycol
PHF	paired helical filament
PIPES	piperazine-N,N′-bis(2-ethanesulfonic acid)
PK	proteinase K
PMSF	phenylmethane sulfonyl fluoride
RNA	ribonucleic acid
RPM	revolutions per minute

SD	standard deviation
SDS PAGE	sodium dodecylsulfate polyacrylamide gel electrophoresis
SEM	standard error of means
SF	straight filament
SM	single molecule
TCEP	tris(2-carboxyethyl)phosphine
TEM	transmission electron microscopy
ThS	thioflavin S
ThT	thioflavin T
TRIS	tris(hydroxymethyl)aminomethane
UV	ultraviolet
UWM	University of Wisconsin, Madison

Chapter 1 Introduction

1.1 Alzheimer's disease

Alzheimer's disease (AD) is a neurodegenerative disease inflicting approximately 5.4 million people in the US alone, according to the Centers for Disease Control (as of Feb 2018). This number is projected to increase dramatically with the aging baby-boomer population. AD manifests itself in the form of dementia and can cause symptoms such as memory loss, difficulty with time and space, and challenges completing every-day tasks at home. This disease is histopathologically hallmarked by inclusions comprised of two different protein aggregates [1]. The first type of aggregate is called a senile plaque, and is composed of a protein fragment named amyloid beta (Aβ) [2]. This fragment is the product of abnormal proteolytic processing of the amyloid precursor protein (APP) [3]. The other proteinaceous component that is associated with AD is called a neurofibrillary tangle (NFT) [4]. NFTs are part of a larger structure called an intraneuronal lesion [5]. These lesions are comprised primarily of amyloid fibrils made of phosphorylated Tau protein [4].

In AD, Tau pathology begins in the locus coeruleus in the entorhinal cortex and spreads through the brain to eventually be found in nearly every region in the later stages [6]. This pathology and subsequent neurodegeneration can be

accelerated by genetic mutation [7], trauma [8]–[9], and unknown mechanisms. The stages of the NFT spread are described as Braak Stages [1], [10]. Braak stages I and II are when NFT involvement is primarily in the entorhinal cortex region of the brain. Stages III and IV possess the characteristics of earlier stages as well as the spread to limbic regions such as the hippocampus. The final stages V and VI are used to describe the extensive neocortical NFT deposition in the advanced disease state.

1.2 Tauopathies: a class of protein misfolding diseases

Deposition of aggregated Tau protein is also found in over twenty other neurodegenerative diseases (besides AD), collectively named Tauopathies. The list of Tauopathies includes diseases such as; chronic traumatic encephalopathy (CTE) [11], corticobasal degeneration, progressive supranuclear palsy (PSP), and a type of Frontotemporal Dementia also known as Pick's disease (for a thorough review see [12]). AD is the best studied and most common variant of these diseases. CTE received more attention recently due to the fact that several high-profile professional athletes have been diagnosed post-mortem with the disease [13]–[15]. This emergent disease demonstrates our fundamental lack of knowledge in this area and how traumatic brain injury can lead to unusual pathology in the brain.

1.3 Microtubule associated proteins

Proteins are comprised of linear chains of amino acid building blocks that typically fold into biologically important three-dimensional (3D) structures. These

3D structures can perform very specific reactions in the cell, but not all biologically important proteins are folded. There is a class of proteins called intrinsically disordered proteins (IDPs). These proteins contain no regular structured regions and are less common than their folded or partially folded counterparts. Disorder in proteins is common, however. For example, 97% of proteins are predicted to have disorder in the first or last five residues in the chain [16]. An example of this are histone proteins that bind and organize DNA in eukaryotes [17].

Although the two-main microtubule associated proteins (MAPs) discussed here, MAP Tau and MAP2 are considered IDPs, they are not completely devoid of structure. Studies show that MAP Tau monomer is not a random coil but rather a loosely associated hairpin structure [18]–[19]. Structural studies have utilized Förster resonance energy transfer (FRET) experiments to demonstrate that the N-terminus and C-terminus of Tau are in close proximity to each other, and to other key residues tested in the microtubule binding repeat (MTBR) region [20]. Due to the apparent backfolding of the ends of the protein, Tau resembles a paperclip. However, these regions do not have regular secondary structure in the traditional sense, except for small transient folds that do not persist for long periods of time in solution [19]–[20].

The other MAP of interest for this work, MAP2, is also considered intrinsically disordered, except for a small sequence in the amino terminal

domain that is implicated in binding to the regulatory subunit of protein kinase A [22].

Native functions

Microtubule associated proteins are a critically important set of proteins that have been shown to stabilize [23] and crosslink [22]–[23] microtubules in a healthy mature neuron. This stabilization effect is attributed largely to the interaction of the microtubule binding repeat region (MTBR, Fig 1.1) with the negatively charged microtubule surface. Microtubule stabilization in the axon is very important as microtubules are one of the main structural components involved in membrane protrusion [25]. Tau and other MAPs are key regulators of microtubule dynamics. The interactions between Tau and microtubules are controlled in part by the phosphorylation state of Tau (see below). The most common amino acid in these repeats is the lysine residue which is a major contributor to the electropositive nature of these repeat regions. MAPs perform their native functions by binding to microtubules through electrostatic interactions in these MTBR regions. The charges are well distributed along the MAP backbone resulting in heat stability [26] and this contributes to the stable random-coil structure required for function in the cell.

Tau Isoforms and splicing

The best studied of these MAPs is MAP Tau. The MTBRs are comprised of either 3 or 4 imperfect repeats consisting of either 31 or 32 amino acids and are present in all isoforms of MAPs expressed in humans [27]–[29]. This feature

is what gives rise to the naming half of the isoforms three-repeat (3R) and the other half the name four-repeat (4R). The presence of the second repeat is determined by alternative splicing of exon 10 in the MAPT gene. Tau protein can be further categorized by whether exons 2 and/or 3 are spliced. This results in zero, one, or two N-terminal inserts in the protein. (Fig 1). With either 3 or 4 repeats and three different combinations of N-terminal inserts, there are 6 isoforms of Tau protein. All 6 are present in the adult human brain [30]–[32].

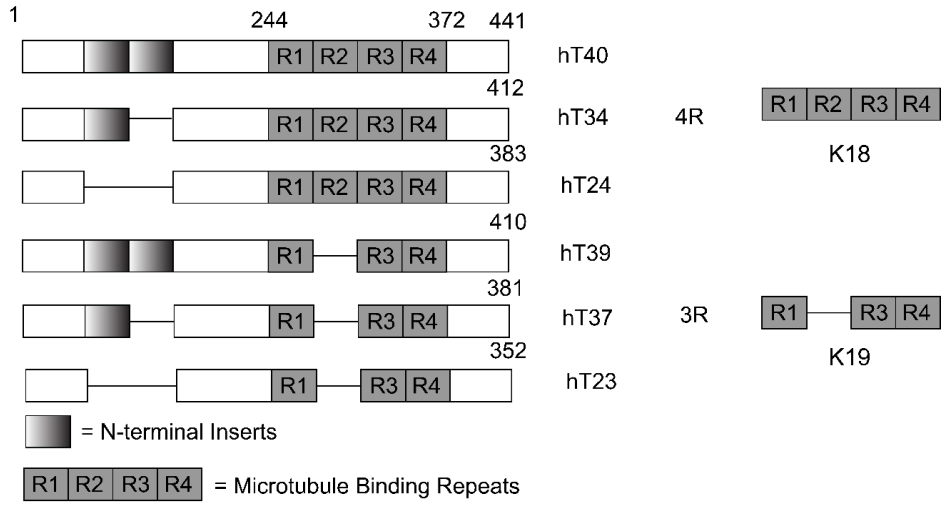

Figure 1.1 Scheme of Tau isoforms in humans. Tau protein exists in 6 splice variants in humans. The variation is determined by whether exons 2, 3 or 10 are expressed. Exons 2 and 3 encode the first and second inserts in the N-terminal regions, respectively. Exon 10 is responsible for the second repeat in the microtubule binding repeat region. K18 and K19 are constructs made of only the MTBRs. The MTBRs are the primary component of Tau fibrils.

There are several other MAP homologues in humans including (but not limited to) MAP1 A and B, MAP2 C and D, and MAP4. The other MAPs have garnered less attention. This may in part be due to the isoform diversity. It has

been demonstrated that MAP2 C and MAP2 D are present in neurons and are localized primarily to the dendrites and cell body [33]–[35].

Phosphorylation and hyperphosphorylation

The phosphorylation state of MAP proteins has been shown to regulate the binding affinity for the microtubule surface [36]–[39]. This is controlled tightly in healthy cells by a variety of enzymes, such as microtubule associated protein kinase (MAPK) [48]–[49] and glycogen synthase kinase 3-β (GSK3β) [42]–[44]. In healthy individuals the average phosphorylation state is 2-3 mol PO_4^{3-}/mol Tau [45]. Tau becomes hyperphosphorylated [46]–[48] in disease (7-9 mol PO_4^{3-}/mol Tau), which reduces the affinity of Tau for the negatively charged microtubule surface [49]. It is thought that the decreased net positive charge and higher soluble concentrations of Tau help to drive aggregation in the cell.

1.4 Amyloids

Structure of amyloids

The amyloid structure is a class of protein fold often associated with disease. Over 25 amyloid-forming proteins have been identified and associated with serious diseases [50]. Amyloids are characterized as fibrillar protein structures, typically with a cross-β-sheet structure where parallel chains of β-strands are arranged perpendicular to the fibril axis (Fig 1.2). X-ray fiber diffraction studies yielded basic information about the spacing between β-strands and β-sheets [51]–[53]. Continuous wave (CW) electron paramagnetic resonance (EPR) spectroscopy has given insight into the core structure of Tau fibrils [54]–

[58] and other amyloids [59]–[61] by demonstrating that the stacked monomers in the fibril adopt a parallel and in-register structure. Amino acids are stacked on identical residues from the next monomer layer along the fibril axis (Fig 1.2 B).

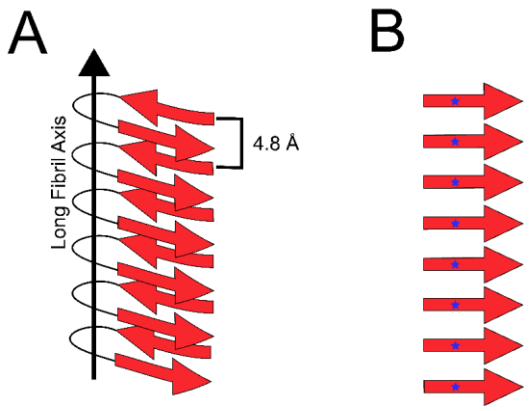

Figure 1.2 Model of amyloid fibril structure. A Amyloid fibril structures are comprised of β sheets with sheet-sheet packing. Each monomer layer is separated by 4.8 Å. B Stacking of monomers is in parallel and in-register fashion. Individual residues are stacked in the fibril along the long fibril axis directly on top of the identical residue in the adjacent monomer (indicated by the blue star).

Another EPR technique used in structural studies of amyloid fibrils is called double electron-electron resonance (DEER) spectroscopy [61]–[64]. This has been used to measure the distance between a fixed pair of nitroxide spin label radicals, introduced at known positions on the protein backbone [59]–[61]. Multiple distances may arise in the analysis, which can be attributed to an ensemble of conformers [58], [63]–[64], [66]. Nuclear magnetic resonance has had success in studying the structure of these fibrils [67]–[70]. CryoEM provided atomic-level resolution and illustrated which repeats in Tau are involved in the core of the fibrils from a patient with Alzheimer disease [71].

Amyloid formation

Conversion of soluble protein to insoluble fibrillar aggregates is still poorly understood. Amyloid formation generally comes with the loss of native function of the protein or peptide [72]–[75] and can include toxic species along the aggregation pathway [76]–[78]. Aggregation is thought to proceed through the formation of a nucleus that can turn into a small soluble oligomer, which can mature into an insoluble fibril (Fig 1.3) [79]–[83].

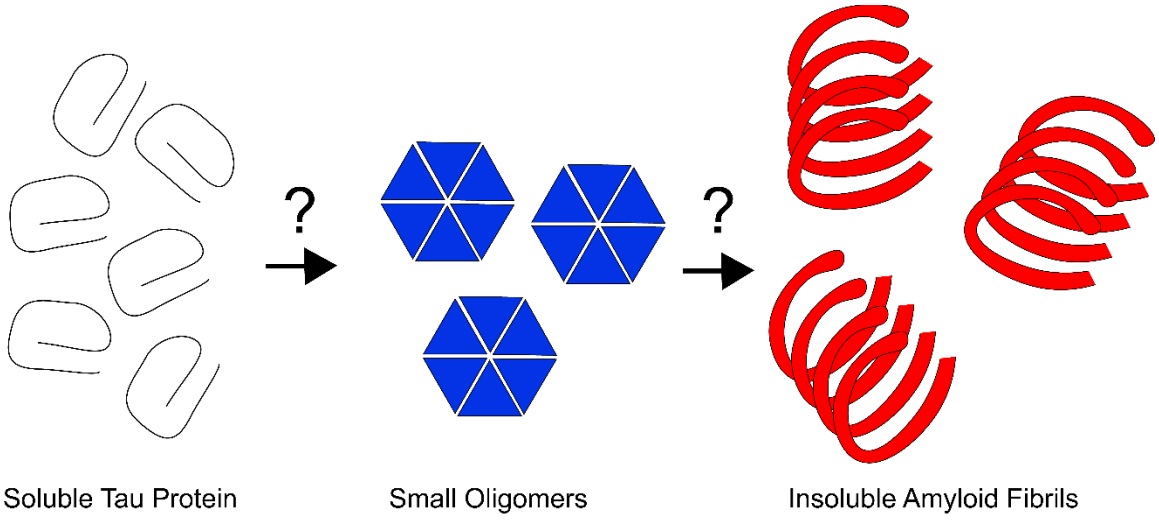

Figure 1.3 Amyloid aggregation pathway scheme. Although the exact mechanism of action and structure of oligomers is unknown, studies show it is the small, still soluble species, that are toxic to cells [84]–[88].

The structure of early pathway aggregates is difficult to study with techniques commonly applied to other proteins, such as X-ray crystallography. There have been attempts at studying the early stages of the Tau aggregation pathway, however [89]. In the case of oligomers, less is known about their structure, but it has been demonstrated that toxic species in the aggregation

pathway are oligomers [90]–[92]. One problem with the study of oligomers is trying to discern which size or stage of these oligomers are toxic but it has been shown that small aggregates can propagate through neuronal networks [93]–[96]. This leads to toxicity because the process of templating in a new cell can begin when the small fibrils are internalized in the neighboring cell [93], [97]–[99]. Therefore, a method by which to study these structures is essential.

1.5 Conformation and conformational ensembles of Tau amyloids

The conformation of amyloids depends on the initial nuclei that form [50]. These nuclei drive aggregation by templating the exact same misfolded state onto the endogenous population [55], [100]. It follows that different sets of nuclei may form in a disease, which could result in the pathology and progression of that disease. It has been shown that the conformation of Tau fibrils can be modulated by single mutations [58]. This means that conformational incompatibilities arising from sequence changes in monomers can drive the structure of these fibrils and that they can evolve over time.

Under conditions in the lab it may be possible to form multiple fibril conformations simultaneously. There are usually a dominant species and sub-species of conformers. These conformational ensembles can evolve resulting in new dominant species [58], [64]. Multiple conformers might also form in the brains of people afflicted with amyloid disease. As the fibrils spread from region-to-region [94]–[95], selection pressures exerted on the fibril species may change. Although the mechanism is unclear, selection pressures may change with

respect to post-translational modifications [48], [87] or mutations of endogenous protein [57], [96]–[97], for example. This may result in an altered conformational ensemble that favors the new conditions.

1.6 Diagnosing, preventing, and treating AD

There is no cure for AD on the market. Many treatments are ineffective by the time the disease is diagnosed. Although recent developments show promise [103]–[104], there are no antemortem diagnosis methods for AD or other Tauopathies besides neurological examinations[107] and cognitive testing [108]–[111]. The onset of Tau hyperphosphorylation and mild cognitive decline [112] is years before these diagnostic methods can provide an accurate diagnosis. The focus of treatment has been in the development of inhibitors to aggregation [113]–[115]. Drugs are generally administered late in progression and are not effective at reversing the disease [116]–[118]. These critical areas of research have been slowed by the lack of structural data available and by the sheer challenge of the problem. Treatment would likely be more effective if administered early, highlighting the need for a rapid and early detection method.

1.7 The scope of my research

I examined several aspects of MAP Tau aggregation. These topics cover monomeric Tau protein and its conversion into Tau protein aggregates. Explicitly the topics include: monomer conformational heterogeneity, aggregation of Tau monomers into fibrils, a study of Tau fibril conformation and conformational selection processes and concludes with a study demonstrating that MAP2 is

capable of capping and blocking Tau aggregation *in-vitro*. These topics are interlinked in that they all provide insight into the process in which healthy monomeric Tau protein is converted into disease state-related Tau protein fibrils.

In Chapter 3 I examined the behavior of monomer species in solution. This is important to understand because a conformational change in the monomer is responsible for the nucleation behavior of Tau. Probing the structure and elucidating monomer behavior may enable investigators to better understand how the initial formation of fibrils occurs. I performed experiments in Chapter 4 which are evidence for the hypothesis that multiple conformations of Tau fibrils exist in-vitro and that amyloid conformational ensembles can evolve. It is thought that different conformations of Tau may form in different diseases, which could drive their specific pathology. Tau fibril conformations may be the result of different monomer conformations during the nucleation and oligomerization process. If the various states of Tau in solution can be characterized, it may be possible to elucidate which structure or structures contribute to various Tauopathies, such as AD. In Chapter 5 I examined the stability of fibrils and their associated cofactors once aggregation has taken place. Dissociative properties of Tau monomers from the fibril must be such that the fibrils do not dissociate upon breakage. If Tau fibrils dissociated spontaneously, it seems unlikely that they would be capable of spreading. Lastly, understanding that Tau fibrils impart their structure onto endogenous monomers may enable researchers to develop therapeutics. One possible therapeutic avenue is to block the Tau monomers

from becoming incorporated on the fibril end. It is possible to block Tau aggregation at the end of the fibril using a capping mechanism in-vitro. Lastly, I demonstrate in Chapter 6 that the microtubule binding repeats of 3R and 4R MAP2 block Tau aggregation and also that MAP2 is binding to the end of the Tau fibril. Investigations of this blockage effect are being investigated in a cellular system now. The study of the conversion of soluble Tau monomer to fibril aggregates is one that is ongoing.

Chapter 2 Methods

2.1 Tau constructs

The longest human 4R isoform, hT40wt, and the shortest 3R isoform, hT23wt, were previously cloned into pET-28b plasmids using the NcoI/XhoI restriction sites in the plasmid. Truncated constructs, K18wt and K19wt, were also generated previously [56]. All mutagenesis was performed using the QuikChange method to introduce different amino-acid substitutions. K18 with a single cysteine on the N-terminus was synthesized and cloned by Biomatik using NcoI/XhoI restriction sites in a pET-28 vector. Aligned constructs used for this work can be found in Appendix A.

2.2 MAP2 constructs

Sequences for the microtubule binding repeats of MAP2 C and MAP2 D (Uniprot #P11137 variant 5) were synthesized by Biomatik and cloned into pET-28 vector using NcoI/XhoI restrictions sites. These constructs had the natural cysteines replaced with serines (C404S and C444S). Constructs containing the cysteines were generated using site-directed mutagenesis as per manufacturer's instructions as previously described. Also, a 4R truncated MAP2 N-terminal cysteine construct was synthesized and cloned by Biomatik into a pET-28 vector

using NcoI/XhoI restriction. Aligned constructs used for this work can be found in Appendix A.

2.3 Plasmid transformation and DNA purification

Plasmid DNA was transformed into BL21 (DE3) cells (Agilent) or XL1-Blue cells (Agilent) for protein expression or DNA amplification purposes, respectively. Transformation was performed as follows, cells were thawed on ice and 25 µL of thawed material was transferred to a 14 mL round bottom polypropylene tube (Corning Falcon). Two microliters of pure DNA were combined with cells and allowed to sit on ice for 30 minutes. Cells were permeabilized by heat shock at 42 °C for 45 seconds and then placed on ice for 2 minutes, then 500 µL of NZY+ (10 g/L NZ-amine, 12.5 mM $MgCl_2$, 12.5 mM $MgSO_4$, 20 mM glucose) media was added and the cells were allowed to incubate at 37 °C for 45 - 60 minutes. Volumes of incubated material were plated on kanamycin plates at either 25-50 µL for purified DNA or 250-500 µL for PCR product.

Plasmid MIDI preparations were performed according to the manufacturers (QIAGEN) instructions. High-copy XL1-Blue cells were transformed with DNA, as above, from either site-directed mutagenesis reactions (Agilent) or previously purified DNA.

Mammalian plasmid MIDI preparations were performed according to manufactures instructions (Omega). DNA was eluted with prewarmed (40 °C) PCR grade H_2O. Eluent was repassed through column to achieve the highest

concentration. DNA was quantified using $A_{280\ nm}$ and purity assessed via the ratio of $A_{260\ nm}$ / $A_{280\ nm}$.

2.5 Recombinant protein expression

Protein expression was performed as follows; previously transformed BL21 (DE3) cells were scraped from either a kanamycin plate or a previously prepared glycerol stock and added to 50 mL of LB (20 g/L, Difco) with 20 µg/mL Kanamycin (Gold Bio). The solution was incubated at 200 RPM and 37 °C for 16-18 hours to produce a starter culture. The resultant culture was mixed with 1.5 L of LB at a ratio of 1:100 supplemented with 20 mg/L Kanamycin (Gold Bio) and incubated at 200 rpm and 37 °C until the $OD_{600\ nm}$ = 0.8 - 1.0. Protein expression was induced with 0.5-1 mM IPTG for 3.5 hours at 37 °C and 200 rpm. The cells were harvested at 5500 x g for 10 minutes. Pellets were taken up in 500 mM NaCl, 20 mM piperazine-N,N'-bis(2-ethanesulfonic acid (PIPES, JT Baker or RPI) pH 6.5, 5 mM ethylenediaminetetraacetic acid (EDTA, Fisher), 50 mM 2-mercaptoethanol (Fisher, electrophoresis grade), and stored at -80 °C.

2.6 Protein purification

Bacterial pellets from previous step were thawed for 20 minutes at 80 °C to precipitate heat insoluble protein. Samples were sonicated on ice at 50% power for 1 minute with a tip sonicator to lyse the cells and release soluble protein. Lysis solution was centrifuged at 20,000 x g for 30 minutes to remove the insoluble cellular material. The supernatant was adjusted to 55% (w/v) ammonium sulfate and rocked for 1-16 hours in order to precipitate the remaining

soluble protein. Precipitated protein was collected by centrifugation at 4,000 x g for 10 minutes. The supernatants were discarded, and the pellets were respun at the same settings. The remaining supernatant was pipetted off and the pellets were taken up in 8 mL of either nanopure water (Tau) or 10 mM PIPES pH 6.5 150 mM NaCl 2 M urea (MAP2 proteins) both supplemented with 4 mM DTT. Additional buffer, salt, and urea was added due to low MAP2 solubility. Samples were combined and sonicated for 1 minute at 50% power to shear DNA and disrupt any small aggregates. These sonicated samples were syringe filtered (Pall Acrodisc 0.45 µM) to remove any particulate and diluted until conductivity was below 20 mS/cm. Protein was loaded onto a cation exchange column (Mono S 10/100 GL, GE Healthcare) using 50 mM NaCl, 20 mM PIPES, 0.5 mM EDTA and eluted with a linear gradient of 1 M NaCl, 20 mM PIPES, and 0.5 mM EDTA. Protein was pooled based on an SDS-PAGE, adjusted to 3 mM DTT, and stored at 4 °C for immediate use or -80 °C for future use. Samples were loaded onto a S75 column (GE Healthcare) for truncated Tau or an S200 column (GE Healthcare) for full length Tau or MAP2 proteins to separate proteins by size. Fractions containing protein were pooled based on UV trace and precipitated overnight as follows; truncated Tau was mixed 1:4 with Acetone (Fisher, Optima Grade) and full length Tau was mixed 1:1 with methanol (Fisher Optima Grade), all were adjusted to 4 mM DTT and incubated overnight at 4 °C. Precipitated protein was collected by centrifugation at 12,000 x g for 10 minutes. Protein pellets were stored at -80 °C under 2 mM DTT (acetone or methanol for

truncated and full-length Tau, respectively) until further use. Representative chromatograms for purification of K18 and MAP2 are attached in Appendix C.

2.7 Protein monomerization

Pellets from previous step were washed three times with either acetone (truncated proteins) or methanol (full length proteins) devoid of DTT and all supernatant was removed each time with a gel loading tip. Protein was dissolved in 8 M guanidinium HCl (Thermo) for 2-24 hours. No more than 300 µL of dissolved protein was loaded onto a PD-10 desalting column (Ge Healthcare) equilibrated with assembly buffer (10 mM HEPES pH 7.4 100 mM NaCl 0.1 mM NaN_3), and 2.0 mL of this assembly buffer less volume of dissolved protein was added and allowed to flow completely through. To elute protein, 2.0 mL of assembly buffer was added to the column and collected for BCA (Pierce) quantification which was performed according to manufacturer's instructions.

2.8 Protein (cysteine residue) conjugation reactions

Cysteines in Tau or MAP2 were covalently conjugated with a variety of labels for this work. Either a single natural residue (C291 or C322 in Tau or C409 or C440 in MAP2, numbered according to Uniprot # P11137, variant 5) or an unnatural cysteine introduced through site-directed mutagenesis or in a construct ordered commercially (Biomatik) were labeled using maleimide (PEG-Biotin, Alexa, and Atto conjugates) conjugation reactions. Briefly, cysteine containing protein pellets dissolved completely in 8 M guanidinium HCl were conjugated by adding a 10:1 molar excess of dye to protein. This reaction was mixed thoroughly

and allowed to proceed for 2-24 hours in the dark. Excess dye and guanidinium was removed using a PD-10 desalting column (GE) and protein eluted as described above. Protein concentration was determined using BCA (Pierce) according to manufacturer's instructions. Fluorescent labeling efficiency was determined using protein diluted to 1 µM according to BCA and measuring dye absorbance in a Cary 100 UV-vis spectrophotometer. Absorbencies were converted to concentrations using the Beer-Lambert Law. Extinction coefficients that were used are as follows: Atto 647N (1.5×10^5 $M^{-1}cm^{-1}$), Atto 633 (1.3×10^5 $M^{-1}cm^{-1}$), Alexa 488 (7.3×10^4 $M^{-1}cm^{-1}$), Alexa 594 (9.2×10^4 $M^{-1}cm^{-1}$).

2.9 Fibril formation

Fibrils were formed by combining 25 µM Tau and 50 µM heparin (Celsus, average MW 4400 kDa) in 100 mM NaCl 10 mM HEPES pH = 7.4 (referred to as assembly buffer from here on) to induce aggregation of monomer. 0.5 mM TCEP was included if cysteines were present to provide a reducing environment. Solutions were made at volumes of at least 500 µL and were stirred for 3 days for truncated Tau and 8 days for full length Tau at room temperature (22 °C) using a Barnstead Thermolyne stir plate set to 220 RPM.

2.10 Seeded reaction

Stirred fibril material was sonicated using a Fisher Sonic Dismembrator Model 100 with power set to 20% for 30 – 120 seconds, depending on the application. Seeded reactions were performed by combining 10 µM fresh monomer and 20 µM heparin to induce aggregation (and 0.5 mM TCEP if

cysteines were present in monomers) with 2 – 10% monomer molar equivalents of sonicated preformed fibrils added to serve as seeds. Monomers were allowed to template and elongate the fibrils for 6 hours. Reactions were ultracentrifuged at 130,000 x g. Pellets (insoluble fraction) and supernatants (soluble fraction) were separated, pellets were resuspended in equivolume (with respect to reaction volume) of 1 X Laemmli sample buffer, and both were analyzed using SDS PAGE (15% for truncated and 12% for full length).

2.11 Consecutive seeding cycle experiment

Consecutive seeding cycles were performed as follows. Fibrils stirring for three days were sonicated 30 seconds at 20% power using a Fisher Sonic Dismembrator Model 100 to generate small fibrillar seeds and added in 10% monomer molar equivalents to 25 µM Tau, 50 µM Heparin in assembly buffer at a final volume of 500 µL. Cycle one was incubated for 1 hour at 37 °C and subsequently sonicated and used as seeds in the second reaction. This process was repeated until the ninth or fourteenth cycle was reached at which point the monomer concentration was increased to 50 µM Tau, heparin concentration was reduced to 12.5 µM, and seeds were added at 5% molar monomer equivalents. 50 µM reactions of cycle 1 (from original seeds), cycle 5 (from cycle 4), cycle 10 (from cycle 9), and cycle 15 (from cycle 14) were allowed to reach completion overnight at 37 °C.

2.12 Breakage sensitivity

50 µM overnight reactions of cycle 1 or cycle 10 samples from consecutive seeding cycle experiments (above) were subjected to 60 seconds of sonication in a QSonica bath sonicator at 5% power, subsequent fibril fragments were diluted to 10 µM and prepared for transmission electron microscopy analysis (below).

2.13 Transmission electron microscopy sample preparation and ImageJ analysis

Concentration of Tau was adjusted to 10 µM total protein using assembly buffer and loaded onto Formvar carbon coated Cu grids by resting the grid on a 10 µL droplet of protein on parafilm for 60 seconds. Excess protein was blotted gently on Whatman filter paper and the grid was placed on a 10 µL droplet of 2% uranyl acetate (Electron Microscopy Sciences) for 60-120 seconds. Grids were blotted and allowed to dry for 10 minutes on filter paper. Images were taken on a Tecnai F12 Biotwin scope using 100 kV high tension on a Gatan camera at University of Colorado, Boulder.

Fibrils were analyzed by ImageJ (NIH version 1.8.0) for length, width, and helical periodicity. The scale was set by measuring the length of the scale bar (153 pixels) and setting the scale in ImageJ to 100 nm. Data sets were collected in ImageJ, sorted in Excel (Version 1801) and plotted in GraphPad (Version 7.04).

2.14 Fibril dissociation experiments

Fibrils formed with RNA were made by stirring 25 µM Tau and 12.5 µg/mL PolyA RNA (Sigma, product number P9403, lot 084M4144V) in assembly buffer for three days at 22 °C. Fibrils were subsequently diluted 1:5, 1:10, 1:20, and 1:40 with assembly buffer and incubated for 12 hours in the absence or presence of 50 µg/mL PolyA RNA.

Fibrils formed with RNA were adjusted to 500 mM NaCl and incubated for 15 minutes at room temperature. The reaction was ultracentrifuged in order to separate insoluble pellet (fibril) from soluble supernatant (monomer). The pellets were then either taken up in 1 X Laemmli buffer for SDS PAGE analysis or taken up in 60 µL 2% sodium dodecyl sulfate (SDS). Pellet samples dissolved in 2% SDS and supernatants were brought up to 1250 µL in assembly buffer (10 mM HEPES pH 7.4 and 100 mM NaCl) and measured on a Cary 100 for absorbance at 280 nm. Triplicates were measured, averaged and standard deviation was plotted in Excel.

2.15 ThioflavinT kinetics

ThioflavinT (ThT) kinetics were measured by combining 10 µM monomeric Tau, 20 µM heparin, 0.5 mM TCEP (if cysteines present), 5-20 µM ThT, and 2-10% seeds (monomer molar equivalent) in assembly buffer and measured on a Tecan M1000 or Omega Fluorstar fluorescent plate reader. Excitation was performed at 440 nm and emission of ThT was monitored at 480 nm for 3 - 10

hours. Data were exported to, and averages of replicates were plotted in, Excel showing either SD or SEM error bars.

To measure ThT kinetics of nucleation, fluorescence was measured in an Omega Fluorostar plate reader. Excitation was performed at 440 nm and emission of ThT was monitored at 480 nm. 25 µM Tau monomer and 50 µM heparin cofactor mixtures were incubated quiescently in a sealed 96 well plate at 37 °C. To ensure the reactions were fully mixed, plates were shaken once for 3 seconds at 100 RPM at the beginning of the experiment.

2.16 Proteinase K sensitivity assay (limited proteolysis)

Reactions of cycle 1 or cycle 10 fibrils formed in consecutive seeding cycle experiment (above) were subjected to limited proteolysis by 7 nM or 70 nM proteinase K for 1 hour at 22 °C. Proteolysis was stopped by addition of 4 mM phenylmethyl sulfonyl fluoride (PMSF) and Laemmli sample buffer to a final concentration of 1x.

2.17 Turbidity analysis

Consecutive seeding cycle reactions of K18 or K19 (above) were measured at 340 nm for light scattering on a Cary 100 UV-vis spectrophotometer. Measurements were taken in biological triplicate and averages plotted with SEM reported.

2.18 MAP2 blockage experiment

Seeded reactions were performed as above with the addition of monomeric MAP2 proteins at substoichiometric concentrations. Briefly, 10 µM

Tau protein and 20 µM heparin were added to serially diluted MAP2 protein at either 5, 2.5, or 1.3 µM final concentration and 10% seeds were added to induce Tau aggregation. Reactions were incubated at 37 °C for 6 hours and thereafter centrifuged at 130,000 x g for 30 minutes. Pellets were separated from supernatants and dissolved in equivolume (with respect to supernatant) of 1 x Laemmli sample buffer and run on 15% SDS-PAGE with pellets and supernatants. Gels were stained with Coomassie-R250. Scanned gels were analyzed by band densitometry on ImageJ and quantified band intensities were plotted in GraphPad. Plotted data was analyzed by one-way ANOVA in GraphPad.

2.19 Atto 647N and 633 fluorescence anisotropy of MAPs

Fluorescence anisotropy of truncated Tau and MAP2 was performed with protein labeled at the natural cysteine in the third repeat (322 for Tau or 440 for MAP2 (numbering described above)) with Atto 647N and 633 (AttoTek). 50 µM Tau monomer was added to 5% preformed K18 fibrils with 6.3 µM Heparin (8:1 ratio) were incubated for 16 hours overnight and sonicated for 2 minutes at 20% power and these fibrils were titrated into a solution containing 100 nM Atto labeled protein. When vertically polarized light is used to excite a fluorophore, fluorescence anisotropy (r) can be determined by the following equation[119] :

$$r = \frac{I_{VV} - I_{VH}}{I_{VV} + 2I_{VH}}$$

Equation 1 Fluorescence anisotropy. I_{VV} is the intensity of vertically polarized fluorescence emission and I_{VH} is the intensity of horizontally polarized fluorescence emission.

Fluorescence emission intensities are measured using parallel (I_{VV}) and perpendicular (I_{VH}) filters, with respect to the excitation. Polarization biases introduced by the instrument can be accounted for by applying a grating factor, or G-factor. The G-factor is determined by the following quotient:

$$G = \frac{I_{HV}}{I_{HH}}$$

Applying the G-factor to the previous equation gives:

$$r = \frac{I_{VV} - GI_{VH}}{I_{VV} + 2GI_{VH}}$$

Fluorescence was initiated with excitation of polarized light at 610 nm (slit width = 2 nm). Fluorescence emission anisotropy readings were measured at 630 nm (slit width = 4 nm). This process was repeated 10 times and averaged on a Horiba Jovan Fluorolog spectrometer for each sample. Each data point was performed in triplicate using independent batches of seeds and those values were averaged and plotted with SD in GraphPad. Fits were added in GraphPad for one site total binding and K_D values were taken from this analysis.

2.20 Alexa 488/594 Förster resonance energy transfer

50 µM Tau monomer was added to 5% seeds and 6.2 µM heparin and incubated at 37 °C for 16 hours. 500 µL of this reaction was sonicated for 2 minutes at 20% power to produce small fibril seeds. 10 µM seeds were added to

1 µM K18 labeled on the N-terminus with Alexa 488 and incubated at 37 °C for 1 hour to allow for templating of labeled protein on the fibril. The samples were measured by excitation at 450 nm and collecting emission spectra from 500-675 nm. Excitation and emission slit widths were set to 5 nm. This was followed by addition of 1 µM protein labeled on the N-terminus with Alexa 594 as an acceptor dye (Tau Alexa 594, truncated 3R MAP2 Alexa 594, or truncated 4R MAP2 Alexa 594). These reactions were incubated for another 1 hour at 37 °C. Following incubation with the acceptor species, samples were measured again by excitation at 450 nm and collecting the emission spectra of the samples from 500-675 nm. Spectra were averaged in biologic triplicate and plotted with SEM reported in Excel.

2.21 Streptavidin-conjugated magnetic bead pulldown

250 µL of 20 µM PEG-Biotinylated (Thermo product # PI21911) Tau or MAP2 was rotated at 40 rpm with 200 µg of hydrophilic streptavidin conjugated magnetic beads (NEB product number S1421S) for 60 minutes. Beads were pulled to bottom of tube with a powerful magnet (see appendix B). Bead pellet was rinsed thoroughly with 1000 µL of assembly buffer and beads were pulled to the bottom of the tube again. The beads were then resuspended in 250 µL assembly buffer containing 5 µM preformed K18 fibrils and rotated again for 60 minutes. Beads were collected and washed again with 1000 µL of assembly buffer. Finally, beads were taken up in 50 µL of 1x Laemmli sample buffer and heated at 95 °C for 10 minutes. Heating at 95 °C unfolds streptavidin and

releases the biotinylated monomer and seed complex. Resultant sample buffer solutions were run on 15% SDS PAGE and stained with Coomassie R250.

2.22 Gold nanoparticle labeling for TEM

25 µM K18 fibrils were sonicated for 60 seconds at 20% power and mixed with 5 µM biotinylated MAP2 and allowed to incubate for 24 hours at 37 °C. Resultant solution was mixed 1:1 with streptavidin coated gold nanoparticles (Aurion) at a final dilution of 1:40 for 90 minutes. These samples were subsequently prepared for TEM analysis as described above.

2.23 Mammalian cell culture

Human embryonic kidney cells (HEK 293) were cultured in Dulbecco's Modified Eagle Medium (DMEM, Gibco) supplemented with 10% fetal bovine serum (FBS, Gibco) at 37 °C and 5% CO_2. For cells undergoing selection 400 µg/mL G418 (Gibco) was included in the media. Cells were subjected to a serial dilution of G418 initially to establish a kill curve. Cells were dead within 7 days at concentrations over 400 µg/mL. At 800 µg/mL cells died within 3 days.

In order to maintain cell cultures long term, the cells must be unadhered from the plate and split. To achieve this, cells were washed with phosphate buffered saline (PBS, Gibco) and enough trypsin reagent (TrypLE, Gibco) was added to cover the plate. Cells were allowed to incubate for 3-5 minutes with trypsin reagent and then were observed under an inverted microscope to assess detachment. To break up any clumps, cells were forced through a pipette tip

against the flask or dish bottom. The resultant solution of cells is split and either, plated or put in a container with bleach for destruction.

In order to freeze mammalian cells, cryopreservant must be used to prevent cellular damage during freezing. A 37 °C solution of 5% (v/v) sterile dimethylsulfoxide (DMSO, Fisher Certified ACS grade, autoclaved) in FBS is added to the suspension of unadhered cells, mixed, and aliquoted in 1 mL cryogenic vials (Fisher # 10-500-25). These samples were slowly cooled to -80 °C by placing the tubes containing cells inside a Styrofoam container inside the freezer. Once frozen, the cryobox (containing tubes) was placed in liquid nitrogen for long term storage.

2.24 Transfection of human cells

Untransfected cells were grown to 20-40% confluency and media was changed to 1% FBS DMEM 2-4 hours before transfection. Low serum media proved to improve transfection efficiency without sacrificing health of cells during incubation with the media. Transfection was achieved by using Lipofectamine (Invitrogen) according to manufactures instructions. After 4-16 hours cells were washed with PBS and placed back into DMEM containing 10% FBS for continued culture.

2.25 Imaging transfected cells

Previously transfected cells were washed with PBS and placed in OptiMEM. Imaging of cells was performed in 8 well plates (CellTreat), 96 well plates (Corning Nunc), and 384 well plates (Greiner Bio). Cells were imaged for

2-4 hours at a time and then placed back under 10% FBS DMEM to continue culture.

2.26 Monoclonal line selection

Transfected cells were grown under selection media containing 400 µg/mL G418 until 60-80% confluent. Cells were then passaged 1:20 and grown again until 60-80% confluency (2-3 days) and then passaged 1:200 or 1:400 and plated on 8 cm sterile glass petri dishes. Individual cells could be observed after several days having grown into small (20-100 cells) colonies. These colonies were observed under an inverted microscope and manually detached using a pipette and placed into a 24 well polystyrene dish containing media and allowed to grow for 0.5-2 weeks or until a large mat of cells developed. Cells were then split 1:6 and 5 x 1 mL aliquots were frozen using the technique described above. The last 1.0 mL was further diluted 1:1 with selection media and placed in either a T25 flask or split amongst wells of a plate for imaging.

These HEK cell experiments are ongoing and at the time of writing had not produced final data. It is for this reason that the methods are included but there is not representative data for these methods. The cell experiments were taken over by Justin Shady.

Chapter 3 Tau monomers exhibit conformational variation in solution

It has been previously shown that the toxic species in the aggregation pathway of Tau protein is the soluble oligomer species [113]–[114]. Studying the conversion of monomeric Tau into toxic oligomers is therefore critically important in order to understand the earliest stages of disease.

Monomeric Tau protein has been shown to be structurally dynamic in solution. Circular dichroism measurements have shown Tau monomer adopts a random coil structure [122]. Other studies show that Tau molecules have intramolecular distances shorter than what would be predicted for a true random coil. These results have led to a model where the regions flanking the microtubule binding repeats fold back and adopt a paperclip-like structure [20]. These studies typically examine freely-diffusing proteins in solution. The measurements are typically characterized by poor signal-to-noise and short windows of measurement. In order to overcome this limitation, we established a collaboration with the Goldsmith group at the University Wisconsin, Madison. This group employs an antibrownian electrokinetic (ABEL) trap [123]–[125] to monitor individual molecules for timescales on the order of seconds. The ABEL trap, a microfluidic fluorescence measurement instrument is capable of tracking

the position of single fluorophores and utilizes real-time feedback voltages to push individual molecules (here proteins) back to the center of the measurement cell. This allows for fluorescence measurements to be taken for multiple seconds [120]–[121]. Histograms of fluorescence anisotropy data are subsequently detailed enough to represent monomeric conformational heterogeneity in solution. Here an ABEL trap is used to examine Tau monomer for conformational variability in solution. This represents the first use of an ABEL trap on an IDP [127].

Fluorescence anisotropy measurements can be used to examine the rotational freedom of fluorescent molecules in solution. When the fluorophore is attached to a protein, it is possible to study the solution-phase behavior of the protein. Polarized light can be used to selectively excite electrons in fluorescent molecules whose excitation dipole is aligned with the incoming polarized light. Fluorescence anisotropy is a measurement of the depolarization of the emission dipole in a fluorescent molecule, relative to the polarization of the incident light used to excite the molecules. As molecules rotate and diffuse in solution, the emission dipole's position in space will change relative to the original directionality of the dipole when it was excited. Fluorescence anisotropy can be calculated by measuring the emission spectra intensities using parallel and perpendicularly aligned polarizers with respect to the polarized light used for the excitation (see equation in section 2.19). Because fluorescence is a short-lived process (on the order of ns), anisotropy measurements can provide a snapshot

of the tumbling of fluorescent molecules. If the molecules are not rotating in the time frame of fluorescence emission, the maximum value for anisotropy is 0.4. Molecules whose emission dipole dephases 90° (that is, aligns with the perpendicularly aligned polarizer) during the fluorescence lifetime, have a minimum value of -0.2.

Fluorescence anisotropy measurements were taken of full-length human Tau protein (hTau40). In order to utilize maleimide chemistry (and only label 1 position), the two native cysteines were removed and replaced with serines (C291S/C322S). A cysteine was introduced with site-directed mutagenesis at position 310 (Y310C). This single cysteine mutant was labeled with Atto 647N and Atto 633 for fluorescence anisotropy measurements in the ABEL trap. Additionally, the Goldsmith group at UWM labeled commercially available microbial transglutaminase (MTG) with ATTO 647N. This globular enzyme contains one native cysteine in its active site and has a relatively similar molecular weight (Fig 3.1 A – B).

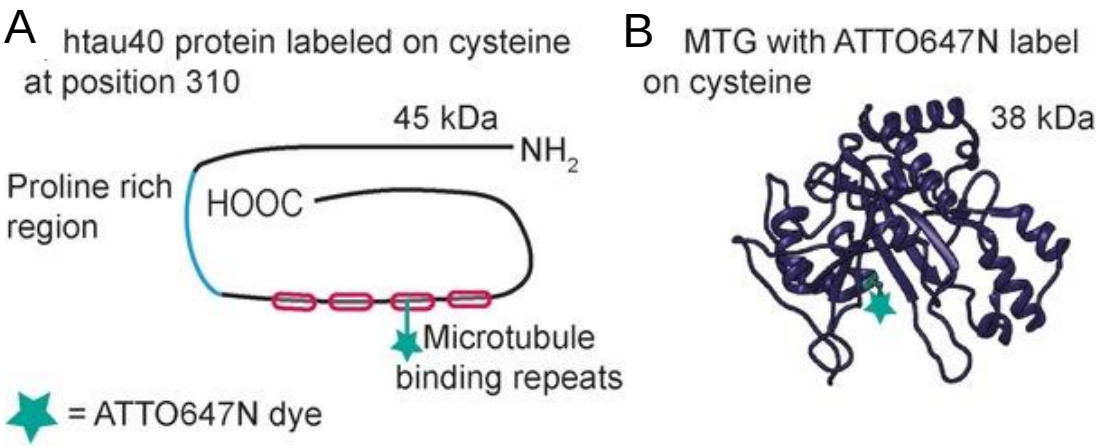

Figure 3.1 Structure for proteins used in this work. A hT40 based on [20], [21] and B Microbial transglutaminase (MTG) based on [128].

In order to study the aggregation pathway of Tau monomer using the ABEL trap, it first must be shown that the protein can be studied using this instrument and methodology. The ABEL trap measurements begin with the feedback voltages off (left side of Fig 3.2 A-E, denoted by off). Feedback voltages are responsible for pushing charged species in the microfluidic measurement in order to trap them for prolonged measurement. Then, upon application of the feedback voltages, fluorescence intensity and anisotropy measurements are taken (Fig 3.2 A – E black trace with red fit trace). Fluorescence anisotropy measurements of Atto 647N conjugated to hT40 were recorded (Figure 3.2 A scale on the right of the graph). Anisotropy of trapped hT40 was observed to be approximately 0.2 (Figure 3.2 A blue trace) and anisotropy for trapped MTG labeled with 647N was 0.3 (Figure 3.2 B blue trace). These results initially contradict intuition. The globular folded nature of MTG would suggest it should be more compact than Tau and should rotate more

quickly than the unfolded Tau molecule. The only native cysteine in MTG exists inside the folded protein structure. The fluorophore is conjugated to this cysteine inside the core of the folded protein. This results in limited rotational freedom of the dye and its C5 linker. Therefore, reduced depolarization and higher anisotropy are observed despite the protein being in a compact, freely rotating, and folded state. Upon denaturation in 6 M guanidinium HCl (GdmCl), the MTG molecule had a marked decrease in anisotropy (0.2), nearly identical for the unfolded Tau molecule (Figure 3.2 C). This is a result of the increased rotational freedom allowed by the unfolding of the protein. Several components can contribute to the reduced anisotropy observed for fluorescent molecules attached to unfolded proteins. The C5 linker which separates the fluorophore and protein backbone would have increased rotational freedom in an unfolded protein. This results in greater depolarization than in the case for the folded enzyme. Additionally, the increase in random motion of the protein backbone would add to the depolarization of the fluorescence emission. This is because solvent exposed fluorophores will have additional freedom to rotate when compared to the active site of the folded enzyme. This result supports previous observations that Tau is largely unfolded. Finally, it was shown that free dye (hydrolyzed) in 50% glycerol has a similar anisotropy to that of the denatured proteins (Figure 3.2 D). These results suggest the fluorescence anisotropy being measured is not an artifact caused by the dye binding to the inner walls of the microfluidic device or other proteins. Protein clumping can be eliminated as a cause for the fluorescence

anisotropy values observed. Emission values would be multiplied by n, where n is the number of proteins clumped together. This was not observed, however.

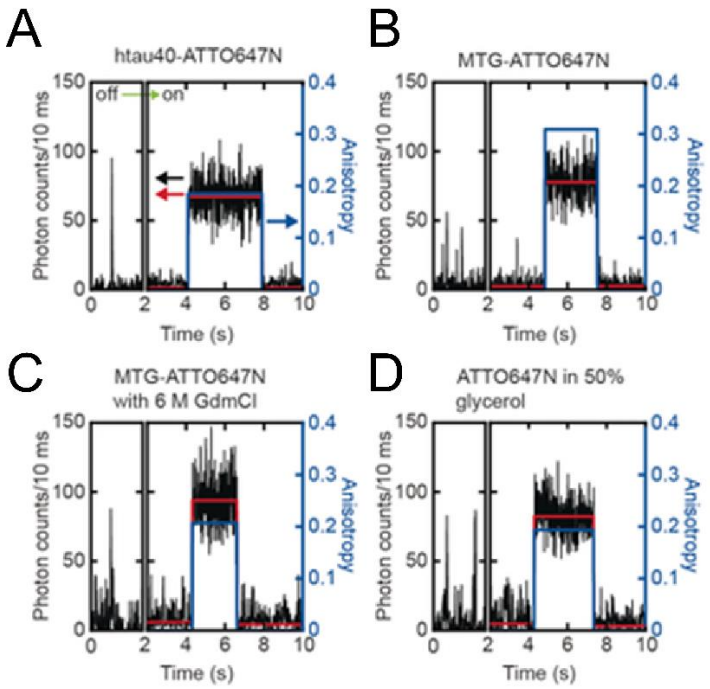

Figure 3.2 Representative traces for molecules in the ABEL trap. A) htau40-ATTO647N, B) MTG-ATTO647N, and C) MTG-ATTO647N denatured with 6 M guanidinium chloride (GdmCl) were trapped in solutions with 25 % glycerol. D) Hydrolyzed ATTO647N was trapped in buffer with 50 % glycerol. Fitting change points in the trapping data are shown in red (left axis), and anisotropy is shown in blue (right axis). Feedback voltages off (left of bar at 2 seconds) and on (right). Trapping data was collected by Lydia Manger at UWM.

The results of many trapping events were binned and plotted as histrograms of anisotropy vs frequency (Fig 3.3). Anisotropic values of 679 trapping events for fluorescently labeled hT40 were fit with Gaussian functions. Tau data was best fit with two Gaussian functions and is bimodal (Fig 3.3 A). The fluorscent anisotropy data for Tau suggests there are at least two populations in

solution, compact and extended forms. 253 trapping events for MTG were fit with one narrow Gaussian function and these results are consistent with a single globular fold for the enzyme (Fig 3.3 B). Tau and MTG were then measured in the presence of 6 M GdmCl. Addition of denaturant should disrupt the folded protein structure in solution. Upon denaturation, the bimodal distribution for Tau becomes a wide single-distribution and the peak for MTG shifts to lower anisotropy (Figure 3.3 C and D). The results match expectations since Tau has been shown to adopt a paperclip-like structure in solution [20], and upon addition of denaturant, the loose structure of Tau should be peturbed. The unfolded proteins exhibit higher rotational freedom around the C5-linkers between the dye and the protein backbone. This allows for lower anisotropy values despite the protein backbone becoming unfolded and tumbling more slowly. It is necessary to add glycerol to these samples in order to improve trapping by slow molecular diffusion. The fluorescence anisotropy of hydrolyzed (free) dye was determined to be 0.18 in 50% glycerol (Figure 3.3). By addition of 80% glycerol (v/v), anisotropy increased to 0.29, indicating the more viscous solution slowed rotational freedom. This slowing is demosntrated by the decrease in emission dipole depolarization, which is due to the increased viscocity of the 80% glycerol solution.This anisotropic behavior models the folded and unfolded states of the proteins. This also suggests the dye is freely diffusing and its diffusion was slowed by the additional solution viscocity.

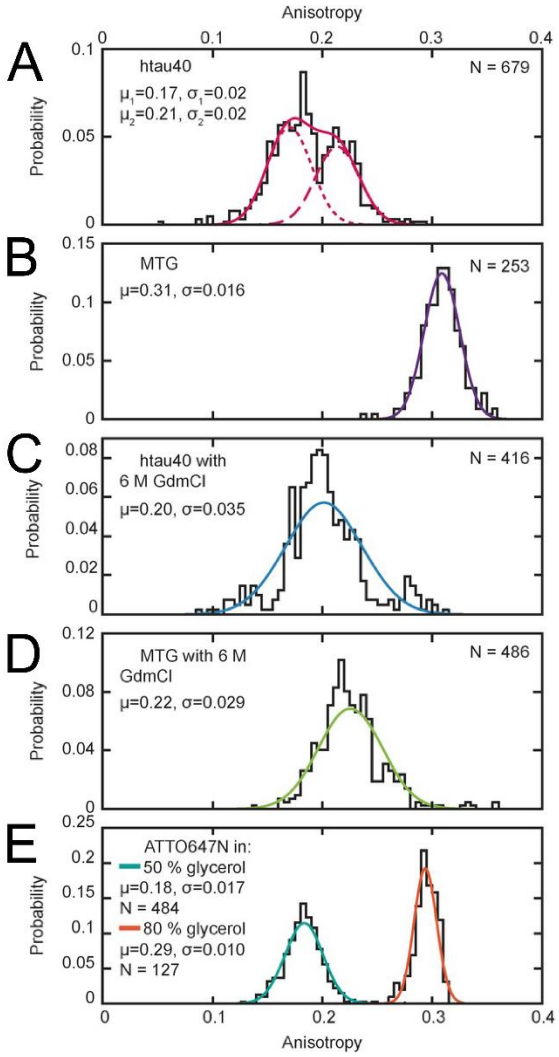

Figure 3.3 Single molecule anisotropy histograms vs probability showing bimodal distribution for only hT40. A hT40 Atto647N exhibits two populations in the fluorescence anisotropy measurements. B Folded microbial transglutaminase (MTG) exhibits one tightly distributed fluorescence anisotropy histogram. C hT40 in the presence of 6 M guanidinium HCl (GdmCl) no longer exhibits two populations. This suggests that intermolecular interactions were disrupted upon addition of the denaturant. D MTG in the presence of 6 M GdmCl has a wider distribution and a lower anisotropy suggesting that the unfolded state has greater emission depolarization due to an increase in rotational freedom of the attached dye. E Hydrolyzed (free) dye in solution at two different glycerol concentrations. This suggests the shift in anisotropy is not due to trapping artifacts. Histograms were prepared Lydia Manger.

These results are indicative that Tau possesses at least two solution-phase families of structures. It is likely the Tau monomer is capable of sampling various transient states within these families. This is demonstrated by broadening of the fluorescence anisotropy distributions of Tau monomer. Whereas the folded MTG distribution is narrow due to limited conformational sampling and compactness of the enzyme's active site. The families of Tau monomer structures can be broadly defined as compact and extended. This data also suggests that Tau exists in dynamic equilibrium between the two states. The structures of Tau monomer interconvert from one population to the other, but not on the timescales observed here. The Gaussian fit distributions are broad and overlapping suggesting that the interconversion is likely a result of conformational sampling of the monomer in solution. The Tau monomers exist in solution in a varying set of structures between the two states, compact and extended. Upon denaturation, Tau loses this bimodal characteristic and adopts a fully loosened random coil structure. This result further suggests the two distinct distributions of Tau structures are a result of solution-phase protein structure.

These experiments are the first to be performed using an ABEL trap to measure Tau. Additional work in this area to elucidate whether or not the intramolecular interactions observed in other studies [20], [129] are long lived (order of seconds) or transient, is planned. These results illustrate that Tau protein is conformationally heterogeneous in solution. The ability of Tau

monomers to adopt a variety of transient folds could contribute to its ability to nucleate and form aggregates in disease.

Chapter 4 Generating and analyzing different Tau conformations

4.1 Successive seeding cycles result in a change in conformational ensemble in K18 but not K19

It has been demonstrated that for other amyloidigenic proteins, that multiple structurally-distinct conformers could be formed in-vitro [56], [130]–[133]. For example, it has been shown that Aβ aggregates formed under either different conditions can evolve from one conformer to another, over the course of time [70]. These studies lead us to wonder if it were possible to generate multiple conformers of Tau in individual samples, and if these conformers were capable of evolving their structure over multiple cycles of seeding. This was observed and could suggest that as Tau fibrils spread through the brain, evolutionary pressures may cause particular structures to propagate in a particular set of conditions.

By stirring Tau monomers and cofactors in solution for several days, nuclei form and mature into amyloid fibrils. Once a fibril nucleus has formed, it will mature and elongate the fibril structure through a process called templating [54]. The formation of the nucleus is the rate-limited step in this process.

To overcome the rate-limiting step in Tau aggregation, fibrils are preformed over the course of three days under stirring conditions at room

temperature. Sonicated fibrils are then added to the reaction (#1) containing 25 µM Tau and 50 µM heparin cofactor is incubated at 37 °C for 1 hour. The sonicated fibrils will serve as a template to accelerate the aggregation of monomer dramatically (Figure 4.1). The reaction is sonicated on ice and then used to seed the next reaction (#2), which again contains monomer and cofactor. This process is repeated until 14 cycles have been completed. At this point the original seed (3 day stirred material), the 4th cycle, 9th cycle, and 14th cycle are used to seed 50 µM Tau and 12.5 µM heparin containing reactions (#1, #5, #10, and #15) for 16 hours at 37 °C for further analysis. The same method of successive cycles of seeding was applied to K19.

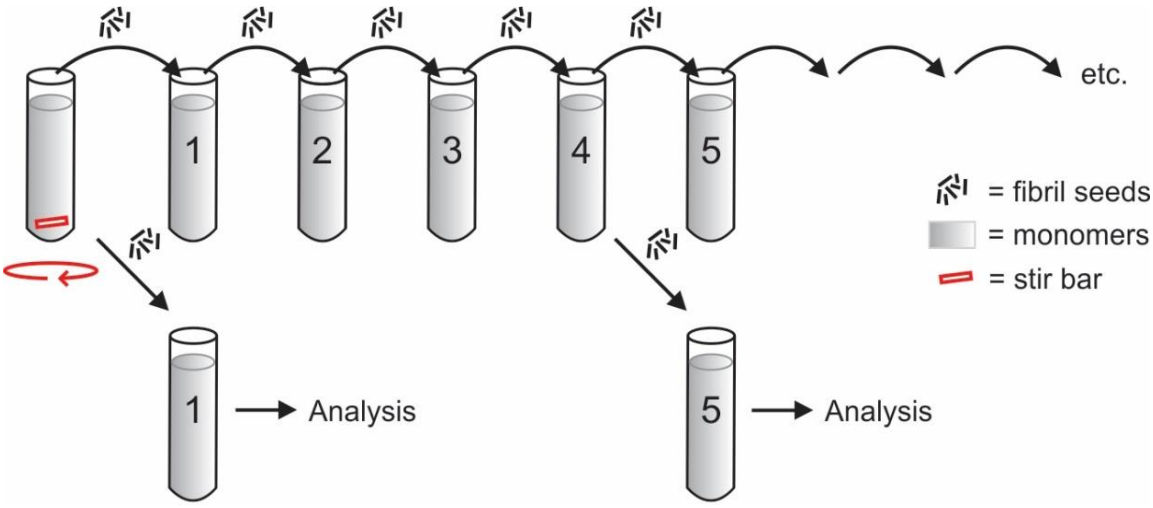

Figure 4.1 Successive seeding cycles scheme. K18 monomers are mixed with a 2-fold molar excess of heparin and allowed to form fibrils for 3 days while stirring. After sonication, the fibril seeds are mixed with fresh K18 monomers to produce a new generation of fibrils referred to as cycle 1. The procedure is repeated up to 15 times. In these templated reactions, fibrils are grown quiescently. At distinct cycles, seeds are removed and used to form an independent set of fibrils for structural analysis.

It has been previously shown that after 5 consecutive cycles of Tau seeding reactions, there is a heterogeneous ensemble of K18 conformers. This was reported by use of double electron-electron resonance (DEER) spectroscopy [63]. DEER spectroscopy can be used to measure distances between unpaired electrons in radicals such as the nitroxide MTSL [58], [63]–[65], [134]. Different conformations of Tau protein will have subtle differences in their folding, which results in changes in the distance measured between the two radicals. One possible explanation for the heterogeneity is that under the conditions provided, multiple amyloid nuclei can form simultaneously.

After one cycle of seeding, measurements showed the sample to be homogeneous [64]. Additional cycles of seeding produced an increasingly heterogeneous ensemble of conformers, which reached an end point at around 10 cycles [64]. The fact that the same protein sequence can form several unique conformations and faithfully template this structure, suggests that Tau monomer exhibits a high degree of structural plasticity in solution.

4.2 Analysis of Tau morphology

Fibrils of differing morphologies have been observed in disease [135]–[137]. In Alzheimer's disease two distinct fibril types have been noted. Tau fibrils possess two monomers per layer stacked in the fibril core. These indivually stacked monomers form a protofilament [71], with two protofilaments associated in the mature fibril [71]. The morphology of AD fibrils is described as either

straight filaments (SF) or paired helical filaments (PHF). Straight filaments have been characterized as flat ribbon-like structures. PHFs are fibrils in which a helical structure has been observed resulting in a characteristic twisted appearance. These morphological differences have been reported on by techniques such as atomic force microscopy (AFM) [138]–[141] and transmission electron microscopy (TEM) [64], [141]–[143]. Using AFM it was previously shown that Aβ fibril morphology and structure coevolved over successive cycles of seeding [144]. Since it was observed using DEER that the structure of Tau fibrils was evolving over multiple cycles of seeding, a question arose. Were these structural changes accompanied by changes in morphology? It was observed that K18 fibril samples from differing cycles did display morphological changes (Fig 4.2 A – D).

Cycle 1 fibrils were observed to have two or more distinct protofilaments (Fig 4.2 A). These protofilamets were straight and had a flat striated-ribbon appearance. These protofilaments were observed to possess variation in the number of parallel filaments, but most often were observed to have 2-3 lateral associations. Cycle 10 fibrils were then analyzed for differences with respect to the Cycle 1 data. Cycle 10 fibrils were characterized by a more heterogeneous mixture of fibrils, consisting of mostly helical filaments (Fig 4.2 C). These filaments were observed to have a helical periodicity of 90 -180 nm (n = 50 for cycle 5 and n = 40 for cycle 10) with a diameter of ~14 nm (n = 100, measured at

the widest part). Cycle 5 samples were observed to have intermediate characteristics with both structures being observed to some extent.

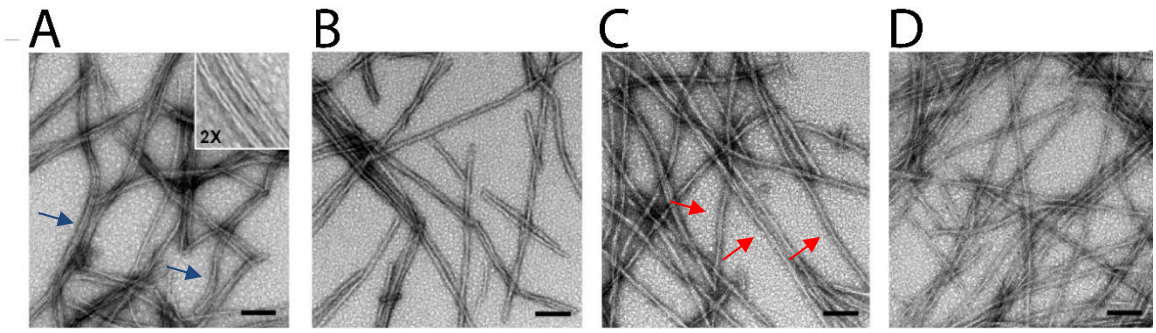

Figure 4.2 Evolution of morphology of K18 fibrils by TEM. TEM analysis of K18 fibrils. Cycle 1 fibrils have a distinct striated ribbon appearance (blue arrows) with varying numbers of parallel filaments (diameter per filament = 7–8 nm), highlighted in the inset. Fibrils at later cycles are dominated by a typical twisted appearance (red arrows, diameter ≈ 14 nm, helix periodicity = 90–180 nm). Scale bars, 100 nm. Panels from left to right represent data for fibrils from cycle 1, cycle 5, cycle 10, and cycle 15, respectively.

The same consecutive cycles of seeding were performed for K19 and the morphology of these fibrils was also examined using TEM. These experiments were done less exhaustively because K19 exhibited a high degree of conformational stability and was not observed to change structure when subjected to multiple cycles of seeding. K19 fibrils were characteristically ribbon-like and within a sample had differing degrees of lateral associations (Fig 4.3). The average number of protofilament associations was fairly consistent amongst differing cycles, however. The individual filaments within the analyzed samples had average diameters ± SD of 26 ± 13 nm (n = 71), 33 ± 11 nm (n = 69), and 32 ± 12 nm (n = 31) for cycles 1, 5, and 10, respectively. The wide distributions and

similar numbers suggest a variety of, but similar distribution of, parallel filament arrangements.

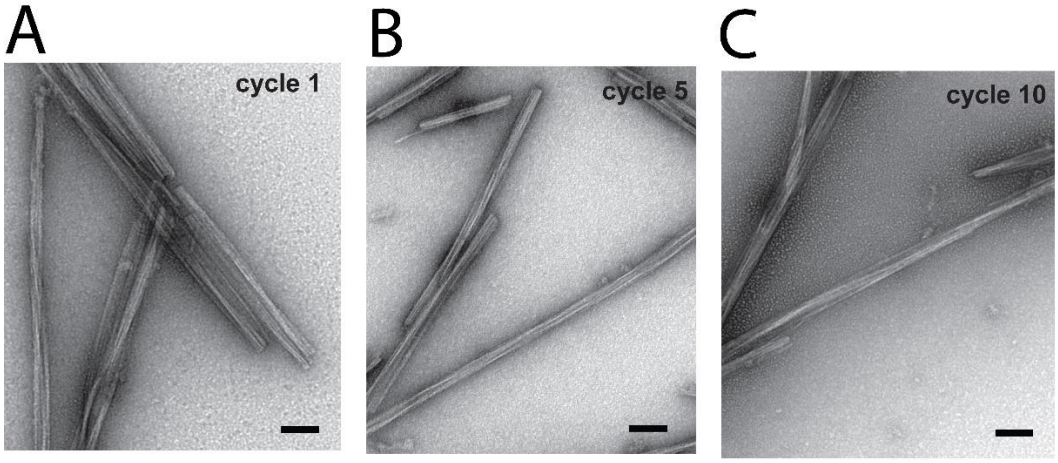

Figure 4.3 Conformational stability of K19 fibrils revealed by TEM. Fibrils were stained with uranyl acetate and analyzed by transmission electron microscopy. Electron micrographs of fibrils from cycle 1 (A), cycle 5 (B), and cycle 10 (C). Scale bars, 100 nm. All K19 fibril ensembles measured (cycles 1, 5, and 10) exhibited similar ribbon-like morphology. Individual protofilaments within these ensembles have a diameter of 7–8 nm with 3-7 protofilaments per fibril.

4.3 Changes in light scattering and proteolytic sensitivity accompany conformational changes

Upon ultracentrifugation, the pellets of fibrils from K18 cycle 1 and cycle 10 samples were visually distinct. The pellets of cycle 1 fibrils were white and tightly packed whereas the fibrils produced after 10 cycles of seeding were translucent and gelatinous. This implies a changing in the packing of the fibrils upon centrifugation which could have resulted from a change in fibril structure. To quantify these observations, a light scattering assay was developed. Turbidity measurements at 340 nm were taken for cycle 1 through cycle 10 samples for

K18 and K19. K18 exhibited a decrease in turbidity over successive seeding cycles (Fig 4.4 A) despite equal amounts of fibrils in solution during each step. These results suggest a change in the packing of the monomers in the fibrils, which resulted in a decrease in light scattering.

In order to support the other data which suggested that the structures of K18 fibrils were changing over multiple cycles of seeding, a proteolysis experiment was designed. It has been demonstrated in the literature that fibrils of differing structures have different proteolytic degradation rates [140]–[141]. A commonly used protease for this is proteinase K (PK). Proteolytic sensitivity differences are suggestive of changes in the packing of the monomers in fibrils of unique structures. The changes in monomer packing result in the accessibility of individual protease cleavage sites within the fibril structure to be more or less accessible. The differences in accessibilities can result in changes in kinetics of proteolytic cleavage. To test for this, fibrils formed from an identical concentration of cycle 1 and cycle 10 samples (Figure 4.4 B, lanes in the gel labeled none) were proteolytically digested. After addition of protease inhibitor to stop the reaction, the samples were run on SDS-PAGE to assess the degree to which the fibrils were digested using PK. It was observed that cycle 10 fibrils consistently degraded faster (Figure 4.4 B). This is evidenced by the appearance of a lower molecular weight band in the cycle ten 10 sample upon addition of 7 nM proteinase K (Fig 4.4 B). With higher concentrations of protease added, a complete disappearance of the original molecular weight band (undigested K18)

is observed for cycle 10 but not cycle 1 (Fig 4.4 B) This suggests the cycle 10 fibrils have different protease accessibilities and therefore different rates of cleavage. A change in the cleavage rate therefore implies a change in structure has occurred. These results demonstrating the change in dominant structure were also supported by DEER measurements [147].

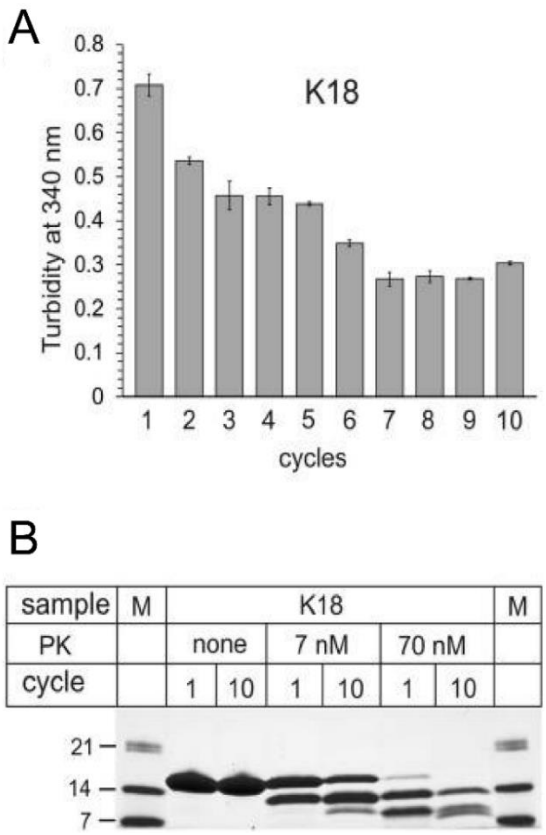

Figure 4.4 Turbidity and limited proteolysis for K18 samples. A Cycle 1 samples possessed the highest turbidity and over several cycles turbidity was observed to decrease. This data is supportive of the fact that conformational changes were occurring over the course of several cycles and the changes in structural diversity were completed before the 10th cycle. Turbidity was measured in Triplicate with SD reported. B Proteinase K (PK) treatment of cycle 1 and cycle 10 fibrils yielded differing digestion products when exposed to protease treatment for 1 hour. Cycle 1 is less sensitive than cycle 10 is more sensitive to this treatment. These results support that the two samples contain different conformational ensembles. (M = molecular weight marker)

Upon ultracentrifugation, the pellets of K19 samples from cycle 1 and 10 both appeared similar. In order to support this quantitatively, light scattering experiments with K19 cycle 1 and cycle 10 fibrils were performed. No changes in turbidity were observed over the course of multiple cycles of seeding (Fig 4.5 A).

To further substantiate that K19 did not undergo structural evolution upon multiple cycles of seeding, protease sensitivity was measured for cycles 1 through 10. However, no changes in proteolytic cleavage were observed (Fig 4.5 B), implying the structure of the dominant species in the sample is not changing in these respects, as described for K18. This supports the previous results that K19 is conformationally stable under these conditions. Proteolysis of K19 cycle 1 and cycle 10 samples was also examined. K19 was more resistant to proteolytic degradation, which necessitated higher (14 and 140 nM instead of 7 and 70 nM) proteinase K concentrations. DEER measurements also suggested that the K19 dominant structures were not evolving over multiple cycles of seeding. Taken together, this data helps to further suggest K19 was not changing dominant structures over multiple cycles of seeding.

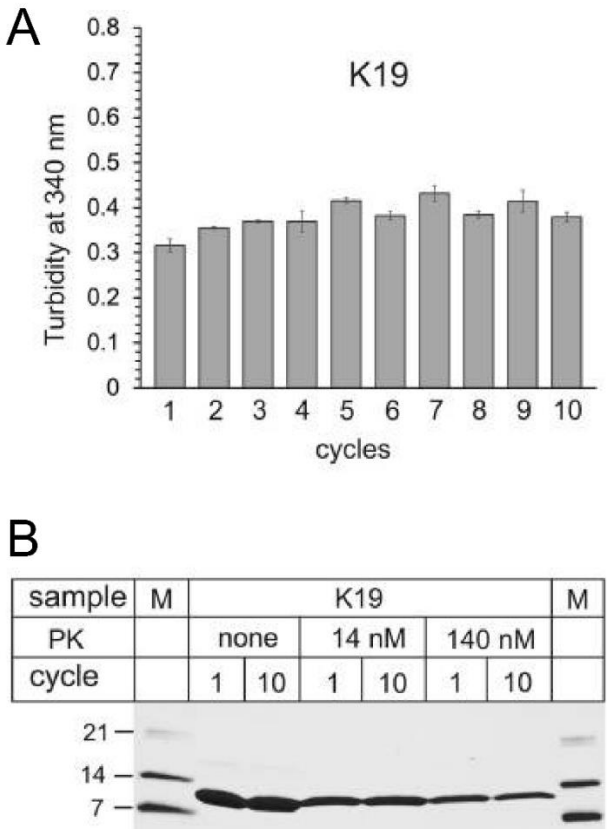

Figure 4.5 Turbidity and limited proteolysis for K19 samples. A K19 samples were also measured for turbidity changes with respect to cycle number. No change in turbidity was observed for K19, supportive of the fact that the conformational ensembles were not observed to evolve with cycles of seeding. Turbidity was measured in triplicate with SD reported. B K19 cycles 1 and 10 were also subjected to Proteinase K digestion. Again, supportive of the data showing no change in structure was occurring, no change in protease sensitivity was observed for the fibrils.

4.4 Fragility and growth rates drive conformational evolution

It was hypothesized that the change occurs over these cycles is due to a difference in the fragility of fibrils. A difference in fragility would result in accelerated growth for fragile fibrils during the period when elongation is occurring under the initial stirring conditions (220 RPM for 3 days at 22 °C). This is because the more fragile fibrils will tend to break more often under agitated

conditions. More broken Tau fibrils lead to more ends, to which Tau can be recruited. To test this, fibrils were sonicated relatively gently (5% power, in a bath sonicator (QSonica) for 1 minute). Electron microscopy samples were prepared, and micrographs were collected. Representative micrographs for each sample (Figure 4.6 A) show that the fibril lengths are very different for cycle 1 and cycle 10 samples after bath sonication. The micrographs were then quantitatively analyzed for fibril length using ImageJ. The cycle 1 sample broke to a greater extent (average = 126 nm, n = 255) than did the cycle 10 sample (average 228 nm, n = 260, Figure 4.6 B).

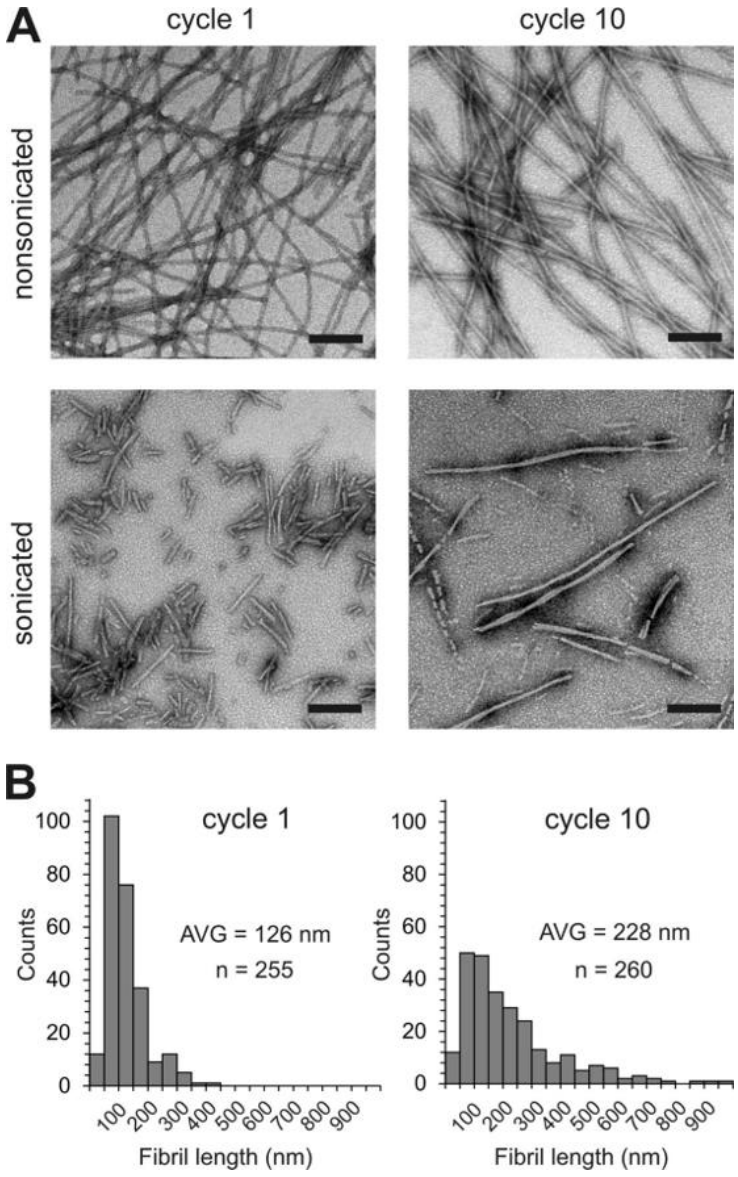

Figure 4.6 K18 fibril fragilities determined using TEM. A cycle 1 and cycle 10 fibrils are analyzed by negative stain EM before (upper panels) and after sonication (lower panels). The fibrils are fractured under mild conditions in a bath sonicator. Scale bars, 200 nm. When subjected to identical stress, cycle 1 fibrils are distinctly shorter than cycle 10 fibrils. B, length distributions for sonicated fibrils from cycle 1 (left panel) and cycle 10 (right panel). The results indicate that cycle 1 fibrils are more fragile than cycle 10 fibrils.

This suggests that selection processes may take place during the stirring step, when fibrils are being initially formed. This selection results in large enhancement of the fragile population. A mechanism of other fibril population enhancement was left to be elucidated. It was hypothesized that the other populations (enhanced in later cycles) grew faster. Quantitative kinetics experiments could demonstrate this hypothesis. Cycle 1 and cycle 10 needed to be sonicated until they were equal size. This would allow for equimolar amounts of fibrils (and therefore ends) to be added in seeded kinetics experiments, in order to evaluate the growth rates of cycle 1 and cycle 10 samples. To test this, the cycle 1 and cycle 10 samples were subjected to 2 minutes of sonication on ice with a tip sonicator set to 20% power. Electron micrographs were collected, and fibril lengths were assessed after tip sonication. The lengths of fibril seeds were quantified using ImageJ. Representative micrographs with the resulting length distributions from the fibril samples are shown (Fig 4.7 A – D).

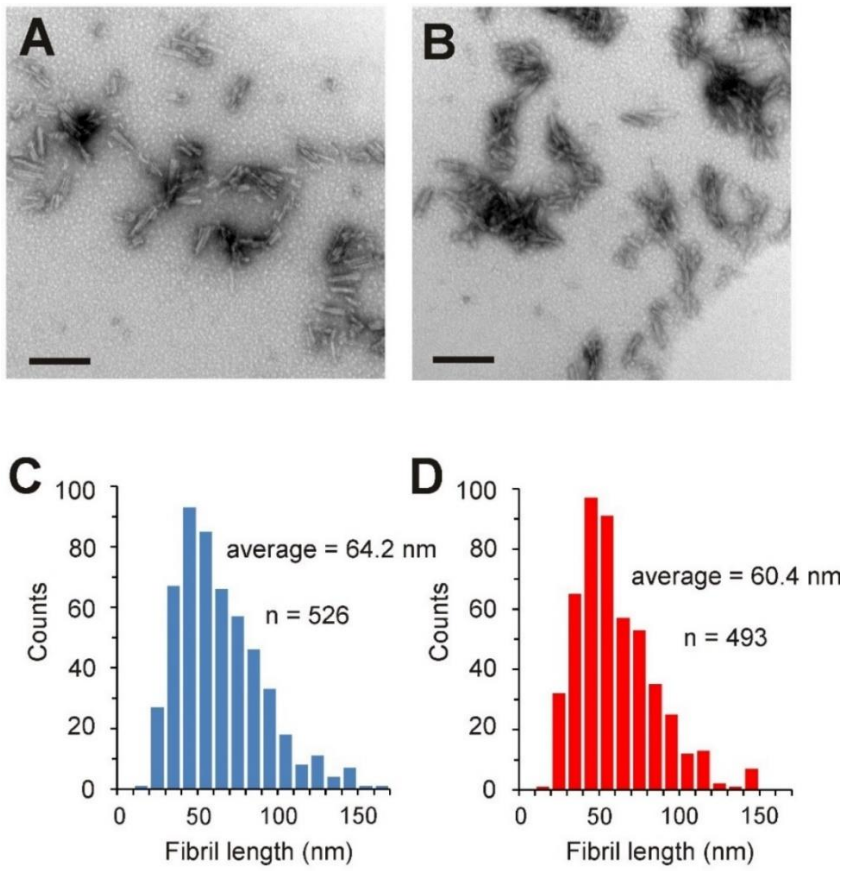

Figure 4.7 Quantified Tau fibril breakage under harsh sonication conditions. Negative stain EM images of cycle 1 (A) and cycle 10 (B) fibrils subjected to harsh sonication conditions with the sonicator tip immersed in the fibril solution. Scale bars, 200 nm. Length distributions of cycle 1 (C) and cycle 10 (D) fibrils. The lengths of 526 fibrils from cycle 1 and 493 fibrils from cycle 10 were measured. The average lengths of cycle 1 and cycle 10 fibrils were 64.2 nm and 60.4 nm, respectively.

Since it was possible to generate nearly identical sizes of preformed fibrils with different conformations, it became possible to quantitatively analyze the samples for seeded kinetic growth rates. To test whether or not the differences in growth rate for cycle 1 and cycle 10 samples were contributing to conformational heterogeneity, thioflavin T kinetics were performed. Thioflavin T is an amyloid

specific dye that binds to β-sheets [142]–[143]. Upon binding the fluorescence emission spectra red shifts and increases in emission intensity [150]–[152]. Monitoring the increase in fluorescence emission intensity of thioflavin T versus time allows for the rates of growth to be monitored. Fibril concentrations were quantified (using the BCA assay) after sonication and therefore the same amount of fibril could be added to each reaction. It was shown that the kinetics of seeded growth were different for cycle 1 and cycle 10 fibril samples (Fig 4.8). Cycle 10 samples (Fig 4.8, red trace) reached completion 2 times faster than the cycle 1 (Fig 4.8, blue trace). The t_{50} was 17 and 8 minutes for cycle 1 and cycle 10, respectively. The results of these experiments were reproduced in triplicates, from independent batches of seeds, which ensured reproducibility and rigor. This data allows for a more complete understanding of the mechanism of selection taking place in the multicycle seeding experiment with K18. Since K19 was not observed to change structure over successive seeding cycles, this analysis of breakage and kinetics was not performed.

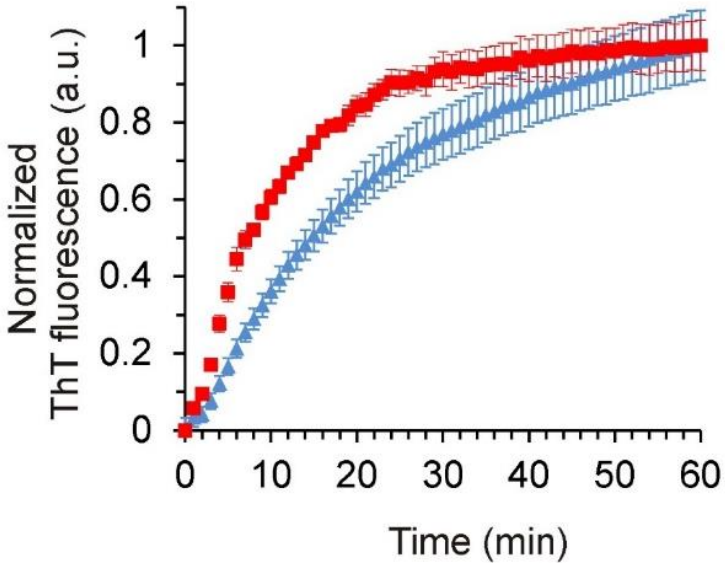

Figure 4.8 Differences in growth rates of K18 conformations. 2% seeds (monomer equivalents) were mixed with 25 μM K18 monomers and 50 μM heparin. Fibril growth of cycle 1 fibrils (blue trace) and cycle 10 fibrils (red trace) was monitored by thioflavin T fluorescence. All values represent average ± SEM (n = 6 replicates).

4.5 3R Tau cannot grow on cycle 1 or cycle 10 material

It has been previously demonstrated that Tau fibrils composed of the MTBRs of 4R Tau cannot recruit 3R Tau. This results in an asymmetric seeding barrier [57], [63], [130]. This phenomenon was first observed using material that was stirred for three days to generate Tau fibrils. Using ultracentrifugation and SDS-PAGE it is possible to separately analyze Tau protein found in the pellet (fibril) or in the supernatant after a seeded reaction. These experiments allow for the examination of whether or not K19 (3R Tau) was being recruited onto the K18 (4R Tau) fibril. Would the cycle 10 conformational ensemble be able to

recruit and template K19? When seeds generated from cycle 1 and cycle 10 were added to K18, both samples fully recruited the K18 monomers (Fig 4.9 A). This demonstrates the seeding competency of the fibrils added to the reaction. Despite their ability to recruit K18, the cycle 1 and cycle 10 samples were not shown to incorporate K19 to an appreciable degree (Fig 4.9). These results suggest the seeding barrier previously observed is robust and does not become diminished after the conformational change (of the K18 seed) produced here (Figure 4.9).

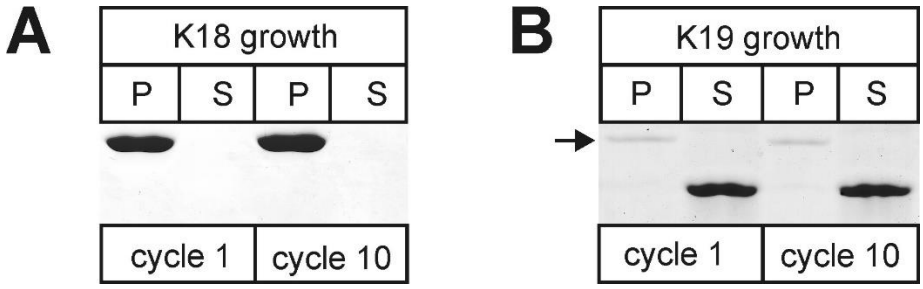

Figure 4.9 Examination of Tau seeding barrier for distinct conformations. 5% seeds (monomer equivalents) from cycle 1 and cycle 10 fibrils were mixed with 25 μM K18 or K19 monomers and 50 μM heparin. Fibrils were allowed to grow for 24 h at 37 °C. Equivalent amounts of pellets (P) and supernatants (S) were analyzed by SDS-PAGE and Coomassie Blue staining. Whereas K18 monomers grow onto K18 seeds (A), K19 monomers do not (B). The arrow in B refers to K18 protein bands that originate from the seeds. The data highlight that both populations of K18 fibril conformers are unable to recruit K19 monomers.

4.6 Fragility and growth rates govern fibril selection

One possible explanation as to why fragile fibrils are enriched in mild stirring conditions could be that if certain populations are more fragile, they will break more often than their less fragile counterparts. Since the end of the fibril is the site of new amyloidogenic growth, the fragile fibrils which generate more

ends, therefore exhibit more growth in these conditions. Long fibrils do not elongate efficiently [153], [154]. Over several days, the dominant species in solution becomes the one which will break the most under the given conditions. Under tip sonication, both fibril species break similarly. This means whichever grows faster in quiescent conditions will evolve as the dominant species through several cycles of templating new monomer onto fibrils from the previous reaction.

Over repetitive cycles of fracture and growth this conformer will become the dominant species (upper reaction path) (Fig 4.10). Inefficient breakage selectively fractures the more fragile conformer (L-shape) (Fig 4.10). If repeated over multiple cycles (continuous stirring) this conformer will become the dominant species (lower reaction path). Note that the depicted conformers are only models. The real structures of Tau fibrils will be more complex and include additional β-sheets. The number of cycles required for evolving a dominant species will depend on the structural composition of the original ensemble and the specific parameters of fracture and growth. In cases where the fragilities and growth rates of different conformers are similar, the populations may have multiple dominant fibril species. It is conceivable that within neuronal cells, molecular chaperones or other machineries could facilitate the breakage of fibrils and influence growth.

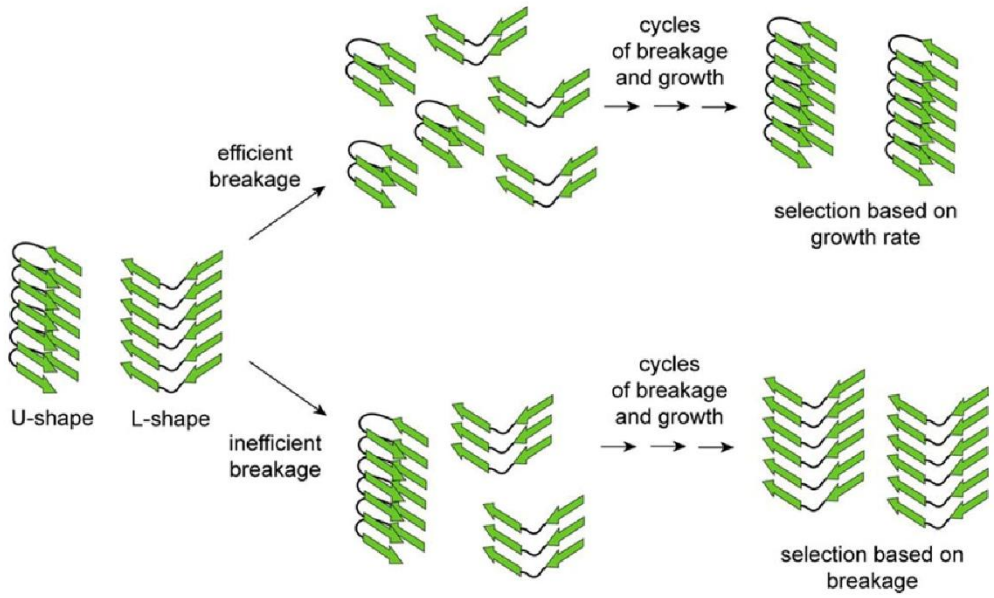

Figure 4.10 Conformational selection based on fracture and growth. In a heterogeneous mixture of Tau fibril conformers, depicted as stacks of β-stranded segments (green arrows) in U- and L-shape conformations, efficient breakage (intense sonication) results in seeds with identical extensions along the fibril axis. Under these conditions the number of fibril ends that can recruit soluble monomers is the same for the different conformers giving the faster growing seed (U-shape) a selective advantage.

It was shown that K18 fibrils can form multiple nuclei under stirring conditions *in-vitro*. Upon changes in the growth conditions, selection processes can evolve the dominant population. Other possible explanations for the change in dominant fibril species do exist, however. Such explanations include secondary nucleation [155]–[157] and strain switching [50], [144], [158]. These results demonstrate a model for how breakage and growth rates may play an important role in disease, and how this process could allow certain populations to become enriched in particular brain regions. Biophysical properties of amyloid

fibrils could drive pathology and subsequently enable the phenotypic diversity found in Tauopathies [159].

Chapter 5 Stability of Tau fibrils

5.1 Limited dilution of Tau fibrils does not cause dissociation

Thermodynamic stability is an important aspect to study when trying to understand protein aggregates. Tau protein is very electropositive at neutral pH. The positive charges in Tau are what allows Tau to perform its native functions of binding to and stabilizing negatively charged microtubules. To induce Tau aggregation in-vitro, a polyanionic cofactor must be added to compensate for the many positive charges in Tau. This cofactor has been shown to bind to the Tau monomer [160], change its conformation [129], and stabilize the fibril [57]. Therefore, it follows that understanding the interaction between the cofactor and the Tau fibril is critical to our understanding how these aggregates form.

It has been suggested in the literature that cofactor molecules may be only required for the initial steps of nucleation [160]. However, it has also been demonstrated that without addition of cofactor, seeded templating of Tau was not observed [57]. Additionally, utilizing a fluorescence anisotropy experiment, it was observed that it was possible to exchange cofactors, which demonstrates the surface accessibility of cofactors. It was observed that not all of the cofactors associated with Tau filaments could become displaced, however [57]. Molecular exchange can only occur with cofactors decorating the outside of the fibril. Some

of the cofactor may be inaccessible to the solvent which suggests some of the cofactors associated with Tau fibrils may be buried in the interior of the fibril core.

In order to test whether the cofactor mediated fibril stabilization was driven by thermodynamic equilibrium, fibril dilution experiments were performed. The experiments below were performed by diluting preformed fibrils in the presence or absence of cofactor, and sedimenting the fibrils after 12 hours of incubation at 37 °C. These results demonstrate that with limited dilution, regardless of whether RNA cofactor was included in the dilution, the fibrils do not dissociate (Figure 5.1, top and bottom).

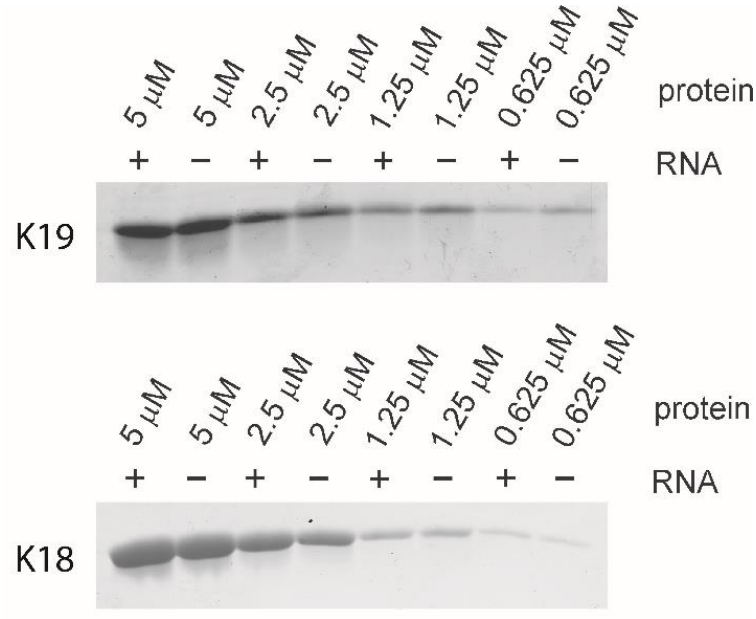

Figure 5.1 Limited dilution of Tau fibrils. Upon dilution in the presence or absence of cofactor, K19 and K18 fibrils were not observed to dissociate. This result suggests that once formed, Tau fibrils are stable and resistant to concentration-dependent depolymerization.

These results are important because they highlight the stability of Tau fibrils, even in the absence of cofactors. Stability is essential for fibrils during cell-to-cell transmission, for example.

5.2 Adding high salt does not dissociate RNA cofactors or Tau fibrils

It was observed that it is possible to inhibit growth of seeded Tau reactions by addition of either 0.5 M or 1.0 M NaCl, depending on the cofactor used [57]. This effect is likely in part due to the increased competition between the polyanionic cofactors (polyRNA or heparin sulfate) and the salt for the positively charged fibril surface. Additionally, it is likely that increased salt concentration could enhance the hydrophobic interaction between monomers in the fibril. This would therefore disfavor fibril dissociation. It is not clear what the contribution of these two effects to fibril elongation are at this time. To understand if cofactors bound to the fibril surface are capable of becoming displaced by salt, fibrils formed with RNA at 100 mM NaCl were adjusted to 500 mM NaCl, incubated for 10 minutes at 37 °C, and sedimented via centrifugation. RNA bound to fibrils was co-sedimented into the insoluble pellets fraction (which contained Tau fibrils and associated RNA). The pellets were taken up in 2% SDS and subsequently adjusted to 1250 µL with assembly buffer. RNA concentration was then quantified in samples using the absorbance at 260 nm (using the following equation: $A_{260\ nm} = 1 = 40$ µg/mL). It was shown that the cofactor/fibril interaction was not diminished significantly by the increase in the salt concentration (Figure

5.2 A). These results are important because they suggest the cofactor/fibril interactions are strong and specific.

It could be possible for fibrils to dissociate upon addition of high salt, despite maintaining a majority of the ionic interactions with cofactors. To test this, fibrils previously formed with RNA and adjusted to 500 mM NaCl for 15 minutes were sedimented, and protein content was compared using SDS PAGE. It was also shown that upon addition of high salt concentrations, the sedimentable material was unchanged (Fig 5.2 B). This result suggests that once the fibrils are formed, that the various interactions between monomers in the fibril are sufficient to disfavor dissociation under these conditions. Although 500 mM salt concentrations are not found *in-vivo* these results are important contributions to understanding the stability of Tau fibrils and their associated cofactors.

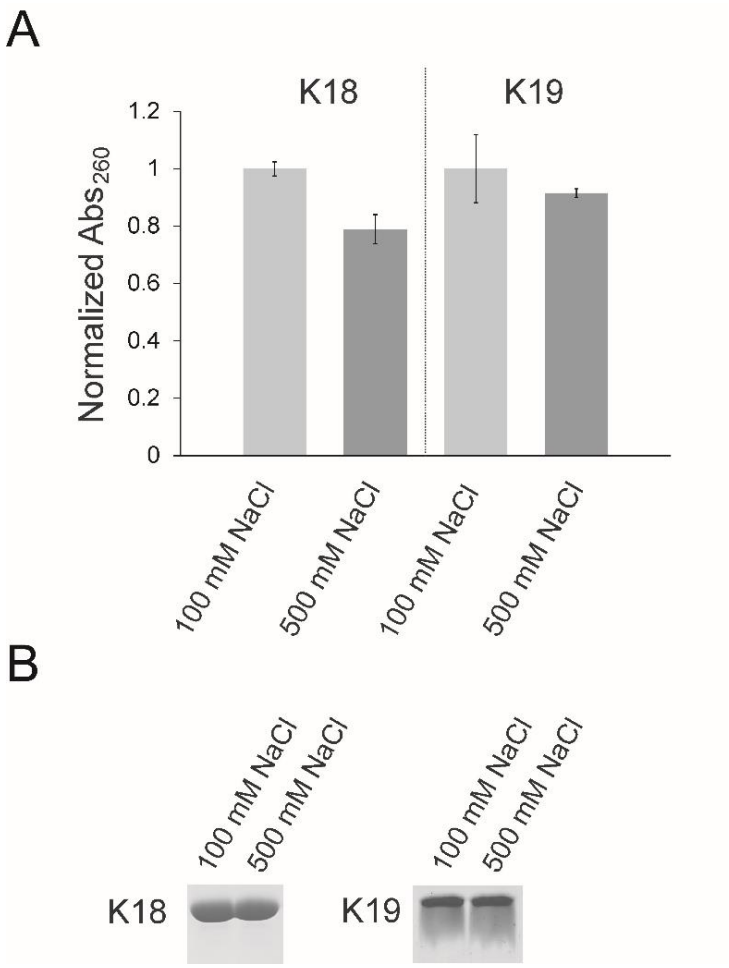

Figure 5.2 Addition of high salt does not dissociate cofactors or monomers. A Normalized intensity of RNA UV280 nm absorbance for K18 and K19. Fibrils were formed at 100 mM NaCl and upon addition of 500 mM NaCl, the RNA cofactor was observed to marginally dissociate (~20% for K18 and 10% for K19). B Identical samples were ultracentrifuged (130,000 x g) and pellets were taken up in 1X Laemmli Sample Buffer and analyzed by 15% SDS PAGE. The results indicate that fibrils do not dissociate upon addition of high salt.

There are alternative explanations that would explain why the higher salt concentrations were unable to dissociate cofactors. For example, any cofactors buried in the fibril's interior would not likely be dissociated from fibrils. These

buried cofactors would be unable to be exchanged and also could contribute to the stability observed for the fibrils in the limited dilution experiments.

Cofactor molecules have been shown to be associated with NFT *in-vivo*. Gaining a deeper understanding of how fibrils associate with cofactors will likely contribute to our understanding of the pathology involving Tau fibrils. For example, it has been shown that sulfonated polysaccharides (such as heparin) are found conjugated to some extracellular membrane proteins, and these can help mediate internalization and transmission of fibrils [161]

These results are important because they suggest that Tau fibrils are stably folded. This is relevant for seeding assays, which rely on fibril stability. Fibrils cannot spontaneously dissociate or fibril seeding experiments would not be possible. This is because as a small amount of seeds are added to a reaction there is a large dilution. If Tau fibrils spontaneously dissociated upon dilution they would be incapable of acting as seeds and would not template new Tau monomer.

Chapter 6 MAP2 Binds to the end of Tau fibrils; Preventing Seeded Aggregation and slows nucleation-Based aggregation

6.1 Sequence similarity between MTBRs of Tau and MAP2

Microtubule associated proteins have been shown to perform similar functions in healthy cells. These functions include binding to and stabilizing or crosslinking the microtubules in neurons [162]–[164]. The semiconserved functions of MAP2 and Tau are due to the high sequence identity in the microtubule binding repeat regions (Fig 6.1).

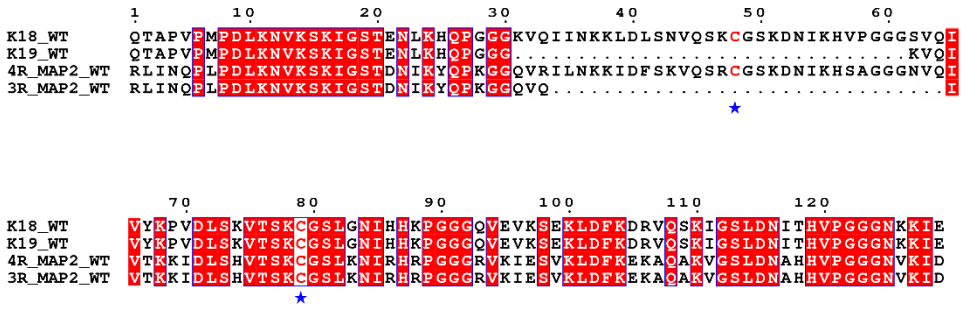

Figure 6.1 Comparison of MAP sequences in MTBRs. MTBRs for 3R (K19) and 4R (K18) Tau and MAP2. Native cysteines are marked by a blue star and red residue letter. Identical regions are boxed in red.

These proteins serve similar functions as monomers in the cell and bind to microtubules through a similar sequence called microtubule binding repeat regions [165]–[167]. NFTs are comprised mainly of phosphorylated Tau [4].

MAP2 epitopes have been shown not to be present as a major component of NFTs. However, this does not exclude small amounts of MAP2 from being present in the mature NFT [188]–[189].

Tau fibrils grow by recruiting monomeric Tau onto their ends. The Tau monomer adopts the structure of the fibril template and extends the fibril. The consequence of this is that identical residues of adjacent monomers, along the fibril axis are stacked on top of one another. The result of this is an elongation of the fibril along the long fibril axis [54], [130]. The templating process can result in different conformations of Tau fibrils being formed (as in Chapter 4). Previously, it was shown that a single point mutation can result in a selection of seed conformation [58]. An extreme case of sequence driven selection occurs with 3R Tau, which will not recruit onto the 4R fibril end. This results in an asymmetric seeding barrier [130]. These incompatibilities with growth might occur due to inability of monomers to adopt different conformations. The incompatibility could be due to subtle or extreme differences in sequence between the species. Considering that the fibrils are comprised of the MTBRs and that these regions in MAP2 and MAPT are highly homologous, it was hypothesized that MAP2 could bind to the end of the Tau fibril, cap it, and thereby inhibiting the recruitment of Tau monomers (Figure 6.2).

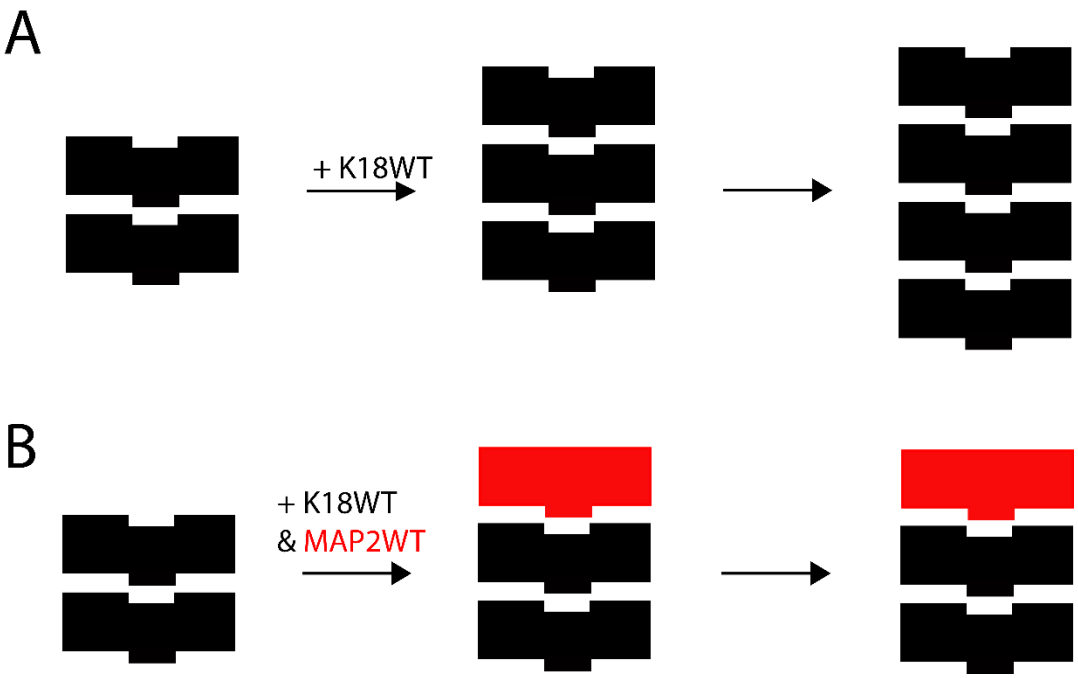

Figure 6.2 Hypothetical model of MAP2 binding to the end of Tau fibrils. A In the absence of MAP2, the Tau protein is capable of continuing the structure until the monomer or heparin is depleted. The structure of Tau fibrils is templated faithfully and the notches in the diagram represent this continuation of structure. B In the case where MAP2 has been added, the Tau fibrils are capable of recruiting one MAP2 molecule, on the end of the fibril, as it possesses the correct structural plasticity to adopt the conformation presented by the Tau fibril. Subsequent layers are incapable of incorporating due to some constraint on the Tau and MAP2 monomer that inhibits its ability to elongate the fibril beyond the initial deposition of a layer.

6.2 Inhibition of seeded Tau fibril elongation

To test whether or not MAP2 could inhibit Tau growth, K18 seeds were added to monomer and heparin to allow for growth that could be monitored by thioflavin T (ThT) fluorescence kinetics (as previously described in Chapter 4.6). The K18 in the absence of MAP2 efficiently aggregated and the aggregation was completed in 4 hours (Figure 6.3). By including either 3R or 4R MAP2 MTBR isoforms in seeded Tau experiments, a consistent and powerful blocking effect

was observed. This effect was demonstrated by sub stoichiometric concentrations of MAP2 (2.5 µM) with respect to Tau monomer (10 µM). It was shown that 3R MAP2 reduced ThT signal by 65% and 4R by 90% (Figure 6.3 A). These effects were measured in quadruplicate and plotted with SEM values. Fibril growth can also be monitored by sedimenting the insoluble material by ultracentrifugation after the reaction is complete. This fractionates fibrillar and monomeric Tau. By dissolving the pellets (insoluble fraction) in the same volume of 1 x Laemmli sample buffer as the original reaction, pellets can be directly compared to supernatants by SDS PAGE. It was shown that addition of substoichiometric concentrations of MAP2 MTBRs to the K18 seeded reaction, resulted in a dose-dependent blockage effect (Figure 6.3 B - D). The reproducibility of these experiments was demonstrated by use of three independent batches of seeds (biological triplicates) which were quantified by gel band densitometry using ImageJ. The resultant quantifications were analyzed in GraphPad using a one-way ANOVA test. The 3R MAP2 resulted in 60%-75% reduction ($p < 0.0001$) in K18 aggregation (Fig 6.3 B and C). 4R MAP2 was slightly more potent and resulted in 65-80% ($p < 0.0001$) reduction in K18 aggregate formation (Figure 6.3 B and D). It was noticed that the MAP2 protein consistently ends up in the pellet fraction of these experiments (Fig 6.3 C -D, bands in pellet (P) lane below the K18 (3R MAP2) and above the K18 (4R MAP2). This would suggest that MAP2 is aggregating under the quiescent reaction conditions. However, the reduction in ThT signal (Figure 6.3 A) would

suggest the MAP2 is not forming fibrillar material in place of Tau. This is because the ThT assay measures the relative amount of β-sheet character of proteins in solution (and therefore the relative monomer to fibril conversion). MAP2 is not appreciably contributing to the ThT signal however (Fig 6.3 A). If it were, blockage would be obfuscated by the increase in fluorescence by MAP2. These results suggest that the MAP2 protein might be either binding to Tau aggregates (but not being incorporated into the fibril structure), or they might be forming non-amyloidogenic aggregates, or both.

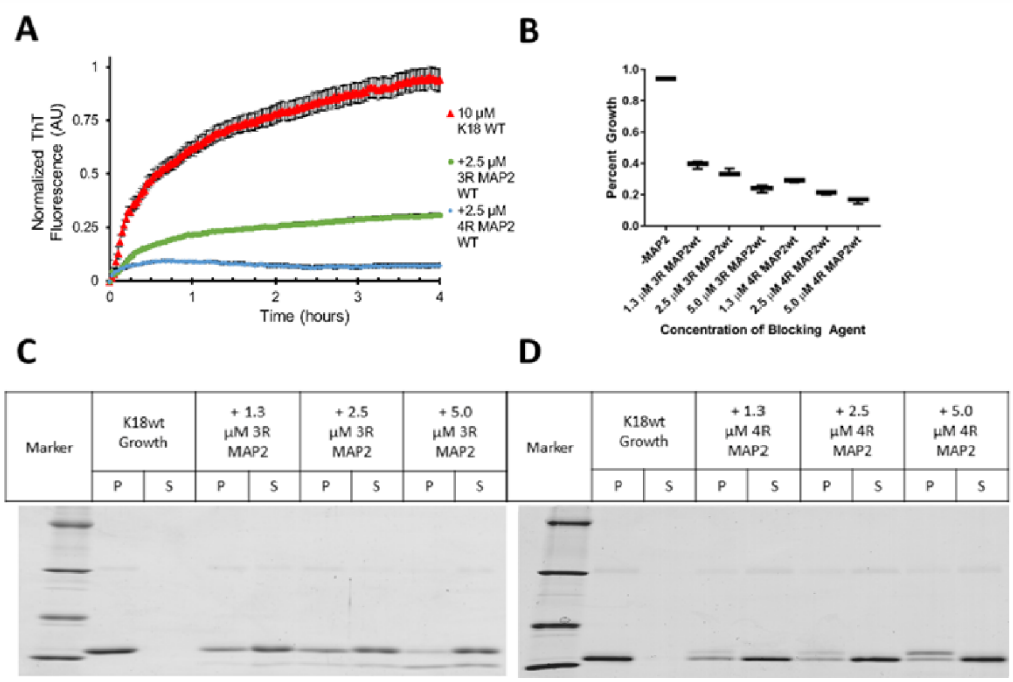

Figure 6.3 3R and 4R MTBRs of MAP2 block K18 growth in seeded reactions. A Thioflavin T kinetics of K18 growth in the absence or presence of 3R or 4R MAP2 MTBRs. B One-way ANOVA analysis of MAP2 blockage in 3 sedimentation experiments (biological replicates). $p < 0.0001$ from one-way ANOVA for each of the different concentrations of MAP2 when compared to –MAP2 reactions. Band intensity was calculated by $I_P/(I_P+I_S)$, where I_P and I_S are the integrated band intensities measured in ImageJ from SDS PAGE gels for the pellet (I_P) and supernatants (I_S). C and D Representative SDS PAGE gels of 3R and 4R MAP2 blocking K18 growth, respectively.

6.3 Inhibition of K18 nucleation by MAP2 MTBRs

Nucleation dependent kinetics can be monitored via ThT also. Once the nuclei form, they begin to elongate and consume monomer via the templating mechanism. This results in an initial lag phase in which the fluorescence emission intensity of ThT in solution is low. Once the nuclei have formed and begin to grow, the ThT binds and the emission intensity in solution increases.

Eventually, the monomer is fully incorporated in the fibril structure and the increase in ThT signal plateaus.

The MAP2 blockage effect was so potent for a seeded reaction, it was hypothesized the MAP2 MTBRs may slow or inhibit nucleation dependent kinetics experiments also. It was shown that in the absence of MAP2 K18 aggregated fully within 5 hours (Figure 6.4). By the addition of 3.2 µM MAP2 MTBRs, a large increase in the time for K18 (25 µM) to aggregate in these reactions was observed (Fig 6.4). The K18 protein in the absence of MAP2, aggregates fully, and has a T_{50} of 2.5 hours. By inclusion of MAP2 protein, the nucleation of Tau slowed to have a T_{50} of 5.5 hours (Fig 6.4). This represents a doubling of the time required to nucleate. The overall signal intensity was also reduced indicating that it is not only slowed by this but the total amount of ThT positive Tau aggregates were reduced by as much as 20% (Fig 6.4). The reduction in ThT positive aggregates again suggests that MAP2 is not being incorporated into the fibril but is inhibiting the Tau protein from fully aggregating.

The fact that the overall reduction in Tau aggregation is less potent than for a seeded experiment can be explained. In a nucleation experiment, K18 monomers in the 96 well plate are shaken in order to induce aggregation. This shaking could break already formed fibrils, thereby negating the effect of MAP2 blockage by exposing new ends to which K18 can grow. If MAP2 were templating onto the fibril, one would expect the signal for a + MAP2 experiment to be higher than for that of the K18 only samples.

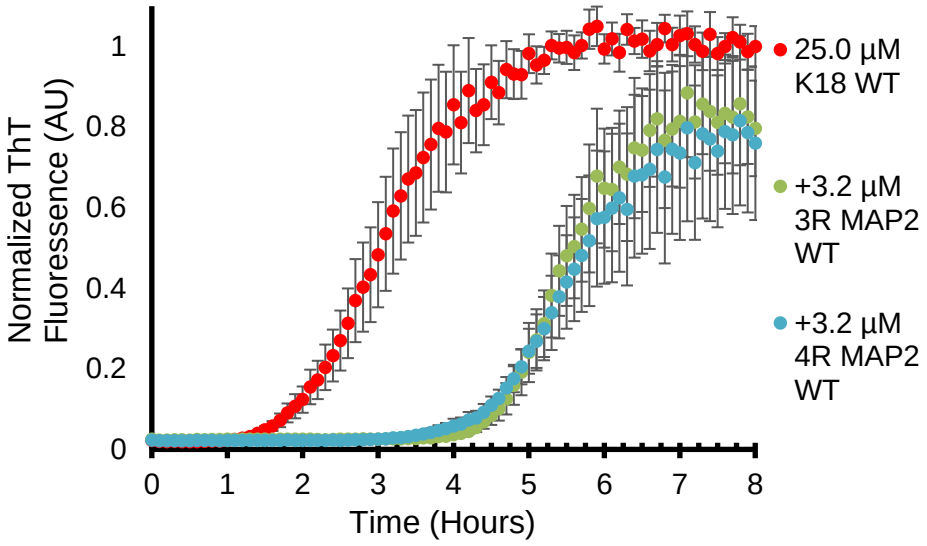

Figure 6.4 MAP2 3R and 4R can slow nucleation of K18 in-vitro. Tau protein and heparin cofactor incubated under shaking conditions nucleates with a T_{50} of 3 hours (red). MAP2 3R and 4R both slow the aggregation rate of Tau to T_{50} of 5.5 hours (green and blue respectively).

6.4 K19 does not block K18 aggregation

K19 also has high sequence similarity to K18. It has been shown that K19 is incapable of growing on K18 (Chapter 4, Figure 4.9). However, it had not been examined whether K19 could interfere with K18 aggregation. In the previous blockage experiments, MAP2 monomers were added at 5.0 µM final concentration. This concentration achieved the maximum decrease in K18 aggregation. It was shown that in a seeded reaction in the absence of K19, K18 fully aggregated (Fig 6.5). To a separate K18 seeded reaction, 5.0 µM K19 was added. It was shown that K19 was not capable of blocking K18 aggregation (Fig 6.5). This result is important because it demonstrates that the inhibition of Tau is

caused by MAP2 sequence dissimilarity not the fact that its highly homologous. If homology were the only factor to consider, the K19 should have caused an obvious decrease in K18 aggregation since K19 shares 75% sequence identity with K18. Instead, this result suggests that the ability for MAP2 to block Tau aggregation is likely caused by the sequence dissimilarity between Tau and MAP2.

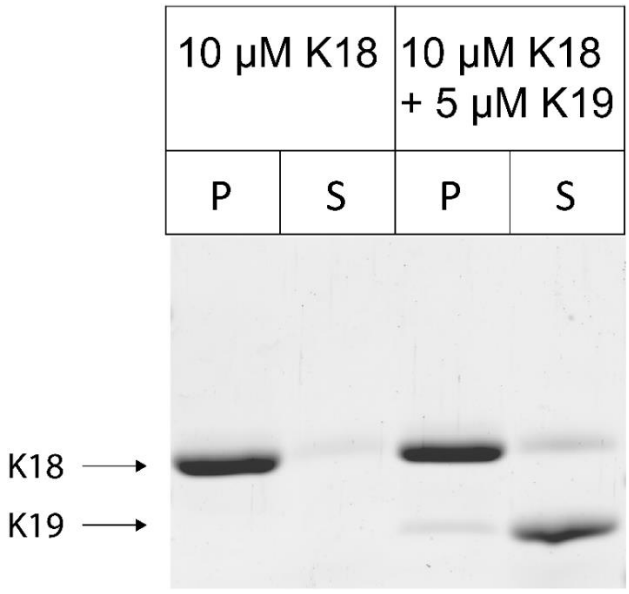

Figure 6.5 K19 does not block K18 aggregation. SDS PAGE of K18 reactions demonstrate that K18 fully aggregates and K19 does not inhibit K18 aggregation appreciably. Upon ultracentrifugation, K18 is in the pellet (P) in both cases. K19 remains soluble and does not grow on K18. P = pellet, S = supernatant

6.5 Heparin sequestration does not account for blockage

It was noticed that when MAP2 and heparin were combined, rapid aggregation of the MAP2 would occur, resulting in a cloudy solution. This occurred even in the absence of seeds. It was observed that if these solutions

are pelleted in the ultracentrifuge and the resultant pellets are analyzed by SDS PAGE, the white precipitate is MAP2. The MAP2 protein would consistently also become insoluble in the sedimentation experiments shown previously, but it was not appreciably increasing the ThT signal in either the seeded or nucleation experiments. These results together suggest that unlike Tau, MAP2 is forming aggregates in the presence of heparin which are not amyloidogenic. To examine the morphology of these aggregates K18, 3R MAP2, or 4R MAP2 were incubated with heparin and K18 seeds for 6 hours at 37 °C (identical to the seeded experiments shown in Chapter 6.2). MAP2 proteins produced white pellets, which resembled those of K18 monomer with seed. When these samples were prepared for TEM analysis, the morphology of the aggregates became evident. K18 produced long fibrils as expected (Fig 6.6 A). MAP2 containing samples were demonstrated to contain large amorphous aggregates rather than fibrils (Fig 6.6 B and C). This result suggested that although MAP2 is capable of interacting with heparin – it seems to preferentially form amorphous aggregates instead of fibrils.

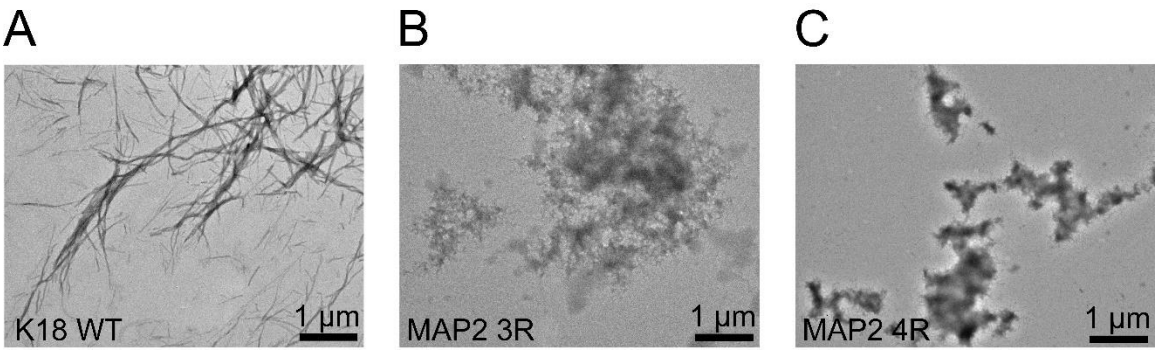

Figure 6.6 TEM of K18 and MAP2 aggregates. A Representative negatively stained electron micrograph of K18 WT fibrils formed after incubation overnight with heparin, cofactor, and seeds. B and C Representative micrograph of amorphous aggregates formed from 3R and 4R MAP2 monomers incubated overnight with heparin cofactor and seeds, respectively.

Since it was observed that MAP2 could block Tau aggregation but also simultaneously aggregated with itself in the presence of heparin, the following question arose. Would it be possible to rescue the Tau fibrilization by additional heparin in the seeded experiments? To test this, experiments with identical conditions to the previous blockage experiments were performed. In addition, reactions in which the heparin concentration was doubled and quadrupled were performed in parallel. The previous experiments in which seeded Tau aggregation was blocked by MAP2 contain 20 µM heparin. This is a four-fold higher concentration than the MAP2 present (5 µM). In the next experiment, the heparin was doubled (40 µM, 8 x higher than MAP) and quadruped (80 µM, 16 x higher than MAP2) in order to determine if more aggregation of Tau would be observed. No increase in the aggregation of Tau upon addition of more heparin was observed for either 3R (Fig 6.7 A and C) or 4R MAP2 (Fig 6.7 B and D).

Heparin titration experiments were performed using three independent batches of K18 seeds (biological triplicates), and the resultant fibrils were ultracentrifuged as before. Pellets were dissolved in 1 x Laemmli sample buffer equal to that of the supernatant. The pellets and supernatants were analyzed on SDS PAGE and the protein bands in the gels were quantified using ImageJ. Band intensity found using gel densitometry was plotted in GraphPad. A one-way ANOVA test was performed to find p-values. The blockage in seeded experiments with 20, 40, or 80 µM heparin by 5 µM of both MAP2 isoforms is very similar (Fig 6.7) to that of the blockage observed in the regular heparin (20 µM) regime (Fig 6.3). This result suggests that sequestration of heparin by spontaneous MAP2 aggregation is not likely responsible for the blockage effect observed for K18 seeded reactions.

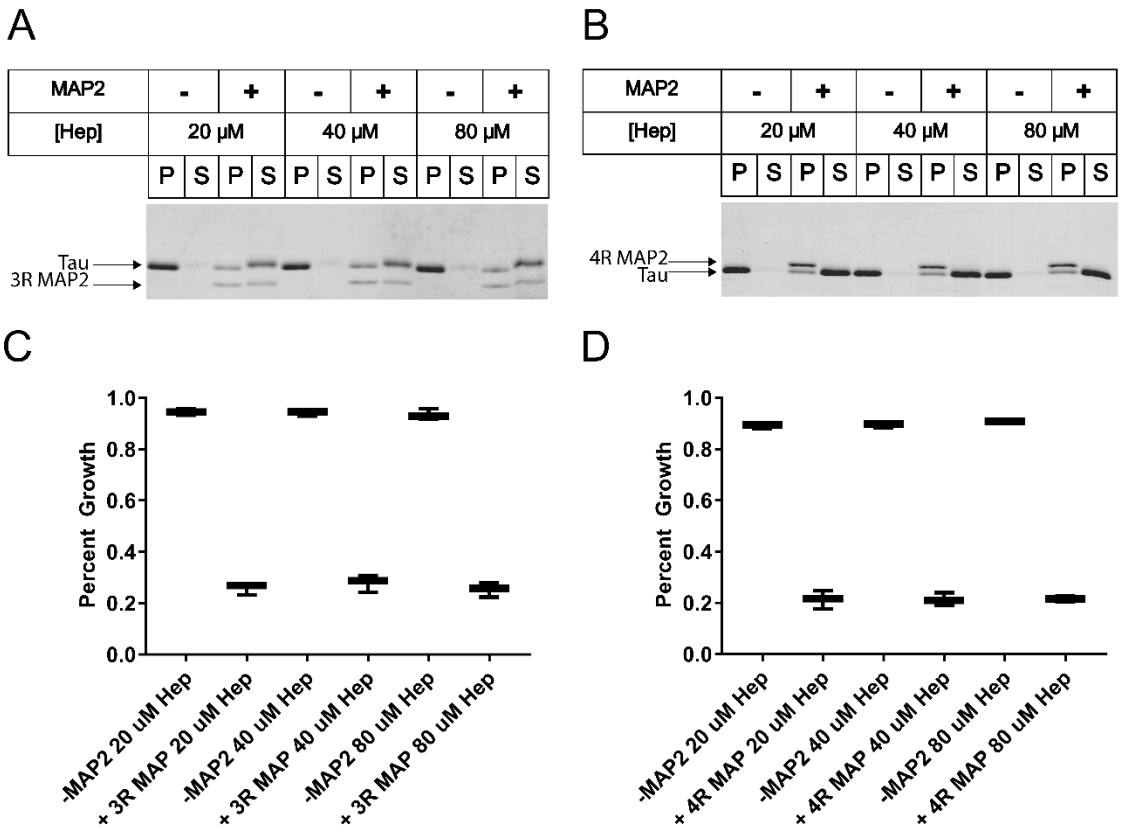

Figure 6.7 Heparin titration does not rescue Tau aggregation. A and B Representative gels of 3R and 4R MAP2 heparin titration experiments, respectively. C and D One-way ANOVA analysis of ImageJ densitometry of heparin titration gels. Experiments were performed in triplicate (biological replicate). From one-way ANOVA, $P < 0.0001$ for each + MAP2 reaction compared to corresponding – MAP2 reaction. P = pellet, S = supernatant

6.6 K18 inhibition by MAP2 is not caused by large aggregates of MAP2

Through these experiments it became evident that MAP2 was not blocking the aggregation of Tau protein by way of binding the cofactor. It was not clear, however, if the aggregates of MAP2 themselves were somehow responsible for the blockage effect observed. So next, MAP2 was incubated in either the presence or absence of heparin for 16 hours at 37 °C. This material was

subsequently used in a K18 blockage experiment as before. K18 monomer and heparin was seeded. Blockage experiments including the MAP2 incubated with or without heparin were performed in parallel. Insoluble protein was sedimented and pellets were compared to supernatants using SDS PAGE. It was shown that if MAP2 is aggregated (Fig 6.8 the lanes labeled Agg) prior to being used as a blocking agent, the blockage effect is abolished nearly completely for both isoforms 3R and 4R, respectively (Figure 6.8 A – B). However, if MAP2 (3R or 4R) was incubated without heparin in assembly buffer, then blockage was observed. This result would suggest the large amorphous aggregates observed under TEM are not responsible for the blockage of K18 seeded reactions.

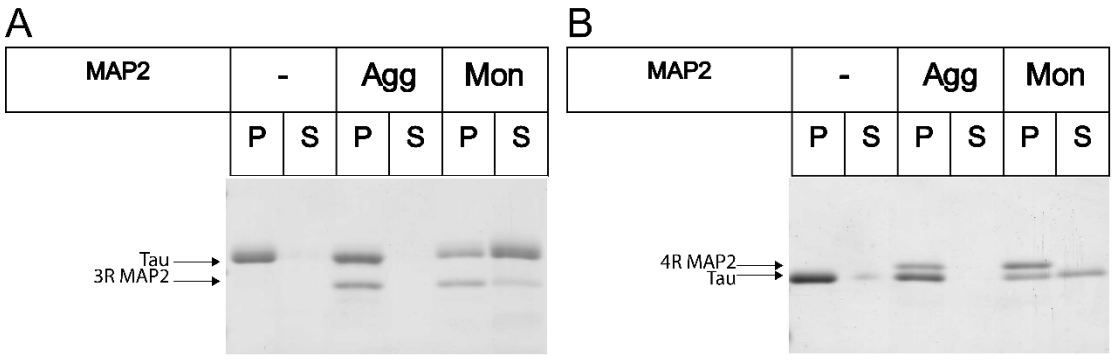

Figure 6.8 Aggregated vs monomeric MAP2 blocking Tau aggregation. K18 WT and heparin with 10% seeds incubated for 6 hours grows fully (- = K18 seeded in the absence of MAP2). Inclusion of 3R (A) or 4R (B) MAP2 incubated with heparin overnight does not result in blockage when subsequently added to a K18 seeded reaction (Agg = aggregated). However, if MAP2 was instead incubated in the absence of heparin overnight, blockage of Tau aggregation is observed for both 3R and 4R MAP2 (Mon = monomeric). P = pellet, S = Supernatant

These results taken together suggest that MAP2 can form aggregates under quiescent conditions, but these aggregates are not amyloids. Additionally, the blockage effect is quite potent when monomeric MAP2 is used but completely abolished with aggregated MAP2. This would suggest that monomeric MAP2 or small aggregates are blocking the Tau from elongating. It was still unclear at this point whether the MAP2 was interacting directly with the fibril or causing any elongation of the fibrils.

6.7 MAP2 does not elongate Tau fibrils

To understand if the MAP2 was interacting with the fibril, it first needed to be established whether or not the K18 fibrils were elongating in the presence of only MAP2 monomer.

The next set of experiments were devised using TEM in order to understand whether or not truncated MAP2 3R and 4R isoforms could be recruited and extend Tau fibrils *in-vitro*. If the MAP2 monomers are extending the fibril length, it should be observable under TEM. K18 seeds were incubated at the same concentration, in the absence of additional monomers. This was important to set a baseline size for the seeds and would also ensure fibril dissociation wasn't skewing the analysis. TEM samples of the seeds added to K18 monomer served as a positive control, to ensure the seeds are truly competent to induce aggregation. Samples of K18 seeds with MAP2 monomers added were then compared using TEM.

Samples of K18 seeds incubated with only buffer had an average size of 108 nm (Figure 6.9 A), and representative micrographs are depicted (Fig 6.9 B). K18 fibrils were shown to increase to an average length of 326 nm (Fig 6.9 C) when incubated with K18 monomer. Fibrils were clearly longer in these samples (Fig 6.9 D). When either 3R or 4R MAP2 monomer was added in the experiment, instead of Tau, K18 fibrils were not observed to increase in size. These fibril samples were observed to be 108 and 106 nm long in the presence of MAP2 3R and 4R respectively (Fig 6.9 E and G). The micrographs of samples containing MAP2 monomers looked indistinguishable from the buffer control samples (compare Fig 6.9 B with F and H). These results indicate that MAP2 is unable to significantly extend the fibrils. This is consistent with the observations that MAP2 is not considered a major component of Tau fibrils or NFTs in the brain[4] and that the ThT signal of K18 seeds did not increase in the presence of MAP2 monomers.

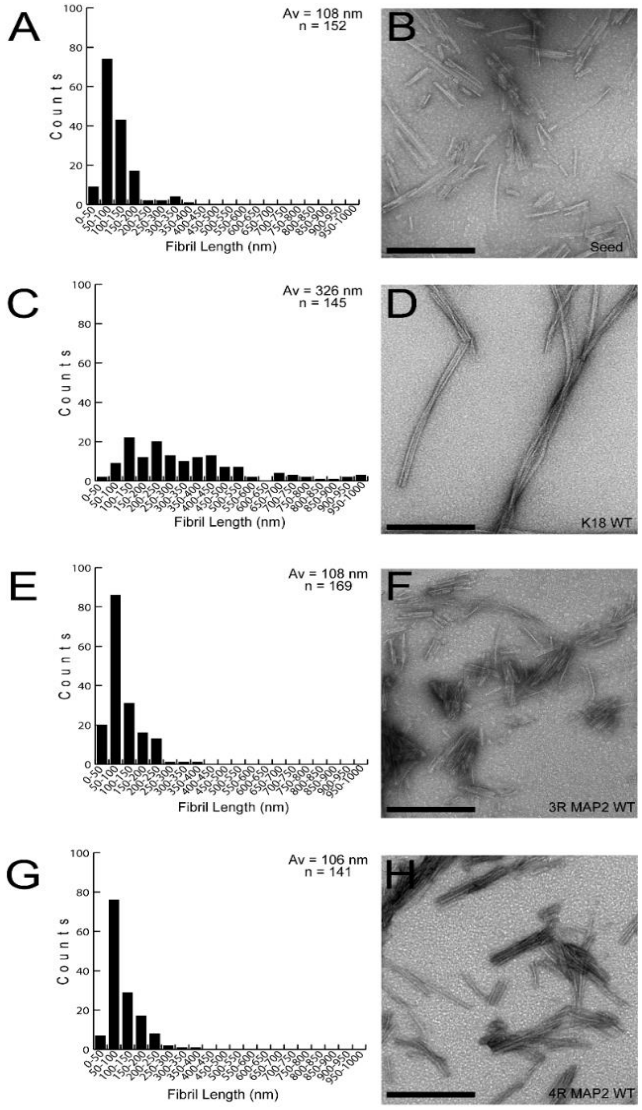

Figure 6.9 Fibril length analysis of MAP monomers with seeds. A Quantification of fibril length measurements for K18 seed only sample. B Representative micrograph of K18 seed used in this experiment. C Quantification of K18 fibril length after seeds were incubated with 10 µM monomer and 20 µM heparin for 6 hours at 37 °C. D Representative EM of K18 fibrils measured. E and G Quantification of K18 fibril length after seeds were incubated with 3R or 4R MAP2 respectively. F and H Representative EMs of seeds incubated with MAP2 3R or 4R for six hours respectively. Scale bar is 100 nm.

6.8 MAP2 binds to Tau fibrils

The previous results exclude large aggregates as being responsible for the MAP2s blocking effect observed. Additionally, the MTBRs of MAP2 isoforms were not observed to elongate Tau fibrils appreciably. Still, it needed to be established if MAP2 was physically binding to the Tau fibril. If Tau aggregation is being blocked by MAP2 interacting with the end of the fibril, it could be possible for the effect to be caused by only a single to a few layers of MAP2. This would not be sufficient increase in length to be observed using TEM. Binding of monomers to fibrils can be observed using fluorescence anisotropy. This is because as monomers bind to the relatively massive fibril, the tumbling of labeled protein in solution will slow. Decreased protein tumbling would reduce the rate of emission dipole depolarization and therefore increase anisotropy (according to equation in section 2.19). To test whether MAP2 was binding to the fibril, a single mutant for 4R MAP2 was generated by removal of the native cysteine found in the 2nd repeat (C409S). The natural cysteine in the 3rd repeat exists in both 3R and 4R MAPs. Both 3R and 4R isoforms of MAP2 and Tau were labeled with Atto 647N maleimide. Initially, anisotropic measurements vs time were taken to establish a rate of binding. When 100 nM of labeled MAP2 isoforms were mixed with 10 μM sonicated Tau fibrils, the labeled proteins were observed to have rapid binding kinetics and the reactions were complete well before the 15-minute collection time (data not shown).

Establishing a binding assay using fluorescence anisotropy would allow for examination of kinetics for MAP2 and K18 seeds. Fluorescence anisotropic increases were observed for K18, 3R MAP2, and 4R MAP2 (Fig 6.10 A – C). Experiments were performed using three independent batches of seeds (biological replicates) and averaged with SEM shown. K18 was used as a positive control and the K19 as a negative control. If the MAP2 is binding to the end of the fibril, an increase in fluorescence anisotropy for the MAP2 proteins and K18 should be observed. Since K19 is incapable of templating on K18, due to the asymmetric seeding barrier, the anisotropy for K19 should not change. The average maximum anisotropic value for experiments containing MAP2 were found to be 0.35 and 0.36 for 3R and 4R, respectively (Figure 6.10 A - B). These curves were plotted in GraphPad and apparent K_D were found to be 2.8 µM and 1.6 µM for 3R and 4R MAP2, respectively. The maximum change in anisotropy for labeled K18 incubated with seeds was observed to be an average of 0.26 with an apparent K_D of 3.9 µM (Figure 6.10 C). The apparent K_D for MAP2 being lower than for Tau could explain how the blocking effect may take place, in-vitro. The MAP2 can bind to the fibril more tightly than a Tau monomer would. This is indicative of strong binding to the fibril. The seeds used in these experiments were formed in the presence of heparin to induce aggregation. It is possible that some heparin in these reactions was not bound to the fibril. Unbound heparin could cause aggregation of MAP2, which could result in artifactually high anisotropy values. The seeds for these experiments were made with an 8 to 1

ratio of Tau to Heparin. This means that with 20 µM of K18 seeds added, and if all of the heparin in solution was not bound to the fibrils, 2.5 µM of free heparin would be have been added to the monomers in the anisotropy experiments. In order to test the degree to which this effected the change in anisotropy 2.5 µM of heparin was added to 3R and 4R MAP2 monomers. Very little to no change was observed for the anisotropy of the MAP2 proteins as compared to only buffer added (data not shown). These results demonstrate that the labeled MAP2 and K18 proteins are binding to the fibril and not to heparin or the cuvette. For K19, as expected, no change in anisotropy was observed for even the highest concentration of K18 seed (Fig 6.10 D).

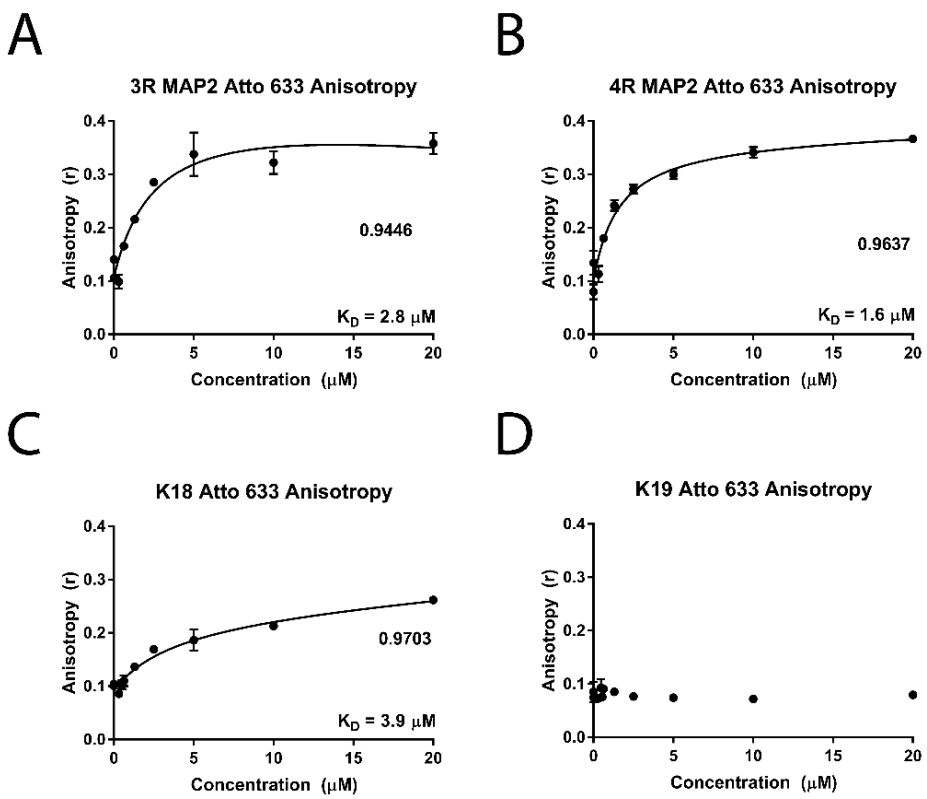

Figure 6.10 Fluorescence anisotropy changes induced in monomers by titration of seed. 100 nM 3R (A) or 4R (B) MAP2 were titrated with 0.310 - 20 μM K18 seeds. The seeds produce large changes in anisotropy for the monomers with K_D values at 2.8 μM and 1.6 μM, respectively. C K18 seeds induce anisotropic changes for K18 also with an apparent K_D of 3.9 μM. D K19 was used as a control since it does not template on K18, even at high seed concentrations. Experiments were performed using three independent batches of K18 seeds. Results are averaged, and SD reported. Curve fitting and K_D analysis was performed in GraphPad.

6.9 MAP2 captures Tau fibrils from solution

The fluorescence anisotropy experiment was indirect evidence of MAP2 binding to Tau fibrils. To support this further a bead-capture experiment was performed. In this experiment commercially-available magnetic beads conjugated to streptavidin (NEB) were purchased. Biotinylation of Tau and MAP2 monomers would allow for these biotinylated monomers to bind to the magnetic beads. By

placing the magnetic bead slurry in a magnetic field, the beads (which are attached to the monomers) can be pulled from solution and washed. If K18 seeds can bind to MAP2 monomers, then these magnetic beads with biotinylated monomers should be capable of capturing the fibril seeds from solution. If the monomers are binding to the fibril, then the beads should be capable of isolating fibrils attached to the biotinylated monomers by way of interaction with the streptavidin conjugated to the magnetic beads. The biotin-streptavidin bond can be disassociated by boiling the beads in 1 X SDS (Laemmli) sample buffer. Utilizing a PEG11-Biotin maleimide labeling reagent (Thermo Fisher), the monomers (K18, K19, 3R MAP2, and 4R MAP2) were labeled utilizing a single cysteine at the N-terminus of each protein. PEGylation is a useful characteristic of this label and is used in order to provide enough of a spacer such that the biotin molecule attached to the proteins can still interact as a ligand to streptavidin.

K18, 3R MAP2, 4R MAP2, and K19, conjugated to biotin, bind to streptavidin coated magnetic beads (faint bands above arrow for K18 and 4R, or below the arrow for 3R and K19, Fig 6.11). K18, 3R MAP2, and 4R MAP2 are capable of binding to K18 seeds (Fig 6.11, the large band indicated with an arrow). K19 and hydrolyzed biotin label were each incapable of binding to K18 (Fig 6.11). This result is important because it shows that the K18 and both 3R and 4R MAP2 tightly bind to seeds and are released upon boiling of beads in 1X Laemmli sample buffer. This experiment reconfirms the result that K19 does not

interact with K18 fibrils, which is the basis for the asymmetric seeding barrier. Also beads and hydrolyzed biotin label alone are insufficient to pull Tau seeds from solution.

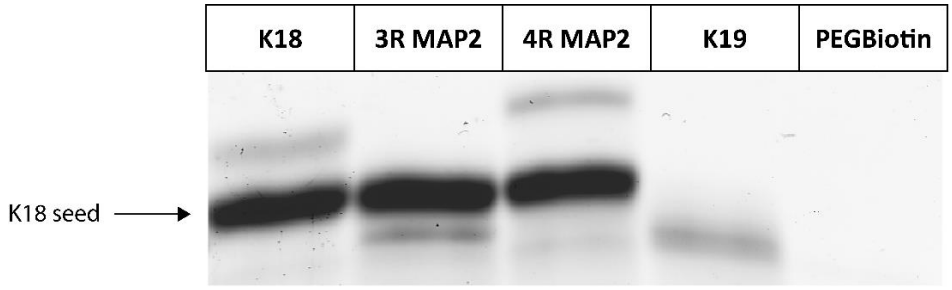

Figure 6.11 Streptavidin conjugated magnetic beads pull seeds out of solution by way of biotinylated monomers. Biotinylation at the N-terminus of K18, 3R MAP2, 4R MAP2 resulted in an ability to bind to beads and K18 seeds. The bound seeds are eluted with biotinylated monomers during boiling in 1 X Laemmli sample buffer. Biotinylated K19 and hydrolyzed PEGBiotin reagent did not however demonstrate the ability to bind to seeds. Notice faint bands for streptavidin can be seen for all lanes (most prominent in 4R sample) at bottom of gel. This is a result of unfolding the tetrameric streptavidin complex. Some streptavidin is liberated during boiling in 1 X Laemmli buffer because only 1-2 streptavidin molecules per tetramer is covalently conjugated to the bead.

6.10 MAP2 binds to the end of Tau fibrils

One way to demonstrate that proteins are within close proximity, is to utilize Forster resonance energy transfer (FRET) experiments. In order to perform FRET, a donor and acceptor fluorophore are required. FRET requires two fluorophores to have sufficient spectral overlap between the emission spectrum of the donor and excitation spectrum of the acceptor. If sufficient overlap exists, a non-radiative energy transfer can occur in which the energy of an excited electron in the donor fluorophore (high energy) is transferred to and excites an electron in the acceptor fluorophore (lower energy). Additionally,

because this phenomenon is non-radiative, it only occurs when fluorophores are in close proximity to one another (here 60 Å for Alexa488/Alexa 594). This phenomenon can be measured by exciting the donor fluorophore and monitoring emission for the acceptor. Due to the energy transfer phenomenon, the intensity of the donor species is reduced while the acceptor species intensity increases.

If it is the case that MAP2 is binding specifically and tightly to the end of the fibril, it is expected that this phenomenon could be observed by FRET. In these experiments K18 Alexa 488 (donor) monomer was incorporated onto the fibril end. The samples were excited at 450 nm and emission was measured from 500 – 675 nm. To these reactions, Alexa 594 (acceptor) labeled proteins (K18, 3R MAP2, and 4R MAP2) were added to the previous reactions. The resultant emission spectra were measured again. It was shown that upon addition of K18, 3R MAP2, or 4R MAP2, that donor intensity decreased (peak at 520 in Figure 6.12 A - C) and acceptor intensity increased (peak at 611 nm in Figure 6.2 A – C). Three independent batches of seeds were used, ensuring consistency and rigor. The emission spectra were normalized for the intensity at 520 (donor peak), averaged, and plotted with SEM (Fig 6.12 A-C). When K18 Alexa 594 was added as an acceptor species, FRET was observed with the characteristic drop in donor intensity (at 520 nm, black arrow) and increase in acceptor intensity (at 611 nm, red arrow). The reduction of the donor peak (520 nm) relative to the increase in acceptor peak (611 nm) is evidence that energy transfer is occurring between the labels and demonstrates the labels are in close proximity. Since we

know that K18 grows efficiently on the end of the fibril, it can be extrapolated that the MAP2 protein is also interacting with the end of the fibril due to the increase in acceptor emission observed. If MAP2 were binding randomly along the long axis of the fibril, it would be expected that the FRET signal would be weaker than that of K18. Since intensities for the acceptor peak are similar, it is likely that MAP2 is also binding to the end of the fibril.

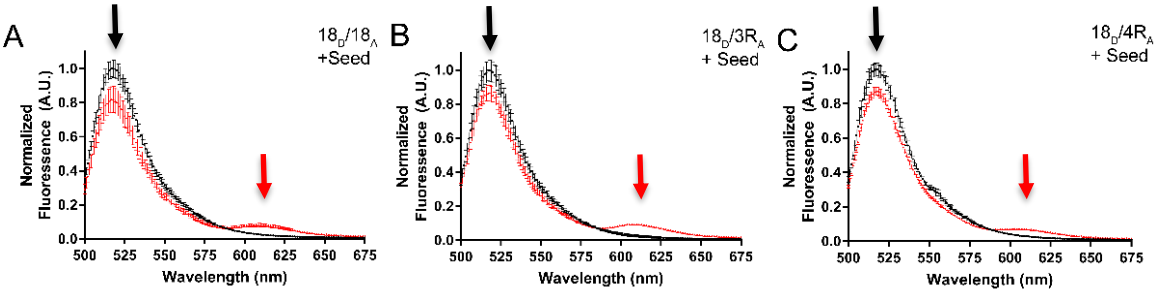

Figure 6.12 FRET of Alexa labeled monomers. 1 µM labeled K18 was mixed with 10 µM K18 seeds and incubated 1 hour at 37 °C. Emission spectra were taken and 1 µM of the indicated acceptors were added (K18, 3R MAP2, or 4R MAP2). A FRET experiment of Alexa 488 and Alexa 594 labeled K18 grown on K18 results in energy transfer due to close proximity of labeled monomers on the end of the fibril. B and C FRET signals for Alexa labeled MAP2 3R and 4R respectively. Energy transfer occurs to a similar degree with MAP2 proteins, indicating that they are likely binding to the end of the fibril in a similar manner to that of K18.

To ensure this FRET signal was not a result of excess heparin in solution (from the seeds, and a similar argument as in the anisotropy experiments) resulting in monomer aggregation, the monomers were incubated together with 2.5 µM heparin. This amount is equal to the amount of heparin that the seeds added would have contributed. If all of the heparin was unbound and free in

solution. It was shown that by addition of 2.5 µM heparin, no increase in FRET signal was observed for K18 (Fig 6.13 A). Likewise, 3R and 4R MAP2 were not observed to have an increase in FRET signal when only heparin was added (Fig 6.13 B and C). This result is important because it suggests strongly the binding observed is specific to the fibril and not an artifact of labeling or unbound heparin.

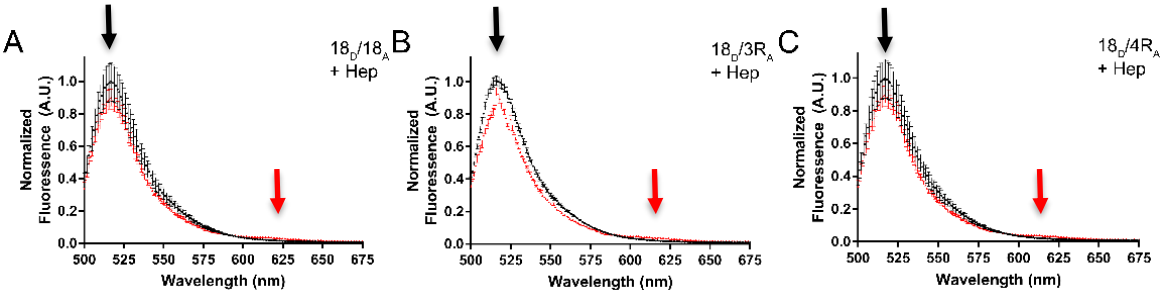

Figure 6.13 No FRET signal is observed when only heparin is added. 1 µM labeled K18 was mixed with [heparin] carried over from seeds in previous experiment (Fig 6.12) and incubated 1 hour at 37 °C. Emission spectra were taken and 1 µM of the indicated acceptors were added (K18, 3R MAP2, or 4R MAP2). Without the addition of seed, no FRET is observed for any of the 3 reactions (A K18, B 3R MAP2, or C 4R MAP2) despite equimolar heparin concentrations as in seeded experiment above.

If these monomers are indeed interacting with the end of the fibril, it should be possible to again use the biotinylated monomers in a different type of experiment than before. Commercially available products that contain streptavidin conjugated to gold nanoparticle exist. It is also possible to observe these gold nanoparticles under transmission electron microscopy. This type of experiment would allow for direct observation of the MAP2 at the end of the Tau fibril, by way of observing a black dot of a known size (here 6 nm Au) at the location in which the monomer has bound. It was necessary to use the constructs

generated for the bead-capture experiments, namely the proteins with a single cysteine residue at the N-terminus. This would ensure the PEG11-biotin conjugation would be pointing towards the solution, where it would be able to interact with the streptavidin conjugated nanogold. Tau fibrils were allowed to incubate with biotinylated 3R and 4R MAP2 and then were mixed with equivolume of diluted streptavidin conjugated gold nanoparticles (Aurion). It was observed that a 1:20 dilution of nanoparticles with assembly buffer produced the best results. After incubation with the gold nanoparticles for 1 hour, samples were prepared for TEM analysis. It was shown that MAP2 proteins were binding to the end of Tau fibrils (Fig 6.14 A - B). Since these MAP2 monomers were conjugated with biotin, and this biotin was accessible to the streptavidin on the gold nanoparticles, it was observed that a single or few nanoparticles were found on the end of the Tau fibrils. This result demonstrates visually that MAP2 3R and 4R isoforms are binding to the end of the Tau fibril.

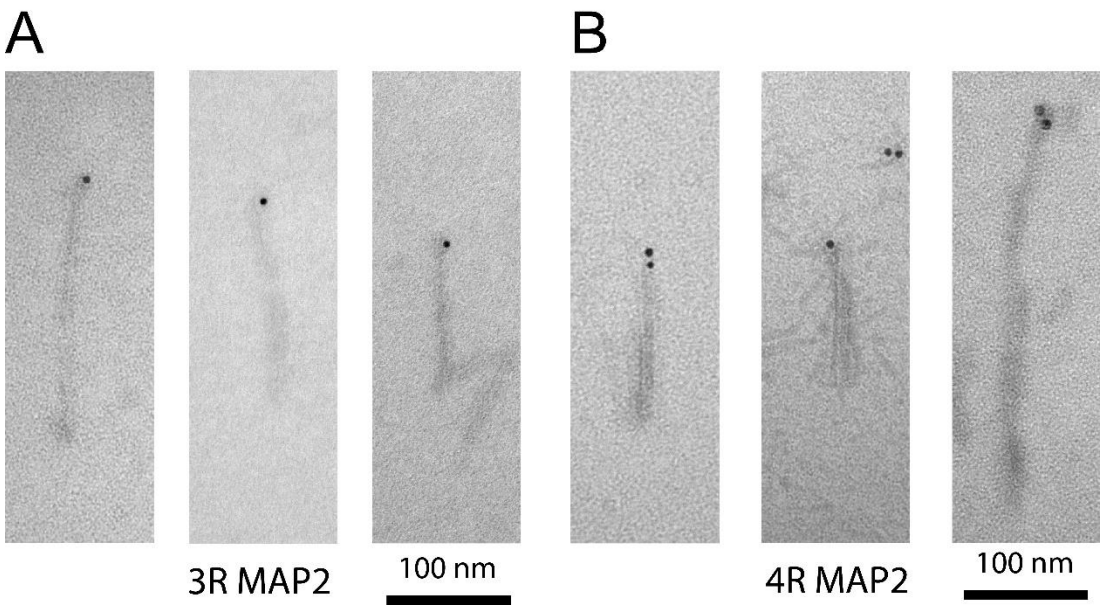

Figure 6.14 Streptavidin gold binds to end of fibrils incubated with biotinylated MAP2 monomers. A 3R and B 4R MAP2 conjugated to biotin binds to the end of K18 fibrils, indicated by the presence of the gold nanoparticle at the fibril's end. Streptavidin binding to biotinylated monomers causes the nanoparticle to show up only where MAP2 is present.

Now with direct evidence for MAP2 binding to the end of Tau fibrils, it became clear how the mechanism of action for blockage is likely occurring. In the absence of MAP2, Tau proteins elongate into long fibrils unhindered. If MAP2 monomers are included in the reaction, it is possible for the MAP2 monomers to bind to the end of the Tau fibrils, but not allow for the next Tau monomer to bind. Taken together, the results of anisotropic KD determination, magnetic bead experiment, FRET, and gold nanoparticle data demonstrate in a logically consistent fashion that the MAP2 protein binds to the end of Tau fibrils in a specific and tight manner. Additionally, these results demonstrate that the number of MAP2 layers that form on the end of the fibril is as few as a single

layer. It also seems likely that the MAP2 protein, which is not interacting with the end of the fibril, but that is sedimented in the earlier experiments, is likely due to amorphous aggregates forming with excess heparin. The heparin titration experiments show that the blockage effect is not caused by reduced heparin concentration, however. It is still unknown whether or not the MAP2 protein is interacting in an identical fashion as Tau, but it is suggested by the FRET experiments that the MAP2 is probably binding parallel and in-register or the FRET labels would likely be too far apart to have similar signal intensities to Tau labeled with Alexa 594.

Chapter 7 Discussion

7.1 Full length monomeric Tau resides in multiple conformational states

Measurements of the structure of Tau in solution demonstrated various intramolecular interactions. Particularly, FRET experiments on monomeric Tau resulted in distance distributions shorter than would be expected for a true random coil [19], [129]. One study utilized introduction of Tryptophan residues and cysteines (labeled with a fluorophore, IAEDANS) to measure FRET efficiencies and calculate the distances between the pair of fluorophores. This study demonstrates that the monomer alone in solution can adopt a global hairpin-type structure [20]. Another study utilized FRET to demonstrate that upon addition of heparin, the MTBR of Tau compacts, and the N and C termini are forced outwards[129]. This could demonstrate the initial step towards oligomerization of positively-charged monomers on the polyanionic heparin scaffold. Due to limitations with the instrumentation used, molecules must be observed in bulk solution or only briefly at the single molecule level (on the order of milliseconds [168]).

One way to avoid these pitfalls is to utilize an instrument called the anti-Brownian electrokinetic trap (ABEL trap) [123], [169]. This instrument is capable of tracking the molecular trajectory and utilizing electromotive force to direct

analytes of interest. Keeping analytes in the measurement cell enables prolonged (on the order of seconds) measurements of individual proteins [123]–[124], [165]. Prolonging measurement time provides better signal-to-noise and allows for new conformational information to be elucidated.

ABEL trap instruments have been utilized to study other proteins previously [123], [125] but the first use of this type of instrument on an intrinsically disordered protein has been shown here and confirmed that fundamental solution-phase behavior of monomeric Tau can be examined [127]. This proof of concept will enable development of more advanced studies that could incorporate cofactors and/or seeds to investigate the mechanism of monomer to fibril conversion.

It was shown in collaboration with the Goldsmith group at University Wisconsin, Madison, that full length human Tau (the longest isoform) is present in a bimodal distribution of fluorescence anisotropies. However, when either a folded globular protein (microbial transglutaminase or MTG), denatured MTG, or free dye were measured, the samples only consist of a distribution of anisotropy best fit by one Gaussian function. This implies that these latter cases only have one global structure. Upon denaturation, Tau no longer exhibited this bimodal distribution. This is indicative of structural perturbation by the denaturant. To ensure this was due to disruption of intramolecular interactions in the monomeric state of Tau, several additional experiments were performed. First, hydrolyzed dye and unlabeled Tau (mutated to have no cysteines) were mixed, and bulk

anisotropy measurements were taken. Then the same experiment was performed using the ABEL trap. The results suggest it is likely the dye is not interacting with the protein in a non-specific manner ([127] See page 12 in the supplement). Additionally, when a less hydrophobic dye was used (Atto 633), the anisotropic distributions were very similar ([127] supplement, Fig S5). This also substantiates the claim that the dye is not interacting with the protein and causing artifactual anisotropic distributions. Utilizing molecular dynamics simulations, dyes conjugated to proteins have been shown to track the proximal residues [171]. If these results were purely a consequence of unfolded proteins in solution, then the denatured MTG would likely exhibit a bimodal anisotropic distribution, which it does not. This feature must be attributed to Tau itself, and not a consequence of being an unfolded protein. These findings are in agreement with other studies which show Tau has transient intramolecular interactions which result in a structure that is more compact than expected for a random-coil [20].

Transient structure in other IDPs has been shown. For example, Huntingtin protein is an amyloidogenic protein containing polyglutamine expansions in the primary sequence and is considered to have intrinsically disordered regions [167]–[168] and a collapsed solution-phase structure has also been demonstrated for polyglutamine chains [174]. Aβ fragments are also highly flexible in solution. NMR of soluble Aβ has shown that conformational sampling occurs and structural disorder is prevalent [175]. These transient structures are important because they preclude true amyloid formation but might be associated

with oligomeric states and early polymerization. It is thought that hydrophobic regions can become exposed during this conformational sampling. These hydrophobic patches may serve as aggregation hotspots.

This work is being followed up with additional measurements on hT40 mutants labeled with Atto 647N. Also, time-resolved anisotropy measurements of the hT40 310 labeled with Atto 647N have been recorded. The future work utilizing this instrument could be useful in developing a better understanding of how initial aggregation occurs, and what factors may drive the oligomerization of Tau.

7.2 Amyloid fibril selection and evolution

The ability to form distinct fibril conformers from proteins with identical sequence, and to perpetuate these conformers by template-assisted conversion, is a unique property of amyloids [69], [131]–[133], [176], [177]. Structural polymorphism requires that the recruited proteins exhibit a high degree of plasticity as they are molded into different conformational states, Tau proteins possess such plasticity. It has been shown that K18 fibrils, when subjected to 5 cycles of seeding and growth, formed a heterogeneous mixture of conformers [63]. Upon further examination, it was demonstrated that the K18 fibrils formed from stirred material were relatively homogenous [64]. After consecutive cycles of seeding and growth, the once dominant polymorph had become a sub-population. To understand the context of this phenomena, it is helpful to consider that structural evolution has been observed for other amyloids.

Strain switching and conformational polymorphism are well documented phenomena within the context of amyloids [144], [158], [178]. It was shown that for prion protein, fibrils formed under different agitation conditions were structurally unique [179]. These fibrils were shown to have differing properties with respect to cross-β-core structure and morphology. Importantly, these unique structural features arose when independent reactions from identical batches of protein were agitated differently. Polymorphism was a result of monomers adopting unique structures upon differing agitation modes, and not from preformed nuclei within the stock monomer samples. Here we present sample homogeneity formed during agitation and then subsequent selection of minor subpopulations due to differences in their growth rate, which resulted in heterogeneity in the later cycle samples.

Another example of structural polymorphism leading to strain switching induced by differences in agitation has been shown for Aβ [70]. This study demonstrated that if amyloidogenic proteins were incubated either quiescently or agitated, that unique structures would arise. Aβ fibrils formed under agitation were also shown to interconvert to the quiescently formed fibril structure, if these fibrils were mixed together. The structural conversion took place over the course of 35 days [70]. This process was demonstrated to be due to in part to dissociation of monomers from the less thermodynamically stable fibril. This allowed for elongation and growth of the more stable Aβ polymorph. It was also demonstrated, in this work, that a change in agitation allowed for a new

dominant structure of Tau fibril to evolve [64]. Since each reaction was sonicated and added to new monomers, the fastest growing Tau fibril would become dominant over time, rather than the more stable structure. Tau fibrils did not appreciably dissociate to allow a similar mechanism of action, as measured for Aβ, however. This could be due to cofactor interactions, causing increased thermodynamic stability.

Surface catalyzed secondary-nucleation mechanisms have also been suggested to cause strain switching within a single fibril [150]–[151], [187]. Secondary nucleation is a phenomenon in which a new amyloid nucleus forms on the surface of the fibril, along the long axis. This mechanism would seem to imply branching of fibrils, though this has not been observed. It has been suggested that these small fibrils detach from the surface easily and begin elongation independent of the nucleation site. If fibrils are capped, fragmentation-based pathways may allow for Tau to break, and then elongate despite having been previously capped. Fibrils have been observed to break into pieces as small as trimers and still be seeding competent [95]. However, short fibrils (>10mer) appear to be most seeding competent [96].

It was demonstrated that Tau fibrils are found in the brains of people with chronic traumatic injury [11], [180], [181]. This disease is thought to be caused by repeated concussion or head trauma [8], [9], [182]. This highlights the need to further investigate the breakage properties of amyloids. Fragile fibrils may spread more rapidly, as small fibrils have been shown to be selectively

endocytosed [93], [96]. Further work needs to be done in order to better understand how mechanisms of breakage can contribute to structural polymorphism of amyloids found in disease. Selection processes can interconvert the dominant Tau fibril species in solution. Changes in structure were monitored by various techniques including: TEM, proteolytic sensitivity, and light scattering. A study on α-synuclein showed that structural evolution, with respect to these same biophysical properties, also occurred [183]. Additionally, it was shown that there were different degrees of toxicity from different α-synuclein fibril species when applied to SH-SY5Y cell culture. Using cell culture and mouse models, Tau inclusions formed exogenously can result in unique, faithfully-propagating, strains of Tau fibrils. These phenotypes could be induced in aggregate free cells by addition of fibril-containing cellular lysate [177], [184].

Differences in disease phenotypes may be linked to fibril conformation or the ability of the fibril to faithfully propagate during cell-to-cell transmission. Therefore, it is important to examine the conformational heterogeneity of amyloid fibrils to more fully understand the processes which lead to different disease phenotypes.

7.3 Tau fibril stability

Amyloid fibrils made of Tau are very stably folded [185]. Proteins in the amyloid fold typically form zipper-like structures [186]–[188], which results in high stability. Bovine spongiform encephalopathy (BSE) prion amyloids are capable of surviving the meat rendering process, and even incineration of medical and

agriculture byproducts[189]. Inactivation of prions and amyloids can be achieved under harsh conditions of strong alkalinity and high temperatures [190]. This stability could contribute to why the Tau fibrils were not dissociated upon limited dilution. The dissociation of fibril and cofactor interactions may take place under more extreme dilution conditions than examined here (>40x). The limit of detection for these proteins on Coomassie stained SDS PAGE meant it was not possible to examine greater dilutions. Silver staining or immunostaining could be used to achieve greater sensitivity, but with greater background. ABEL traps can overcome this limitation due to higher signal-to-noise. An ABEL trap may be used in the future to examine fibril dissociation leading to greater understanding of molecular behavior of Tau fibrils.

Neither K18 nor K19 fibrils were observed to release associated cofactors under high salt conditions (500 mM). Similarly, the fibrils themselves did not dissociate appreciably under high salt conditions. It is likely that some of the cofactor may be very tightly associated with Tau along the long fibril axis. The cofactor has been proposed to stabilize the parallel and in-register arrangement of the many positive charges found in Tau [177]–[178]. The fact that cofactors can be partially exchanged [57] demonstrated that at least some of the cofactors associated to the fibril are non-permanent. However, since neither increased salt concentration nor dilution released bound cofactors appreciably, it is likely a compensatory structure must replace bound cofactors [57]. The cofactor exchange process could be responsible for cell internalization processes [161].

Fibrils initially formed with heparin were shown to bind to sulfonated polysaccharides on the surface of cells in culture, and this process mediated micropinocytosis of the fibrils [161]. Additionally, it has been shown that polyanionic molecules (cofactors) are associated with NFTs [179]–[180]. This suggests that cofactor mediated stabilization likely occurs in-vivo. The exact role for polyanionic cofactors in disease is unclear, however, hyperphosphorylated Tau found in disease has been shown to aggregate without a cofactor [195]. Although high-resolution structural data has become available for the AD fibril [71], it is not clear whether fibrils formed *in-vitro* have the same structure. The cryo-EM structure of Tau fibrils showed electron density in the interior of the fibril but was not of high enough resolution to precisely understand what this electron density is due to [71]. It is possible that this density is due to the presence of a polyanionic cofactor. Heterogeneity within the structure of the cofactor would obscure the molecular resolution for these structures. Further work needs to be done to characterize the extent of cofactor mediated stabilization in disease fibrils, and the position(s) of these cofactors within the fibril structure.

7.4 MAP2 aggregation

It has been demonstrated in the literature that NFTs are comprised primarily of phosphorylated Tau. Antibodies raised against epitopes of MAP2 not present in Tau, generally have little reactivity against these NFTs [196]. Claims of epitopes from MAP2 in NFTs have been made, but cross-reactivity of antibodies with Tau could not be fully eliminated [195]–[196]. Evidence for MAP2 amyloid

formation in the literature is scarce, but has been demonstrated in two contradictory studies [197]–[198]. The first study utilized a truncated MAP2 C construct to generate PHF-like structures. A relatively high concentration of recombinant 3R MAP2 MTBRs was incubated in a sitting drop crystallization setup and allowed to aggregate for 1 - 4 weeks. The PHF-like structures formed bound the amyloid specific dyes, ThT and ThS, and were examined using TEM. The second study demonstrated the ability for MAP2 C to form SF-like structures under similar concentrations and sitting-drop crystallography conditions. The ability for MAP2 C to form PHF in this study was predicated on mutating a region of MAP2 C to the sequence of Tau. By changing this sequence in MAP2 C to the sequence found in Tau (4 amino acid substitutions), the ability of MAP2 C to form SF was diminished greatly, while the ability to form PHFs was enhanced. Another study demonstrated that if two amino acids are changed from the sequence of MAP2 to Tau, and vice versa, the aggregation of these proteins can be modulated [200]. In the case of the mutant Tau, amyloid formation was decreased and an increased likelihood of granule or amorphous aggregation was observed. The results of the experiments involving the mutated MAP2 show that the propensity of MAP2 to form amyloid aggregates was increased when it contained the sequence derived from Tau. These results are interesting because the sequence that was mutated is known to be one of two very important six-residue stretches within the larger sequence that comprises Tau amyloid aggregates. These small regions within the MTBR region of Tau are known as

the hexapeptide repeats. In fact, fibrils from only these hexapeptide regions have been observed. These studies highlight that it may be possible for MAP2 to form amyloid structures under particular conditions.

There have been almost no studies on MAP2 D aggregation. The full length and MTBRs of MAP2 D expressed here, aggregated during the initial purification procedure used. This required the use of 2 M urea to solubilize the protein (see methods). It was demonstrated that the aggregation behavior of MAP2 in the presence of heparin cofactor results in large amorphous aggregates, which do not resemble amyloid fibrils.

7.5 Inhibition of Tau

It was shown here that MAP2 binds to the end of K18 fibrils with a lower K_D (1.6 µM for MAP2 4R and 2.8 µM for MAP2 3R vs 3.9 µM for K18 on itself) than Tau for itself. If MAP2 is going to be a useful inhibitor of Tau aggregation, it must interact with the fibril directly and specifically. When K19 was used as a control, no binding was observed. This is consistent with the asymmetric seeding barrier that has been previously described [57], [63], [130]. There are very few other studies that demonstrate that MAP2 may inhibit Tau aggregation. One such study has been published on a possible inhibitory role of MAP2 C on Tau nucleation. MAP2 C was shown to inhibit Tau nucleation when a negatively-charged lipid cofactor (arachidonic acid) was used [201]. It was not fully explored whether or not MAP2 was interacting with the arachidonic acid. Arachidonic acid can be used in place of other polyanionic cofactors in Tau research [202]. The

inhibition of Tau protein in this study was negated by phosphorylation of MAP2 C. Phosphorylation of MAP2 C could result in lowered affinity for the anionic micelles, used to induce Tau aggregation. With less MAP2 C binding to the micelles, perhaps the Tau was again able to nucleate and form amyloid fibrils. This study did not investigate 4R MAP2.

There are other cases of experiments in which Tau aggregation is blocked by some type of inhibitor. Many of these examples are of small molecules [121], [203]–[205], but there are cases of a peptide being used [206]. Seidler et al demonstrated that mutated fragments of the Tau MTBRs made from D-amino acids can block the aggregation of K18. This study shows that by using a known disease related mutation, ΔK280, a steric zipper is formed between the β-sheets and this can block the Tau aggregation [207]. This mechanism of action is different than our proposed mechanism, because it is taking place on the side of the protofilament. Experiments in our lab demonstrate that this mutant (K18 ΔK280) can also be blocked by MAP2 (data not shown) which is promising because an eventual drug to treat Tau aggregation should target a variety of sequences.

Other studies demonstrating a blocking effect on Tau aggregation typically involve small molecule inhibitors. Some of these small molecules have been derived from methylene blue (MB). MB and other phenothiazines have been shown to inhibit Tau aggregation in-vitro [208]. These molecules have had limited success at stopping disease progression in zebrafish, however [209]. These

molecules are thought to oxidize the cysteines in Tau, as is the case for vitamin B12 [205]. The cysteines in Tau have been shown to be important in aggregation [210]–[212]. A small molecule that has been studied more exhaustively than most others is (−)-epigallocatechin gallate [120], [211]–[212]. One paper suggests its ability to block aggregation occurs by either stabilizing a conformation of monomer that is incapable of forming nuclei or by changing the monomer to an inert state [121]. This could be important for preventing the initial aggregation from occurring. This mechanism would not affect aggregation in a seeded environment, such as when fibrils are transmitted from neuron to neuron [100]–[101], [213].

Chaperone proteins have been shown to regulate protein refolding in the cellular environment. Heat shock proteins (HSPs) are a class of chaperones. HSP expression is usually regulated tightly and can be increased in response to cellular stress, such as protein aggregation. HSP70 is a highly conserved chaperone protein. It has been shown to bind and inhibit Tau fibril elongation also [216]. The cellular machinery that may be responsible for disassembling Tau fibrils in neurons has yet to be discovered. Studies do show that different combinations of HSPs may be necessary to achieve noticeable clearance of amyloids [217]–[219]. It is possible that the proper combination of chaperones that would allow disaggregation of amyloids, does exist. Once a fibril has grown to a sufficient length, natural fibril fragmentation pathways must cause breakage and subsequent seeding for pathology to spread. Mechanisms of breakage could

include trauma or some undiscovered combination of chaperones. If we could harness an interaction between natural or synthetic blocking agents and Tau fibrils, natural mechanisms such as proteolytic degradation or chaperones mediated disassembly may clear the aggregates.

One final area of AD aggregation inhibitors to discuss is that of antibody-based drugs. These drugs have proven to be effective in mice [220]. Many of these Aβ antibodies capture the monomer in an incompatible format, thereby prohibiting aggregation. As an example, Bapineuzumab was shown to be safe in Phase 2 trials [221] but produced no statistical difference in disease progression of mild-to-moderate AD when compared to a placebo in 3 double-blind studies [219]–[220]. So far, other antibodies have had similar results [224]–[226]. These studies demonstrate that it is possible to engineer monomer-capturing antibodies which have encouraging results *in-vitro*. As for Tau, there are antibody-based approaches demonstrating the ability to inhibit cell-to-cell transmission of Tau fibrils in the preclinical stages that show promising results thus far [224]–[225]. Further studies to demonstrate the exact region or regions of MAP2 that result in the blockage of Tau, shown here, will need to be performed. Eventually, it may be possible to engineer a peptide that resembles the sequence of MAP2, which provides the same structural interference and results in reduced aggregation in patients. The potent and rapid blocking effect demonstrated by the work here could help shape how inhibitors are designed in the future.

7.6 MAP2 binds to and caps the end of Tau fibrils

The end of the fibril is the location in which new monomers are added [54]. The structural information stored in the amyloid fold (such as sheet-sheet packing and protofilament contact residues) defines the structure of fibrils during the conversion of soluble Tau into fibrillar aggregates. This information is stored in the “strain” or conformation. Conformational templating allows for the faithful replication of the structure as parallel and in-register aggregates [54].

The structure of Tau fibrils can be perturbed by changing a single amino acid residue [58]. This is because the core of the fibril is tightly packed and changing the R-group of a single amino acid can generate unfavorable interactions that restrict an incoming monomer from binding to and elongating the fibril. This change in structure could the due to selection processes rather than strain switching in one fibril. It is conceivable that if some minimum number of MAP2 monomers bind to the end of a Tau fibril, they might provide enough perturbation in structure that the Tau protein can no longer grow on this fibril. This interaction may be driven by the sequence similarities between the MAP2 and Tau. However, changes to the structure then cause Tau monomer incompatibilities because of the sequence dissimilarity to MAP2. There are 27 amino acid changes between the two sequences of truncated 4R MAP2 and K18. These differences are likely to be responsible for the inability of MAP2 to be recruited to an appreciable amount and elongate the Tau fibrils. This is also likely the reason K19 was incapable of blocking K18 seeded aggregation.

Although it is not possible to seed 3R Tau monomer on 4R fibrils [63], [130], it is possible to form mixed fibrils where both 3R and 4R Tau are part of the same fibril [56]. It seems that the fact that the second repeat is missing from 3R MAP2 is inconsequential with respect to its ability to block. That region of the protein may not need to be included in the fibril core for templating to occur. Fibrils from AD have recently been shown to be composed of the third and fourth repeats [71]. This may explain why 3R MAP2 may be able to successfully block the aggregation of 4R Tau, like the 4R MAP2 isoform.

It was shown that MAP2 binds to the end of K18 fibrils and blocks Tau aggregation. The differences in the MAP2 and Tau sequences are likely responsible for the incapability of Tau monomers to grow on MAP2 capped fibrils but the sequence similarity between the proteins may be the reason for this binding. Although MAP2 does not grow on the Tau fibril as Tau would, it seems to be possible for a single MAP2 molecule to bind to the end. Perturbations in structure caused by differences in the two protein sequences could disfavor additional monomers from binding. If the conformation of the fibril is perturbed enough, it could also be that Tau is no longer capable of adopting the structure and continuing to elongate the fibril. There is literature to support that conformation of fibrils may not be perfectly imparted on the new monomer, and conformational strain may switch within a single fibril [144], [158]. A similar mechanism that results in capping, rather than true strain switching and

elongation, could help explain why MAP2 seems to block Tau aggregation with a single layer.

Tau fibril seeds and MAP2 monomers were initially preincubated together for some time before the capped fibril seeds were added to fresh monomer and heparin. These experiments resulted in potent blockage of Tau (data not shown) and established the potential for MAP2 as a blocking agent. These types of experiments were adjusted to the more physiologically-relevant experimental design discussed below. By adding the fibril seeds to a mixture of MAP2 monomer, Tau monomer, and heparin, a competition between MAP2 and Tau was forced. Small Tau fibrils have been shown to be progressively transported down neuronal networks [215] and selectively endocytosed [93]. These small Tau fibrils are thought to be much like the seeds used in recombinant experiments. As previously stated, fibrils as small as trimers have been observed, are internalized, and can induce aggregation in cells. The simultaneous introduction of fibril material to monomers (of MAP2 and Tau) and cofactor yielded a more biologically relevant competition-style experiment where MAP2 and Tau proteins would have to compete for the same sites on the fibril end. If after endocytosis of Tau fibrils, MAP2 is present – it might be possible for the internalized fibril ends to become capped – and therefore inhibit the growth. Mechanisms that slow the progression of Tau deposition in disease are of great interest. This is because there are no long-term treatment options for people afflicted with AD and other diseases. Additional work on mechanisms by which

Tau fibril spread can be mitigated is needed. It will be critical in the future to verify that MAP2 is able to block Tau seeding in the cell. Experiments towards this goal are currently ongoing.

References

[1] H. Braak and E. Braak, “Neuropathological stageing of Alzheimer-related changes,” *Acta Neuropathol.*, vol. 82, no. 4, pp. 239–259, 1991.

[2] M. D. Kane *et al.*, “Evidence for seeding of beta -amyloid by intracerebral infusion of Alzheimer brain extracts in beta -amyloid precursor protein-transgenic mice.,” *J. Neurosci.*, vol. 20, no. 10, pp. 3606–11, 2000.

[3] Y. Zhang, R. Thompson, H. Zhang, and H. Xu, “APP processing in Alzheimer’s disease,” *Mol. Brain*, vol. 4, no. 1, p. 3, 2011.

[4] K. S. Kosik, C. L. Joachim, and D. J. Selkoe, “Microtubule-associated protein tau (tau) is a major antigenic component of paired helical filaments in Alzheimer disease.,” *Proc. Natl. Acad. Sci. U. S. A.*, vol. 83, no. 11, pp. 4044–8, 1986.

[5] K. Voss, B. Combs, K. R. Patterson, L. I. Binder, and T. C. Gamblin, “Hsp70 alters tau function and aggregation in an isoform specific manner,” *Biochemistry*, vol. 51, no. 4, pp. 888–898, 2012.

[6] A. Fellgiebel and I. Yakushev, “Diffusion tensor imaging of the hippocampus in MCI and early Alzheimers Disease,” *J. Alzheimer’s Dis.*, vol. 26, no. SUPPL. 3, pp. 257–262, 2011.

[7] V. Vogelsberg-Ragaglia *et al.*, “Distinct FTDP-17 missense mutations in tau produce tau aggregates and other pathological phenotypes in transfected CHO cells.,” *Mol. Biol. Cell*, vol. 11, no. 12, pp. 4093–104, 2000.

[8] C. M. Baugh *et al.*, “Chronic traumatic encephalopathy: Neurodegeneration following repetitive concussive and subconcussive brain trauma,” *Brain Imaging Behav.*, vol. 6, no. 2, pp. 244–254, 2012.

[9] M. Sundman, P. M. Doraiswamy, and R. A. Morey, “Neuroimaging assessment of early and late neurobiological sequelae of traumatic brain injury: Implications for CTE,” *Frontiers in Neuroscience*, vol. 9, no. SEP. 2015.

[10] H. Braak and E. Braak, “Frequency of stages of Alzheimer-related lesions in different age categories,” *Neurobiol. Aging*, vol. 18, no. 4, pp. 351–357, 1997.

[11] K. Perrine, J. Helcer, A. J. Tsiouris, D. J. Pisapia, and P. Stieg, “The Current Status of Research on Chronic Traumatic Encephalopathy,” *World Neurosurgery*, vol. 102. pp. 533–544, 2017.

[12] V. M.-Y. Lee, M. Goedert, and J. Q. Trojanowski, “Neurodegenerative Tauopathies,” *Annu. Rev. Neurosci.*, vol. 24, no. 1, pp. 1121–1159, 2001.

[13] B. I. Omalu, R. L. Hamilton, M. I. Kamboh, S. T. DeKosky, and J. Bailes, “Chronic traumatic encephalopathy (cte) in a national football league player: Case report and emerging medicolegal practice questions,” *J. Forensic Nurs.*, vol. 6, no. 1, pp. 40–46, 2010.

[14] B. I. Omalu, S. T. DeKosky, R. L. Minster, M. I. Kamboh, R. L. Hamilton,

and C. H. Wecht, “Chronic traumatic encephalopathy in a National Football League player,” *Neurosurgery*, vol. 57, no. 1, pp. 128–133, 2005.
[15] J. Mez *et al.*, “Clinicopathological Evaluation of Chronic Traumatic Encephalopathy in Players of American Football,” *Jama*, vol. 318, no. 4, pp. 360–370, 2017.
[16] C. J. Oldfield and A. K. Dunker, “Intrinsically Disordered Proteins and Intrinsically Disordered Protein Regions,” *Annu. Rev. Biochem.*, vol. 83, no. 1, pp. 553–584, 2014.
[17] J. C. Hansen, X. Lu, E. D. Ross, and R. W. Woody, “Intrinsic protein disorder, amino acid composition, and histone terminal domains,” *Journal of Biological Chemistry*, vol. 281, no. 4. pp. 1853–1856, 2006.
[18] S. Elbaum-Garfinkle, T. Ramlall, and E. Rhoades, “The role of the lipid bilayer in tau aggregation,” *Biophys. J.*, vol. 98, no. 11, pp. 2722–2730, 2010.
[19] S. Jeganathan, M. Von Bergen, E. M. Mandelkow, and E. Mandelkow, “The natively unfolded character of Tau and its aggregation to Alzheimer-like paired helical filaments,” *Biochemistry*, vol. 47, no. 40, pp. 10526–10539, 2008.
[20] S. Jeganathan, M. Von Bergen, H. Brutlach, H. J. Steinhoff, and E. Mandelkow, “Global hairpin folding of tau in solution,” *Biochemistry*, vol. 45, no. 7, pp. 2283–2293, 2006.
[21] M. D. Mukrasch *et al.*, “Structural polymorphism of 441-residue Tau at single residue resolution,” *PLoS Biol.*, vol. 7, no. 2, pp. 0399–0414, 2009.
[22] L. Dehmelt and S. Halpain, “Protein family review The MAP2 / Tau family of microtubule-associated proteins,” *Genome Biol.*, vol. 6, pp. 1–10, 2004.
[23] E. Mandelkow and E. M. Mandelkow, “Microtubules and microtubule-associated proteins,” *Curr. Opin. Cell Biol.*, vol. 7, no. 1, pp. 72–81, 1995.
[24] G. Wiche, “High-MA microtubule-associated proteins : properties and functions,” vol. 259, pp. 1–12, 1989.
[25] E. W. Dent, S. L. Gupton, and F. B. Gertler, “The growth cone cytoskeleton in Axon outgrowth and guidance,” *Cold Spring Harb. Perspect. Biol.*, vol. 3, no. 3, pp. 1–39, 2011.
[26] J. B. Ashman, E. S. Hall, J. Eveleth, and K. Boekelheide, “Tau, the neuronal heat-stable microtubule-associated protein, is also present in the cross-linked microtubule network of the testicular spermatid manchette.,” *Biol. Reprod.*, vol. 46, no. 1, pp. 120–129, 1992.
[27] R. L. Neve, P. Harris, K. S. Kosik, D. M. Kurnit, and T. A. Donlon, “Identification of cDNA clones for the human microtubule-associated protein tau and chromosomal localization of the genes for tau and microtubule-associated protein 2,” *Mol. Brain Res.*, vol. 1, no. 3, pp. 271–280, 1986.
[28] M. Goedert, M. G. Spillantini, M. C. Potier, J. Ulrich, and R. A. Crowther, “Cloning and sequencing of the cDNA encoding an isoform of microtubule-

associated protein tau containing four tandem repeats: differential expression of tau protein mRNAs in human brain," *EMBO J.*, vol. 8, no. 2, pp. 393–9, 1989.
[29] G. Lee, R. L. Neve, and K. S. Kosik, "The microtubule binding domain of tau protein," *Neuron*, vol. 2, no. 6, pp. 1615–1624, 1989.
[30] M. Goedert and R. Jakes, "Expression of separate isoforms of human tau protein: correlation with the tau pattern in brain and effects on tubulin polymerization.," *EMBO J.*, vol. 9, no. 13, pp. 4225–4230, 1990.
[31] M. Goedert, M. G. Spillantini, R. Jakes, D. Rutherford, and R. A. Crowther, "Multiple isoforms of human microtubule-associated protein tau: sequences and localization in neurofibrillary tangles of Alzheimer's disease," *Neuron*, vol. 3, no. 4, pp. 519–526, 1989.
[32] M. Goedert, M. G. Spillantini, N. J. Cairns, and R. A. Crowther, "Tau proteins of alzheimer paired helical filaments: Abnormal phosphorylation of all six brain isoforms," *Neuron*, vol. 8, no. 1, pp. 159–168, 1992.
[33] Y. Kanai and N. Hirokawa, "Sorting mechanisms of Tau and MAP2 in neurons: Suppressed axonal transit of MAP2 and locally regulated microtubule binding," *Neuron*, vol. 14, no. 2, pp. 421–432, 1995.
[34] S. A. Lewis, A. Villasante, P. Sherline, and N. J. Cowan, "Brain-specific expression of MAP2 detected using a cloned cDNA probe," *J. Cell Biol.*, vol. 102, no. 6, pp. 2098–2105, 1986.
[35] R. P. Tucker, L. I. Binder, C. Viereck, B. a Hemmings, and a I. Matus, "The sequential appearance of low- and high-molecular-weight forms of MAP2 in the developing cerebellum.," *J. Neurosci.*, vol. 8, no. 12, pp. 4503–12, 1988.
[36] J. Biernat, N. Gustke, G. Drewes, E. Mandelkow, and E. Mandelkow, "Phosphorylation of Ser262 strongly reduces binding of tau to microtubules: Distinction between PHF-like immunoreactivity and microtubule binding," *Neuron*, vol. 11, no. 1, pp. 153–163, 1993.
[37] A. Sengupta, J. Kabat, M. Novak, Q. Wu, I. Grundke-Iqbal, and K. Iqbal, "Phosphorylation of tau at both Thr 231 and Ser 262 is required for maximal inhibition of its binding to microtubules," *Arch. Biochem. Biophys.*, vol. 357, no. 2, pp. 299–309, 1998.
[38] A. D. Alonso, I. Grundke-Iqbal, H. S. Barra, and K. Iqbal, "Abnormal phosphorylation of tau and the mechanism of Alzheimer neurofibrillary degeneration: sequestration of microtubule-associated proteins 1 and 2 and the disassembly of microtubules by the abnormal tau.," *Proc. Natl. Acad. Sci. U. S. A.*, vol. 94, no. 1, pp. 298–303, 1997.
[39] A. C. Alonso, T. Zaidi, I. Grundke-Iqbal, and K. Iqbal, "Role of abnormally phosphorylated tau in the breakdown of microtubules in Alzheimer disease.," *Proc. Natl. Acad. Sci. U. S. A.*, vol. 91, no. 12, pp. 5562–6, 1994.
[40] L. Martin *et al.*, "Tau protein kinases: Involvement in Alzheimer's disease," *Ageing Research Reviews*, vol. 12, no. 1. pp. 289–309, 2013.

[41] C. J. Leugers, J. Y. Koh, W. Hong, and G. Lee, “Tau in MAPK Activation,” *Front. Neurol.*, vol. 4, 2013.
[42] M. Llorens-Marítin, J. Jurado, F. Hernández, and J. Avila, “GSK-3β, a pivotal kinase in Alzheimer disease.,” *Front. Mol. Neurosci.*, vol. 7, no. May, pp. 1–46, 2014.
[43] U. Wagner, M. Utton, J. M. Gallo, and C. C. Miller, “Cellular phosphorylation of tau by GSK-3 beta influences tau binding to microtubules and microtubule organisation.,” *J. Cell Sci.*, vol. 109 (Pt 6, pp. 1537–1543, 1996.
[44] K. Spittaels *et al.*, “Glycogen synthase kinase-3β phosphorylates protein tau and rescues the axonopathy in the central nervous system of human four-repeat tau transgenic mice,” *J. Biol. Chem.*, vol. 275, no. 52, pp. 41340–41349, 2000.
[45] K. Iqbal, C. X. Gong, and F. Liu, “Hyperphosphorylation-induced tau oligomers,” *Front. Neurol.*, vol. 4 AUG, 2013.
[46] E. Kopke, Y. C. Tung, S. Shaikh, C. A. Del Alonso, K. Iqbal, and I. Grundke-Iqbal, “Microtubule-associated protein tau. Abnormal phosphorylation of a non- paired helical filament pool in Alzheimer disease,” *J. Biol. Chem.*, vol. 268, no. 32, pp. 24374–24384, 1993.
[47] W. Noble, D. P. Hanger, C. C. J. Miller, and S. Lovestone, “The importance of tau phosphorylation for neurodegenerative diseases,” *Frontiers in Neurology*, vol. 4 JUL. 2013.
[48] L. Martin, X. Latypova, and F. Terro, “Post-translational modifications of tau protein: Implications for Alzheimer’s disease,” *Neurochem. Int.*, vol. 58, no. 4, pp. 458–471, 2011.
[49] B. Li, M. O. Chohan, I. Grundke-Iqbal, and K. Iqbal, “Disruption of microtubule network by Alzheimer abnormally hyperphosphorylated tau,” *Acta Neuropathol.*, vol. 113, no. 5, pp. 501–511, 2007.
[50] D. Eisenberg and M. Jucker, “The amyloid state of proteins in human diseases,” *Cell*, vol. 148, no. 6. pp. 1188–1203, 2012.
[51] M. Sunde, L. C. Serpell, M. Bartlam, P. E. Fraser, M. B. Pepys, and C. C. F. Blake, “Common core structure of amyloid fibrils by synchrotron X-ray diffraction,” *J. Mol. Biol.*, vol. 273, no. 3, pp. 729–739, 1997.
[52] H. Inouye, D. Sharma, W. J. Goux, and D. A. Kirschner, “Structure of core domain of fibril-forming PHF/tau fragments,” *Biophys. J.*, vol. 90, no. 5, pp. 1774–1789, 2006.
[53] E. C. Landahl *et al.*, “X-ray diffraction from intact tau aggregates in human brain tissue,” in *Nuclear Instruments and Methods in Physics Research, Section A: Accelerators, Spectrometers, Detectors and Associated Equipment*, 2011, vol. 649, no. 1, pp. 184–187.
[54] M. Margittai and R. Langen, “Template-assisted filament growth by parallel stacking of tau.,” *Proc. Natl. Acad. Sci. U. S. A.*, vol. 101, no. 28, pp. 10278–83, 2004.

[55] M. Margittai and R. Langen, “Side chain-dependent stacking modulates tau filament structure,” *J. Biol. Chem.*, vol. 281, no. 49, pp. 37820–37827, 2006.
[56] A. Siddiqua and M. Margittai, “Three- and four-repeat tau coassemble into heterogeneous filaments: An implication for Alzheimer disease,” *J. Biol. Chem.*, vol. 285, no. 48, pp. 37920–37926, 2010.
[57] P. D. Dinkel, M. R. Holden, N. Matin, and M. Margittai, “RNA Binds to Tau Fibrils and Sustains Template-Assisted Growth,” *Biochemistry*, vol. 54, no. 30, pp. 4731–4740, 2015.
[58] V. Meyer *et al.*, “Single mutations in tau modulate the populations of fibril conformers through seed selection,” *Angew. Chemie - Int. Ed.*, vol. 53, no. 6, pp. 1590–1593, 2014.
[59] M. Chen, M. Margittai, J. Chen, and R. Langen, “Investigation of alpha-synuclein fibril structure by site-directed spin labeling.,” *J. Biol. Chem.*, vol. 282, no. 34, pp. 24970–9, 2007.
[60] J. P. Klare, “Site-directed spin labeling EPR spectroscopy in protein research,” *Biological Chemistry*, vol. 394, no. 10. pp. 1281–1300, 2013.
[61] M. Margittai and R. Langen, “Spin Labeling Analysis of Amyloids and Other Protein Aggregates,” *Methods in Enzymology*, vol. 413. pp. 122–139, 2006.
[62] G. Jeschke, “DEER Distance Measurements on Proteins.,” *Annu. Rev. Phys. Chem.*, vol. 63, no. January, pp. 419–46, 2012.
[63] A. Siddiqua *et al.*, “Conformational basis for asymmetric seeding barrier in filaments of three- and four-repeat tau,” *J. Am. Chem. Soc.*, vol. 134, no. 24, pp. 10271–10278, 2012.
[64] V. Meyer, M. R. Holden, H. A. Weismiller, G. R. Eaton, S. S. Eaton, and M. Margittai, “Fracture and growth are competing forces determining the fate of conformers in tau fibril populations,” *J. Biol. Chem.*, vol. 291, no. 23, pp. 12271–12281, 2016.
[65] V. Meyer *et al.*, “Room-temperature distance measurements of immobilized Spin-labeled Protein by DEER/PELDOR,” *Biophys. J.*, vol. 108, no. 5, pp. 1213–1219, 2015.
[66] V. Meyer and M. Margittai, “Spin labeling and characterization of tau fibrils using electron paramagnetic resonance (EPR),” in *Methods in Molecular Biology*, vol. 1345, 2016, pp. 185–199.
[67] A. Sillen, J. M. Wieruszeski, A. Leroy, A. Ben Younes, I. Landrieu, and G. Lippens, “High-resolution magic angle spinning NMR of the neuronal tau protein integrated in Alzheimer’s-like paired helical fragments,” *J. Am. Chem. Soc.*, vol. 127, no. 29, pp. 10138–10139, 2005.
[68] O. C. Andronesi *et al.*, “Characterization of Alzheimer’s-like paired helical filaments from the core domain of tau protein using solid-state NMR spectroscopy,” *J. Am. Chem. Soc.*, vol. 130, no. 18, pp. 5922–5928, 2008.
[69] R. Tycko, “Solid-State NMR Studies of Amyloid Fibril Structure,” *Annu. Rev. Phys. Chem.*, vol. 62, no. 1, pp. 279–299, 2011.

[70] W. Qiang, K. Kelley, and R. Tycko, “Polymorph-specific kinetics and thermodynamics of β-amyloid fibril growth,” *J. Am. Chem. Soc.*, vol. 135, no. 18, pp. 6860–6871, 2013.
[71] A. W. P. Fitzpatrick *et al.*, “Cryo-EM structures of tau filaments from Alzheimer’s disease,” *Nature*, vol. 547, no. 7662, pp. 185–190, 2017.
[72] K. F. Winklhofer, J. Tatzelt, and C. Haass, “The two faces of protein misfolding: Gain- and loss-of-function in neurodegenerative diseases,” *EMBO Journal*, vol. 27, no. 2. pp. 336–349, 2008.
[73] R. A. Saccon, R. K. A. Bunton-Stasyshyn, E. M. C. Fisher, and P. Fratta, “Is SOD1 loss of function involved in amyotrophic lateral sclerosis?,” *Brain*, vol. 136, no. 8. pp. 2342–2358, 2013.
[74] H. Paine, “Does loss of the normal protein function contribute to the pathogenesis of Huntington’s disease?,” *Bioscience Horizons*, vol. 8. 2015.
[75] C. Hetz, K. Maundrell, and C. Soto, “Is loss of function of the prion protein the cause of prion disorders?,” *Trends in Molecular Medicine*, vol. 9, no. 6. pp. 237–243, 2003.
[76] J. Bieschke *et al.*, “Small-molecule conversion of toxic oligomers to nontoxic β-sheetg-rich amyloid fibrils,” *Nat. Chem. Biol.*, vol. 8, no. 1, pp. 93–101, 2012.
[77] M. S. Celej, R. Sarroukh, E. Goormaghtigh, G. D. Fidelio, J.-M. Ruysschaert, and V. Raussens, “Toxic prefibrillar α-synuclein amyloid oligomers adopt a distinctive antiparallel β-sheet structure,” *Biochem. J.*, vol. 443, no. 3, pp. 719–726, 2012.
[78] Y. S. Fang *et al.*, “Full-length TDP-43 forms toxic amyloid oligomers that are present in frontotemporal lobar dementia-TDP patients,” *Nat. Commun.*, vol. 5, 2014.
[79] J. Lee, E. K. Culyba, E. T. Powers, and J. W. Kelly, “Amyloid-β forms fibrils by nucleated conformational conversion of oligomers,” *Nat. Chem. Biol.*, vol. 7, no. 9, pp. 602–609, 2011.
[80] L. Yu *et al.*, “Structural characterization of a soluble amyloid beta-peptide oligomer.,” *Biochemistry*, vol. 48, no. 9, pp. 1870–1877, 2009.
[81] A. Laganowsky *et al.*, “Atomic view of a toxic amyloid small oligomer,” *Science (80-.).*, vol. 335, no. 6073, pp. 1228–1231, 2012.
[82] R. Wetzel, “Kinetics and thermodynamics of amyloid fibril assembly,” *Accounts of Chemical Research*, vol. 39, no. 9. pp. 671–679, 2006.
[83] C. G. Glabe, “Common mechanisms of amyloid oligomer pathogenesis in degenerative disease,” *Neurobiology of Aging*, vol. 27, no. 4. pp. 570–575, 2006.
[84] C. A. Lasagna-Reeves *et al.*, “Alzheimer brain-derived tau oligomers propagate pathology from endogenous tau,” *Sci. Rep.*, vol. 2, 2012.
[85] C. A. Lasagna-Reeves, D. L. Castillo-Carranza, M. J. Guerrero-Muñoz, G. R. Jackson, and R. Kayed, “Preparation and characterization of neurotoxic tau oligomers,” *Biochemistry*, vol. 49, no. 47, pp. 10039–10041, 2010.

[86] C. A. Lasagna-Reeves *et al.*, “Identification of oligomers at early stages of tau aggregation in Alzheimer’s disease,” *FASEB J.*, vol. 26, no. 5, pp. 1946–1959, 2012.
[87] M. A. Meraz-Ríos, K. I. Lira-De León, V. Campos-Peña, M. A. De Anda-Hernández, and R. Mena-López, “Tau oligomers and aggregation in Alzheimer’s disease,” *Journal of Neurochemistry*, vol. 112, no. 6. pp. 1353–1367, 2010.
[88] S. Maeda *et al.*, “Granular tau oligomers as intermediates of tau filaments,” *Biochemistry*, vol. 46, no. 12, pp. 3856–3861, 2007.
[89] A. Takashima, “Hyperphosphorylated tau is a cause of neuronal dysfunction in tauopathy,” *Journal of Alzheimer’s Disease*, vol. 14, no. 4. pp. 371–375, 2008.
[90] M. D. C. Cárdenas-Aguayo, L. Gómez-Virgilio, S. DeRosa, and M. A. Meraz-Ríos, “The role of tau Oligomers in the onset of Alzheimer’s disease neuropathology,” *ACS Chemical Neuroscience*, vol. 5, no. 12. pp. 1178–1191, 2014.
[91] C. A. Lasagna-Reeves *et al.*, “Identification of oligomers at early stages of tau aggregation in Alzheimer’s disease,” *FASEB J.*, vol. 26, no. 5, pp. 1946–1959, 2012.
[92] D. W. Peterson, H. Zhou, F. W. Dahlquist, and J. Lew, “A soluble oligomer of tau associated with fiber formation analyzed by NMR,” *Biochemistry*, vol. 47, no. 28, pp. 7393–7404, 2008.
[93] J. W. Wu *et al.*, “Small misfolded tau species are internalized via bulk endocytosis and anterogradely and retrogradely transported in neurons,” *J. Biol. Chem.*, vol. 288, no. 3, pp. 1856–1870, 2013.
[94] B. B. Holmes *et al.*, “Proteopathic tau seeding predicts tauopathy in vivo,” *Proc. Natl. Acad. Sci.*, vol. 111, no. 41, pp. E4376–E4385, 2014.
[95] H. Mirbaha, B. B. Holmes, D. W. Sanders, J. Bieschke, and M. I. Diamond, “Tau Trimers Are the Minimal Propagation Unit Spontaneously Internalized to Seed Intracellular,” vol. 290, no. 24, pp. 14893–14903, 2015.
[96] S. J. Jackson *et al.*, “Short Fibrils Constitute the Major Species of Seed-Competent Tau in the Brains of Mice Transgenic for Human P301S Tau.,” *J. Neurosci.*, vol. 36, no. 3, pp. 762–72, 2016.
[97] N. Kfoury, B. B. Holmes, H. Jiang, D. M. Holtzman, and M. I. Diamond, “Trans-cellular propagation of Tau aggregation by fibrillar species,” *J. Biol. Chem.*, vol. 287, no. 23, pp. 19440–19451, 2012.
[98] B. Frost, R. L. Jacks, and M. I. Diamond, “Propagation of Tau misfolding from the outside to the inside of a cell,” *J. Biol. Chem.*, vol. 284, no. 19, pp. 12845–12852, 2009.
[99] H. Mirbaha, B. B. Holmes, D. W. Sanders, J. Bieschke, and M. I. Diamond, “Tau trimers are the minimal propagation unit spontaneously internalized to seed intracellular aggregation,” *J. Biol. Chem.*, vol. 290, no. 24, pp. 14893–14903, 2015.

[100] W. P. Esler *et al.*, “Alzheimer’s disease amyloid propagation by a template-dependent dock-lock mechanism.,” *Biochemistry*, vol. 39, no. 21, pp. 6288–6295, 2000.
[101] N. V. Mohamed, T. Herrou, V. Plouffe, N. Piperno, and N. Leclerc, “Spreading of tau pathology in Alzheimer’s disease by cell-to-cell transmission,” *Eur. J. Neurosci.*, vol. 37, no. 12, pp. 1939–1948, 2013.
[102] F. Clavaguera *et al.*, “Transmission and spreading of tauopathy in transgenic mouse brain,” *Nat. Cell Biol.*, vol. 11, no. 7, pp. 909–913, 2009.
[103] M. Hasegawa, M. J. Smith, and M. Goedert, “Tau proteins with FTDP-17 mutations have a reduced ability to promote microtubule assembly,” *FEBS Lett.*, vol. 437, no. 3, pp. 207–210, 1998.
[104] M. Goedert and M. G. Spillantini, “Tau mutations in frontotemporal dementia FTDP-17 and their relevance for Alzheimer’s disease,” *Biochimica et Biophysica Acta - Molecular Basis of Disease*, vol. 1502, no. 1. pp. 110–121, 2000.
[105] P. B. Rosenberg and A. E. Hillis, “Biomarkers for Alzheimers disease: Ready for the next step,” *Brain*, vol. 132, no. 8. pp. 2002–2004, 2009.
[106] F. K. Salawu, J. T. Umar, and A. B. Olokoba, “Alzheimers disease: A review of recent developments,” *Ann. Afr. Med.*, vol. 10, no. 2, pp. 73–79, 2011.
[107] J. Dauwels, F. Vialatte, and A. Cichocki, “Diagnosis of Alzheimers Disease from EEG Signals: Where Are We Standing?,” *Curr. Alzheimer Res.*, vol. 7, no. 6, pp. 487–505, 2010.
[108] F. L. Seixas, B. Zadrozny, J. Laks, A. Conci, and D. C. Muchaluat Saade, “A Bayesian network decision model for supporting the diagnosis of dementia, Alzheimers disease and mild cognitive impairment,” *Comput Biol Med*, vol. 51, pp. 140–158, 2014.
[109] M. S. Albert *et al.*, “The diagnosis of mild cognitive impairment due to Alzheimer’s disease: Recommendations from the National Institute on Aging-Alzheimer’s Association workgroups on,” *Alzheimer’s Dement.*, vol. 7, no. 3, pp. 270–279, 2011.
[110] Z. S. Nasreddine *et al.*, “The Montreal Cognitive Assessment, MoCA: A brief screening tool for mild cognitive impairment,” *J. Am. Geriatr. Soc.*, vol. 53, no. 4, pp. 695–699, 2005.
[111] M. F. Folstein, S. E. Folstein, and P. R. McHugh, “‘Mini-mental state’. A practical method for grading the cognitive state of patients for the clinician,” *J. Psychiatr. Res.*, vol. 12, no. 3, pp. 189–198, 1975.
[112] C. M. Wischik, C. R. Harrington, and J. M. D. Storey, “Tau-aggregation inhibitor therapy for Alzheimer’s disease,” *Biochemical Pharmacology*, vol. 88, no. 4. pp. 529–539, 2014.
[113] S. Coutadeur *et al.*, “A novel DYRK1A (Dual specificity tyrosine phosphorylation-regulated kinase 1A) inhibitor for the treatment of Alzheimer’s disease: Effect on Tau and amyloid pathologies in vitro,” *J.*

Neurochem., vol. 133, no. 3, pp. 440–451, 2015.
[114] K. Hochgräfe *et al.*, “Preventive methylene blue treatment preserves cognition in mice expressing full-length pro-aggregant human Tau,” *Acta Neuropathol. Commun.*, vol. 3, p. 25, 2015.
[115] K. Yanamandra *et al.*, “Anti-tau antibodies that block tau aggregate seeding invitro markedly decrease pathology and improve cognition in vivo,” *Neuron*, vol. 80, no. 2, pp. 402–414, 2013.
[116] A. K. Hakala, D. Fergusson, and J. Kimmelman, “Nonpublication of trial results for new neurological drugs: A systematic review,” *Annals of Neurology*, vol. 81, no. 6. pp. 782–789, 2017.
[117] J. Cummings, K. Zhong, and D. Cordes, “Drug development in Alzheimer’s disease— The role of default mode network assessment in phase II,” *Eur. Neurol. Rev.*, vol. 13, no. 2, 2017.
[118] S. O. Bachurin, E. V. Bovina, and A. A. Ustyugov, “Drugs in Clinical Trials for Alzheimer’s Disease: The Major Trends,” *Medicinal Research Reviews*, vol. 37, no. 5. pp. 1186–1225, 2017.
[119] J. R. Lackowicz and F. Anisotropy, “Fluorescence Anisotropy,” *Princ. Fluoresc. Spectrosc.*, pp. 353–382, 2006.
[120] J. E. Gerson and R. Kayed, “Formation and propagation of tau oligomeric seeds,” *Frontiers in Neurology*, vol. 4 JUL. 2013.
[121] H. J. Wobst, A. Sharma, M. I. Diamond, E. E. Wanker, and J. Bieschke, “The green tea polyphenol (-)-epigallocatechin gallate prevents the aggregation of tau protein into toxic oligomers at substoichiometric ratios,” *FEBS Lett.*, vol. 589, no. 1, pp. 77–83, 2015.
[122] O. Schweers, E. Schönbrunn-Hanebeck, A. Marx, and E. Mandelkow, “Structural studies of tau protein and Alzheimer paired helical filaments show no evidence for beta-structure.,” *J. Biol. Chem.*, vol. 269, no. 39, pp. 24290–7, 1994.
[123] A. E. Cohen and W. E. Moerner, “Controlling Brownian motion of single protein molecules and single fluorophores in aqueous buffer.,” *Opt. Express*, vol. 16, no. 10, pp. 6941–56, 2008.
[124] A. P. Fields and A. E. Cohen, “A Flexible Anti-Brownian Electrokinetic (ABEL) Trap for Single-Molecule Immobilization in Solution,” *Biophys. J.*, vol. 96, no. 3, p. 288a, 2009.
[125] Q. Wang, R. H. Goldsmith, Y. Jiang, S. D. Bockenhauer, and W. E. Moerner, “Probing single biomolecules in solution using the anti-brownian electrokinetic (ABEL) trap,” *Acc. Chem. Res.*, vol. 45, no. 11, pp. 1955–1964, 2012.
[126] S. D. Bockenhauer, T. M. Duncan, W. E. Moerner, and M. Börsch, “The regulatory switch of F1-ATPase studied by single-molecule FRET in the ABEL Trap.,” *Proc. SPIE--the Int. Soc. Opt. Eng.*, vol. 8950, p. 89500H, 2014.
[127] L. H. Manger *et al.*, “Revealing Conformational Variants of Solution-Phase

Intrinsically Disordered Tau Protein at the Single-Molecule Level," *Angew. Chemie - Int. Ed.*, vol. 56, no. 49, pp. 15584–15588, 2017.
[128] T. Kashiwagi *et al.*, "Crystal structure of microbial transglutaminase from Streptoverticillium mobaraense," *J. Biol. Chem.*, vol. 277, no. 46, pp. 44252–44260, 2002.
[129] S. Elbaum-Garfinkle and E. Rhoades, "Identification of an aggregation-prone structure of tau," *J. Am. Chem. Soc.*, vol. 134, no. 40, pp. 16607–16613, 2012.
[130] P. D. Dinkel, A. Siddiqua, H. Huynh, M. Shah, and M. Margittai, "Variations in filament conformation dictate seeding barrier between three- and four-repeat tau," *Biochemistry*, vol. 50, no. 20, pp. 4330–4336, 2011.
[131] D. W. Sanders *et al.*, "Distinct tau prion strains propagate in cells and mice and define different tauopathies," *Neuron*, vol. 82, no. 6, pp. 1271–1288, 2014.
[132] R. Tycko, "Physical and structural basis for polymorphism in amyloid fibrils," *Protein Sci.*, vol. 23, no. 11, pp. 1528–1539, 2014.
[133] R. Tycko, "Amyloid Polymorphism: Structural Basis and Neurobiological Relevance," *Neuron*, vol. 86, no. 3. pp. 632–645, 2015.
[134] G. Jeschke, "DEER Distance Measurements on Proteins," *Annu. Rev. Phys. Chem.*, vol. 63, no. 1, pp. 419–446, 2012.
[135] R. a Crowther, "Straight and paired helical filaments in Alzheimer disease have a common structural unit.," *Proc. Natl. Acad. Sci. U. S. A.*, vol. 88, no. 6, pp. 2288–2292, 1991.
[136] P. Friedhoff, M. von Bergen, E. M. Mandelkow, and E. Mandelkow, "Structure of tau protein and assembly into paired helical filaments.," *Biochim. Biophys. Acta*, vol. 1502, no. 1, pp. 122–132, 2000.
[137] A. d. C. Alonso, T. Zaidi, M. Novak, I. Grundke-Iqbal, and K. Iqbal, "Hyperphosphorylation induces self-assembly of into tangles of paired helical filaments/straight filaments," *Proc. Natl. Acad. Sci.*, vol. 98, no. 12, pp. 6923–6928, 2001.
[138] Y. Li *et al.*, "Characterization of Inter- and Intramolecular Interactions of Amyloid Fibrils by AFM-Based Single-Molecule Force Spectroscopy," *Journal of Nanomaterials*, vol. 2016. 2016.
[139] Z. Wang, C. Zhou, C. Wang, L. Wan, X. Fang, and C. Bai, "AFM and STM study of beta-amyloid aggregation on graphite.," *Ultramicroscopy*, vol. 97, no. 1–4, pp. 73–9, 2003.
[140] C. C. Vandenakker, M. F. M. Engel, K. P. Velikov, M. Bonn, and G. H. Koenderink, "Morphology and persistence length of amyloid fibrils are correlated to peptide molecular structure," *J. Am. Chem. Soc.*, vol. 133, no. 45, pp. 18030–18033, 2011.
[141] N. Norlin *et al.*, "Aggregation and fibril morphology of the Arctic mutation of Alzheimer's Aβ peptide by CD, TEM, STEM and in situ AFM," *J. Struct. Biol.*, vol. 180, no. 1, pp. 174–189, 2012.

[142] A. K. Paravastu, R. D. Leapman, W.-M. Yau, and R. Tycko, “Molecular structural basis for polymorphism in Alzheimer’s beta-amyloid fibrils.,” *Proc. Natl. Acad. Sci. U. S. A.*, vol. 105, no. 47, pp. 18349–54, 2008.
[143] A. K. Paravastu, A. T. Petkova, and R. Tycko, “Polymorphic fibril formation by residues 10-40 of the Alzheimer’s β-amyloid peptide,” *Biophys. J.*, vol. 90, no. 12, pp. 4618–4629, 2006.
[144] N. Makarava, V. G. Ostapchenko, R. Savtchenko, and I. V. Baskakov, “Conformational switching within individual amyloid fibrils,” *J. Biol. Chem.*, vol. 284, no. 21, pp. 14386–14395, 2009.
[145] C. K. Foo, Y. Ohhashi, M. J. S. Kelly, M. Tanaka, and J. S. Weissman, “Radically different amyloid conformations dictate the seeding specificity of a chimeric Sup35 prion,” *J. Mol. Biol.*, vol. 408, no. 1, pp. 1–8, 2011.
[146] C. J. Silva, E. Vázquez-Fernández, B. Onisko, and J. R. Requena, “Proteinase K and the structure of PrP^{Sc}: The good, the bad and the ugly,” *Virus Research*, vol. 207. pp. 120–126, 2015.
[147] V. Meyer, M. R. Holden, H. A. Weismiller, G. R. Eaton, S. S. Eaton, and M. Margittai, “Fracture and growth are competing forces determining the fate of conformers in tau fibril populations,” *J. Biol. Chem.*, 2016.
[148] A. I. Sulatskaya, I. M. Kuznetsova, and K. K. Turoverov, “Interaction of thioflavin T with amyloid fibrils: Stoichiometry and affinity of dye binding, absorption spectra of bound dye,” *J. Phys. Chem. B*, vol. 115, no. 39, pp. 11519–11524, 2011.
[149] M. Biancalana and S. Koide, “Molecular mechanism of Thioflavin-T binding to amyloid fibrils,” *Biochim. Biophys. Acta - Proteins Proteomics*, vol. 1804, no. 7, pp. 1405–1412, 2010.
[150] M. Groenning, “Binding mode of Thioflavin T and other molecular probes in the context of amyloid fibrils-current status,” *Journal of Chemical Biology*, vol. 3, no. 1. pp. 1–18, 2010.
[151] M. Biancalana and S. Koide, “Molecular mechanism of Thioflavin-T binding to amyloid fibrils,” *Biochimica et Biophysica Acta - Proteins and Proteomics*, vol. 1804, no. 7. pp. 1405–1412, 2010.
[152] E. S. Voropai *et al.*, “Spectral properties of thioflavin T and its complexes with amyloid fibrils,” *J. Appl. Spectrosc.*, vol. 70, no. 6, pp. 868–874, 2003.
[153] M. J. Cannon, A. D. Williams, R. Wetzel, and D. G. Myszka, “Kinetic analysis of beta-amyloid fibril elongation,” *Anal. Biochem.*, vol. 328, no. 1, pp. 67–75, 2004.
[154] K. Milto, A. Botyriute, and V. Smirnovas, “Amyloid-Like Fibril Elongation Follows Michaelis-Menten Kinetics,” *PLoS One*, vol. 8, no. 7, 2013.
[155] S. I. A. Cohen *et al.*, “Proliferation of amyloid- 42 aggregates occurs through a secondary nucleation mechanism,” *Proc. Natl. Acad. Sci.*, vol. 110, no. 24, pp. 9758–9763, 2013.
[156] J. S. Jeong, A. Ansaloni, R. Mezzenga, H. A. Lashuel, and G. Dietler, “Novel mechanistic insight into the molecular basis of amyloid

polymorphism and secondary nucleation during amyloid formation," *J. Mol. Biol.*, vol. 425, no. 10, pp. 1765–1781, 2013.
[157] R. Gaspar *et al.*, "Secondary nucleation of monomers on fibril surface dominates α-synuclein aggregation and provides autocatalytic amyloid amplification," *Q. Rev. Biophys.*, vol. 50, 2017.
[158] I. V. Baskakov, "Switching in amyloid structure within individual fibrils: Implication for strain adaptation, species barrier and strain classification," *FEBS Letters*, vol. 583, no. 16. pp. 2618–2622, 2009.
[159] M. E. Orr, A. C. Sullivan, and B. Frost, "A Brief Overview of Tauopathy: Causes, Consequences, and Therapeutic Strategies," *Trends in Pharmacological Sciences*, vol. 38, no. 7. pp. 637–648, 2017.
[160] G. Ramachandran and J. B. Udgaonkar, "Understanding the kinetic roles of the inducer heparin and of rod-like protofibrils during amyloid fibril formation by tau protein," *J. Biol. Chem.*, vol. 286, no. 45, pp. 38948–38959, 2011.
[161] B. B. Holmes *et al.*, "Heparan sulfate proteoglycans mediate internalization and propagation of specific proteopathic seeds.," *Proc. Natl. Acad. Sci. U. S. A.*, vol. 110, no. 33, pp. E3138-47, 2013.
[162] J. Teng, Y. Takei, A. Harada, T. Nakata, J. Chen, and N. Hirokawa, "Synergistic effects of MAP2 and MAP1B knockout in neuronal migration, dendritic outgrowth, and microtubule organization," *J. Cell Biol.*, vol. 155, no. 1, pp. 65–76, 2001.
[163] J. Chen, Y. Kanai, N. J. Cowan, and N. Hirokawa, "Projection domains of MAP2 and tau determine spacings between microtubules in dendrites and axons," *Nature*, vol. 360, no. 6405, pp. 674–677, 1992.
[164] H. Kadavath *et al.*, "Tau stabilizes microtubules by binding at the interface between tubulin heterodimers," *Proc. Natl. Acad. Sci.*, vol. 112, no. 24, pp. 7501–7506, 2015.
[165] M. F. Chau, M. J. Radeke, C. De Inés, I. Barasoain, L. A. Kohlstaedt, and S. C. Feinstein, "The microtubule-associated protein tau cross-links to two distinct sites on each α and β tubulin monomer via separate domains," *Biochemistry*, vol. 37, no. 51, pp. 17692–17703, 1998.
[166] J. Al-Bassam, R. S. Ozer, D. Safer, S. Halpain, and R. A. Milligan, "MAP2 and tau bind longitudinally along the outer ridges of microtubule protofilaments," *J. Cell Biol.*, vol. 157, no. 7, pp. 1187–1196, 2002.
[167] S. Kar, J. Fan, M. J. Smith, M. Goedert, and L. A. Amos, "Repeat motifs of tau bind to the insides of microtubules in the absence of taxol," *EMBO J.*, vol. 22, no. 1, pp. 70–77, 2003.
[168] A. J. Trexler and E. Rhoades, "NIH Public Access," *Biophysics (Oxf).*, vol. 48, no. 11, pp. 2304–2306, 2010.
[169] A. E. Cohen and W. E. Moemer, "Method for trapping and manipulating nanoscale objects in solution," *Appl. Phys. Lett.*, vol. 86, no. 9, pp. 1–3, 2005.

[170] Q. Wang and W. E. Moerner, “Optimal strategy for trapping single fluorescent molecules in solution using the ABEL trap,” *Appl. Phys. B Lasers Opt.*, vol. 99, no. 1–2, pp. 23–30, 2010.
[171] G. F. Schröder, U. Alexiev, and H. Grubmüller, “Simulation of fluorescence anisotropy experiments: Probing protein dynamics,” *Biophys. J.*, vol. 89, no. 6, pp. 3757–3770, 2005.
[172] E. L. Altschuler, N. V. Hud, J. A. Mazrimas, and B. Rupp, “Structure of polyglutamine [1],” *FEBS Letters*, vol. 472, no. 1. pp. 166–167, 2000.
[173] E. L. ALTSCHULER, N. V. HUD, J. A. MAZRIMAS, and B. RUPP, “Random coil conformation for extended polyglutamine stretches in aqueous soluble monomeric peptides,” *J. Pept. Res.*, vol. 50, no. 1, pp. 73–75, 2009.
[174] S. L. Crick, M. Jayaraman, C. Frieden, R. Wetzel, and R. V. Pappu, “Fluorescence correlation spectroscopy shows that monomeric polyglutamine molecules form collapsed structures in aqueous solutions,” *Proc. Natl. Acad. Sci.*, vol. 103, no. 45, pp. 16764–16769, 2006.
[175] S. Côté, R. Laghaei, P. Derreumaux, and N. Mousseau, “Distinct dimerization for various alloforms of the amyloid-beta protein: Aβ1-40, Aβ1-42, and Aβ1-40(D23N),” *J. Phys. Chem. B*, vol. 116, no. 13, pp. 4043–4055, 2012.
[176] B. Frost, J. Ollesch, H. Wille, and M. I. Diamond, “Conformational diversity of wild-type tau fibrils specified by templated conformation change,” *J. Biol. Chem.*, vol. 284, no. 6, pp. 3546–3551, 2009.
[177] S. K. Kaufman *et al.*, “Tau Prion Strains Dictate Patterns of Cell Pathology, Progression Rate, and Regional Vulnerability In Vivo,” *Neuron*, vol. 92, no. 4, pp. 796–812, 2016.
[178] T. Sneideris, K. Milto, and V. Smirnovas, “Polymorphism of amyloid-like fibrils can be defined by the concentration of seeds,” *PeerJ*, vol. 3, p. e1207, 2015.
[179] N. Makarava and I. V. Baskakov, “The same primary structure of the prion protein yields two distinct self-propagating states,” *J. Biol. Chem.*, vol. 283, no. 23, pp. 15988–15996, 2008.
[180] D. H. Daneshvar, L. E. Goldstein, P. T. Kiernan, T. D. Stein, and A. C. McKee, “Post-traumatic neurodegeneration and chronic traumatic encephalopathy,” *Molecular and Cellular Neuroscience*, vol. 66, no. PB. pp. 81–90, 2015.
[181] A. L. Woerman *et al.*, “Tau prions from Alzheimer’s disease and chronic traumatic encephalopathy patients propagate in cultured cells,” *Proc. Natl. Acad. Sci.*, vol. 113, no. 50, pp. E8187–E8196, 2016.
[182] R. A. Stern, D. O. Riley, D. H. Daneshvar, C. J. Nowinski, R. C. Cantu, and A. C. McKee, “Long-term Consequences of Repetitive Brain Trauma: Chronic Traumatic Encephalopathy,” *PM and R*, vol. 3, no. 10 SUPPL. 2. 2011.

[183] L. Bousset *et al.*, “Structural and functional characterization of two alpha-synuclein strains,” *Nat. Commun.*, vol. 4, 2013.
[184] D. W. Sanders *et al.*, “Distinct tau prion strains propagate in cells and mice and define different tauopathies,” *Neuron*, vol. 82, no. 6, pp. 1271–1288, 2014.
[185] O. S. Makin, E. Atkins, P. Sikorski, J. Johansson, and L. C. Serpell, “Molecular basis for amyloid fibril formation and stability.,” *Proc. Natl. Acad. Sci. U. S. A.*, vol. 102, no. 2, pp. 315–320, 2005.
[186] J. C. Stroud, “The zipper groups of the amyloid state of proteins,” *Acta Crystallogr. Sect. D Biol. Crystallogr.*, vol. 69, no. 4, pp. 540–545, 2013.
[187] V. Fonte *et al.*, “A glycine zipper motif mediates the formation of toxic β-amyloid oligomers in vitro and in vivo,” *Mol. Neurodegener.*, vol. 6, no. 1, 2011.
[188] S. W. Lee *et al.*, “Steric Zipper of the Amyloid Fibrils Formed by Residues 109-122 of the Syrian Hamster Prion Protein,” *J. Mol. Biol.*, vol. 378, no. 5, pp. 1142–1154, 2008.
[189] L. G. Paisley and J. Hostrup-Pedersen, “A quantitative assessment of the BSE risk associated with fly ash and slag from the incineration of meat-and-bone meal in a gas-fired power plant in Denmark,” *Prev. Vet. Med.*, vol. 68, no. 2–4, pp. 263–275, 2005.
[190] D. Taylor, “Inactivation of the BSE agent,” *Comptes Rendus - Biol.*, vol. 325, no. 1, pp. 75–76, 2002.
[191] J. Kuret, E. E. Congdon, G. Li, H. Yin, X. Yu, and Q. Zhong, “Evaluating triggers and enhancers of tau fibrillization,” *Microscopy Research and Technique*, vol. 67, no. 3–4. pp. 141–155, 2005.
[192] C. N. Chirita, M. Necula, and J. Kuret, “Anionic micelles and vesicles induce tau fibrillization in vitro,” *J. Biol. Chem.*, vol. 278, no. 28, pp. 25644–25650, 2003.
[193] G. Perry *et al.*, “Association of heparan sulfate proteoglycan with the neurofibrillary tangles of Alzheimer’s disease.,” *J. Neurosci.*, vol. 11, no. 11, pp. 3679–83, 1991.
[194] S. D. Ginsberg, P. B. Crino, V. M. Y. Lee, J. H. Eberwine, and J. Q. Trojanowski, “Sequestration of RNA in Alzheimer’s disease neurofibrillary tangles and senile plaques,” *Ann. Neurol.*, vol. 41, no. 2, pp. 200–209, 1997.
[195] A. d. C. Alonso, T. Zaidi, M. Novak, I. Grundke-Iqbal, and K. Iqbal, “Hyperphosphorylation induces self-assembly of into tangles of paired helical filaments/straight filaments,” *Proc. Natl. Acad. Sci.*, vol. 98, no. 12, pp. 6923–6928, 2001.
[196] J. Six *et al.*, “Specific monoclonal antibodies against normal microtubule-associated protein-2 (MAP2) epitopes present in Alzheimer pathological structures do not recognize paired helical filaments,” *Acta Neuropathol.*, vol. 83, no. 2, pp. 179–189, 1992.

[197] J. P. Brion, M. E. Cheetham, A. M. Couck, J. Flament-Durand, D. P. Hanger, and B. H. Anderton, “Characterization of a partial cDNA specific for the high molecular weight microtubule-associated protein MAP2 that encodes epitopes shared with paired helical filaments of alzheimer’s disease,” *Dement. Geriatr. Cogn. Disord.*, vol. 1, no. 6, pp. 304–315, 1990.
[198] M. A. DeTure, E. Y. Zhang, M. R. Bubb, and D. L. Purich, “In vitro polymerization of embryonic MAP-2c and fragments of the MAP-2 microtubule binding region into structures resembling paired helical filaments,” *J. Biol. Chem.*, vol. 271, no. 51, pp. 32702–32706, 1996.
[199] M. A. DeTure, L. Di Noto, and D. L. Purich, “In vitro assembly of Alzheimer-like filaments: How a small cluster of charged residues in Tau and MAP2 controls filament morphology,” *J. Biol. Chem.*, vol. 277, no. 38, pp. 34755–34759, 2002.
[200] C. Xie *et al.*, “Identification of key amino acids responsible for the distinct aggregation properties of microtubule-associated protein 2 and tau,” *J. Neurochem.*, vol. 135, no. 1, pp. 19–26, 2015.
[201] G. Mitra, S. Gupta, A. Poddar, and B. Bhattacharyya, “MAP2c prevents arachidonic acid-induced fibril formation of tau: Role of chaperone activity and phosphorylation,” *Biophys. Chem.*, vol. 205, pp. 16–23, 2015.
[202] M. E. King, T. C. Gamblin, J. Kuret, and L. I. Binder, “Differential assembly of human tau isoforms in the presence of arachidonic acid,” *J. Neurochem.*, vol. 74, no. 4, pp. 1749–1757, 2000.
[203] A. Crowe, C. Ballatore, E. Hyde, J. Q. Trojanowski, and V. M. Y. Lee, “High throughput screening for small molecule inhibitors of heparin-induced tau fibril formation,” *Biochem. Biophys. Res. Commun.*, vol. 358, no. 1, pp. 1–6, 2007.
[204] P. M. *et al.*, “Identification of small molecule inhibitors of tau aggregation by targeting monomeric tau as a potential therapeutic approach for tauopathies,” *Neurodegener. Dis.*, vol. 15, no. 9, p. 1585, 2015.
[205] S. Rafiee, K. Asadollahi, G. Riazi, S. Ahmadian, and A. A. Saboury, “Vitamin B12 Inhibits Tau Fibrillization via Binding to Cysteine Residues of Tau,” *ACS Chem. Neurosci.*, vol. 8, no. 12, pp. 2676–2682, 2017.
[206] P. M. Seidler *et al.*, “Structure-based inhibitors of tau aggregation,” *Nat. Chem.*, pp. 1–7, 2017.
[207] P. M. Seidler *et al.*, “Structure-based inhibitors of tau aggregation,” *Nat. Chem.*, no. November, pp. 1–7, 2017.
[208] S. Taniguchi *et al.*, “Inhibition of heparin-induced tau filament formation by phenothiazines, polyphenols, and porphyrins,” *J. Biol. Chem.*, vol. 280, no. 9, pp. 7614–7623, 2005.
[209] F. van Bebber, D. Paquet, A. Hruscha, B. Schmid, and C. Haass, “Methylene blue fails to inhibit Tau and polyglutamine protein dependent toxicity in zebrafish,” *Neurobiol. Dis.*, vol. 39, no. 3, pp. 265–271, 2010.
[210] Y. Furukawa, K. Kaneko, and N. Nukina, “Tau protein assembles into

isoform- and disulfide-dependent polymorphic fibrils with distinct structural properties," *J. Biol. Chem.*, vol. 286, no. 31, pp. 27236–27246, 2011.
[211] K. Bhattacharya, K. B. Rank, D. B. Evans, and S. K. Sharma, "Role of cysteine-291 and cysteine-322 in the polymerization of human tau into Alzheimer-like filaments," *Biochem. Biophys. Res. Commun.*, vol. 285, no. 1, pp. 20–26, 2001.
[212] O. Schweers, E. M. Mandelkow, J. Biernat, and E. Mandelkow, "Oxidation of cysteine-322 in the repeat domain of microtubule-associated protein tau controls the in vitro assembly of paired helical filaments.," *Proc. Natl. Acad. Sci.*, vol. 92, no. 18, pp. 8463–8467, 1995.
[213] K. Rezai-Zadeh *et al.*, "Green tea epigallocatechin-3-gallate (EGCG) reduces β-amyloid mediated cognitive impairment and modulates tau pathology in Alzheimer transgenic mice," *Brain Res.*, vol. 1214, pp. 177–187, 2008.
[214] A. S. Chesser, V. Ganeshan, J. Yang, and G. V. W. Johnson, "Epigallocatechin-3-gallate enhances clearance of phosphorylated tau in primary neurons," *Nutr. Neurosci.*, vol. 19, no. 1, pp. 21–31, 2016.
[215] S. Calafate *et al.*, "Synaptic Contacts Enhance Cell-to-Cell Tau Pathology Propagation," *Cell Rep.*, vol. 11, no. 8, pp. 1176–1183, 2015.
[216] F. Kundel *et al.*, "Hsp70 inhibits the nucleation and elongation of tau and sequesters tau aggregates with high affinity," *ACS Chem. Biol.*, p. acschembio.7b01039, 2018.
[217] A. Bracher and J. Verghese, "GrpE, Hsp110/Grp170, HspBP1/Sil1 and BAG domain proteins: Nucleotide exchange factors for Hsp70 molecular chaperones," *Subcell. Biochem.*, vol. 78, pp. 1–33, 2015.
[218] N. B. Nillegoda *et al.*, "Crucial HSP70 co-chaperone complex unlocks metazoan protein disaggregation," *Nature*, vol. 524, no. 7564, pp. 247–251, 2015.
[219] J. Shorter, "The mammalian disaggregase machinery: Hsp110 synergizes with Hsp70 and Hsp40 to catalyze protein disaggregation and reactivation in a cell-free system," *PLoS One*, vol. 6, no. 10, 2011.
[220] J. Sevigny *et al.*, "The antibody aducanumab reduces Aβ plaques in Alzheimer's disease," *Nature*, vol. 537, no. 7618, pp. 50–56, 2016.
[221] S. Salloway *et al.*, "A phase 2 multiple ascending dose trial of bapineuzumab in mild to moderate Alzheimer disease," *Neurology*, vol. 73, no. 24, pp. 2061–2070, 2009.
[222] R. Vandenberghe *et al.*, "Bapineuzumab for mild to moderate Alzheimer's disease in two global, randomized, phase 3 trials," *Alzheimers. Res. Ther.*, vol. 8, no. 1, p. 18, 2016.
[223] S. Salloway *et al.*, "Two phase 3 trials of bapineuzumab in mild-to-moderate Alzheimer's disease.," *N. Engl. J. Med.*, vol. 370, no. 4, pp. 322–33, 2014.
[224] S. Budd Haeberlein *et al.*, "Clinical Development of Aducanumab, an Anti-

Aβ Human Monoclonal Antibody Being Investigated for the Treatment of Early Alzheimer's Disease.," *J. Prev. Alzheimer's Dis.*, vol. 4, no. 4, pp. 255–263, 2017.
[225] R. S. Doody *et al.*, "Phase 3 trials of solanezumab for mild-to-moderate Alzheimer's disease," *N Engl J Med*, vol. 370, no. 4, pp. 311–321, 2014.
[226] J. Sevigny *et al.*, "The antibody aducanumab reduces Abeta plaques in Alzheimer's disease," *Nature*, vol. 537, no. 7618, pp. 50–56, 2016.
[227] C. K. Nobuhara *et al.*, "Tau Antibody Targeting Pathological Species Blocks Neuronal Uptake and Interneuron Propagation of Tau in Vitro," *Am. J. Pathol.*, vol. 187, no. 6, pp. 1399–1412, 2017.
[228] T. West *et al.*, "Preclinical and Clinical Development of ABBV-8E12, a Humanized Anti-Tau Antibody, for Treatment of Alzheimer's Disease and Other Tauopathies," *J Prev Alz Dis*, vol. 44, no. 44, pp. 236–241, 2017.

Appendices

Appendix A Alignments

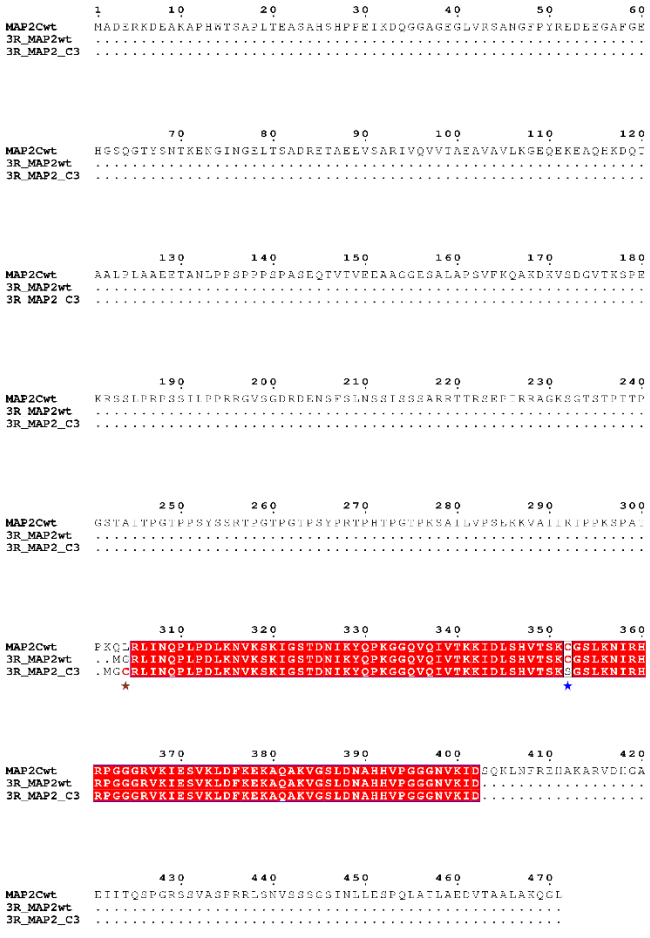

MAP2 C (3R) alignments. Shown here is the full length 3R MAP2 sequence from humans and constructs used in this work. Highlighted in red are the repeat regions. Red residues are cysteines, the blue star is the native cysteine used for Atto647N labeling for anisotropy and brown star is the N-Terminal cysteine labeled with Alexa 594 or PEG11-Biotin maleimide. Uniprot # P11137

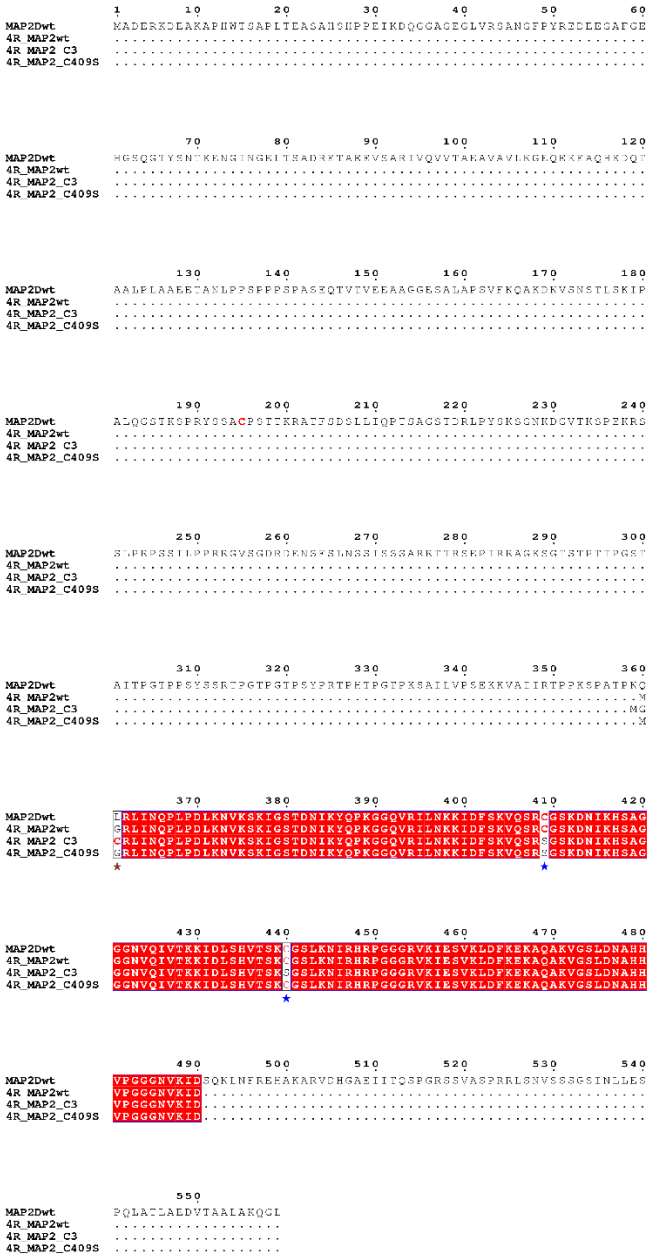

MAP2 D (4R) alignments. Shown here is the full length 4R MAP2 sequence from humans and constructs used in this work. Highlighted in red are the repeat regions. Red residues are cysteines, the blue stars are the native cysteines. Position 440 was used for Atto647N labeling for anisotropy and the brown star is the N-Terminal cysteine labeled with Alexa 594 or PEG11-Biotin maleimide. Uniprot # P11137

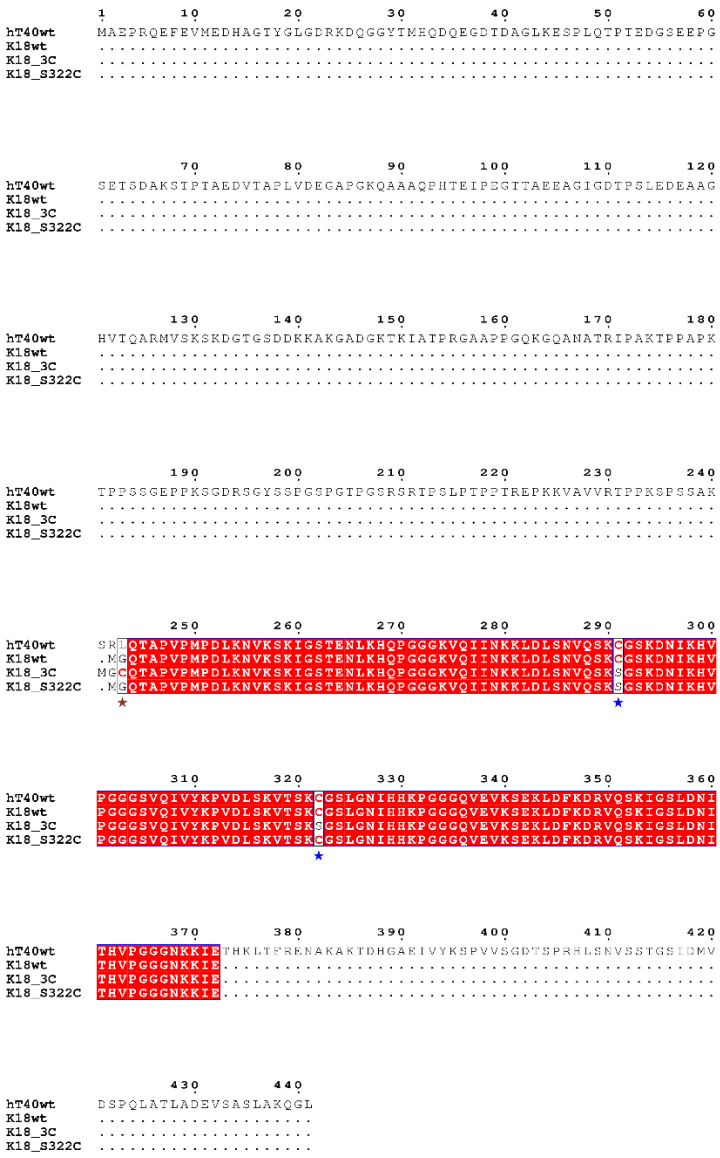

4R Tau alignments. Shown here is the full length 4R Tau sequence from humans. Shown here is the full length 3R MAP2 sequence from humans and constructs used in this work. Highlighted in red are the repeat regions. Red residues are cysteines, the blue stars are the native cysteines. Position 322 was used for Atto647N labeling (anisotropy experiments) and brown star is the N-Terminal cysteine labeled with Alexa 594 or PEG11-Biotin maleimide. Uniprot # P11137

Appendix B Magnetic bead pulldown aparatus

A

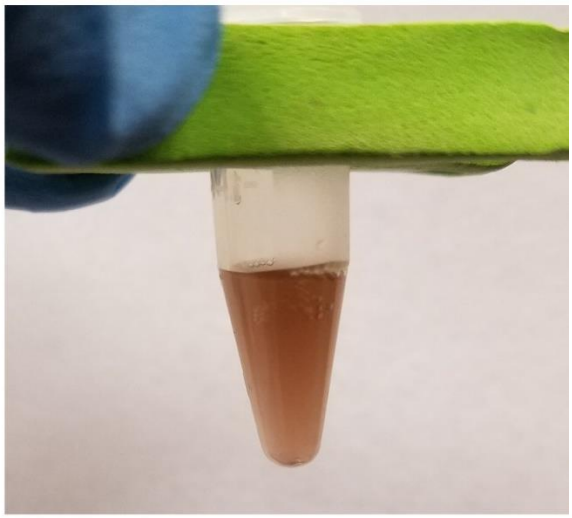

B

Streptavidin coated magnetic bead pulldown setup. A Before applying the magnetic field, beads were homogeneously mixed in solution. B Upon placement of the tube in a strong magnetic field, the beads would be pulled to one magnetic pole, creating a tightly packed pellet.

Appendix C Figures to accompany purification of Tau and MAP2

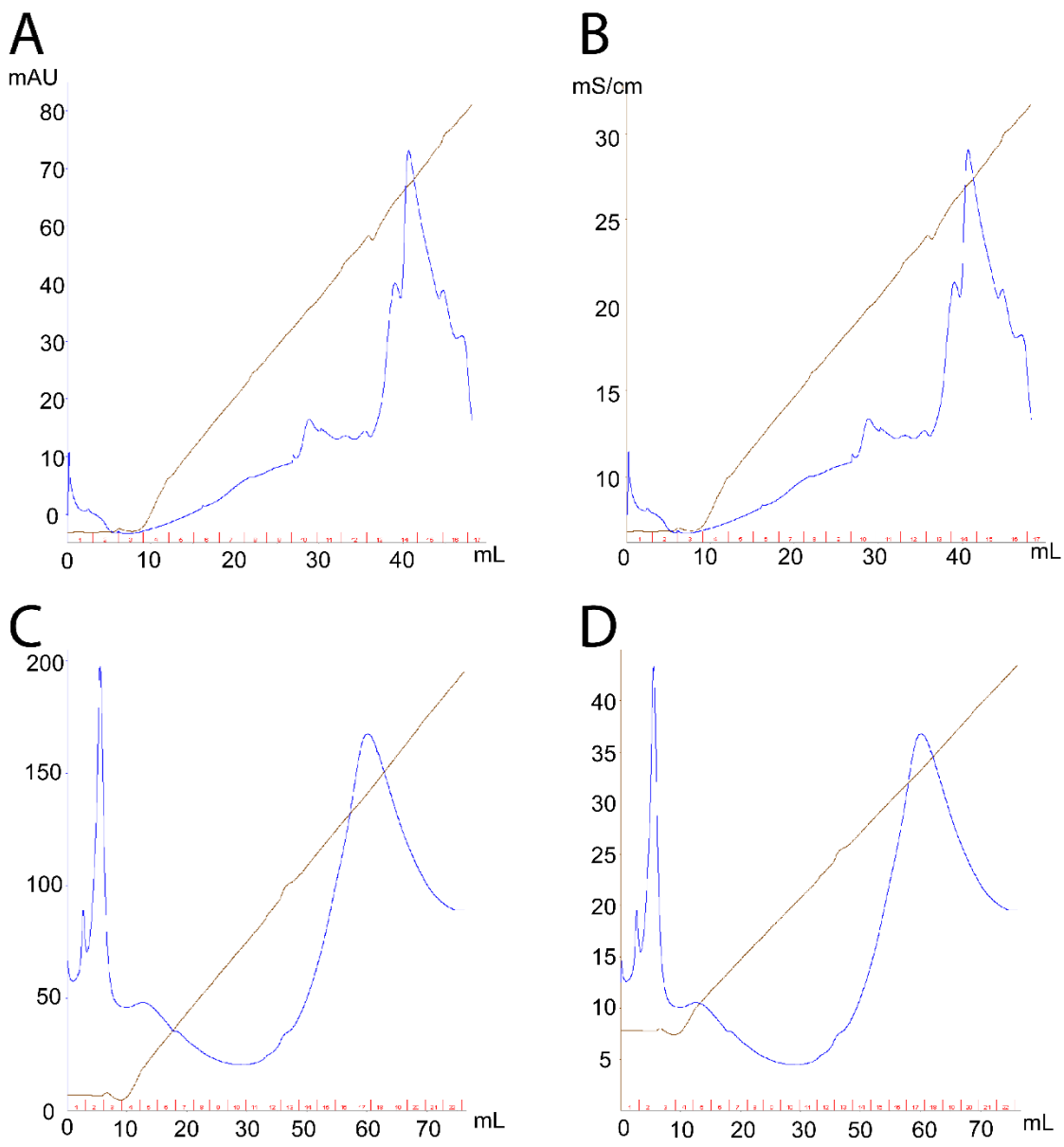

Figure Appendix C 1 Representative cation-exchange chromatograms for K18 and MAP2. Shown here are representative cation-exchange chromatograms for K18 with the y-axis scale of A UV (mAU) and B Conductivity (mS/cm). C and D show a representative chromatogram for MAP2 with y-axis scales for UV (mAU) and conductivity (mS/cm), respectively. Chromatograms for K19 and 3R MAP2 are nearly indistinguishable from the 4R examples shown here.

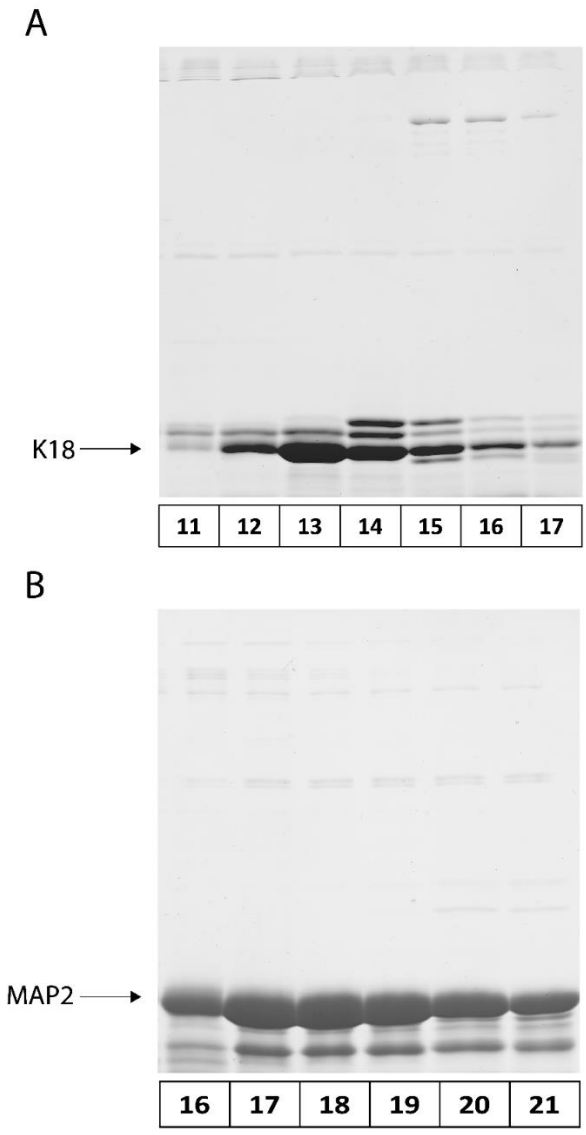

Figure Appendix C 2 Representative ion exchange eluent fractions of K18 and truncated 4R MAP2 analyzed by SDS PAGE. Representative eluent fractions from MonoS GL10/100 (GE) column for truncated A Tau (#11 - #17) and B 4R MAP2 (#14 - #20). MAP2 elutes at a higher conductivity.

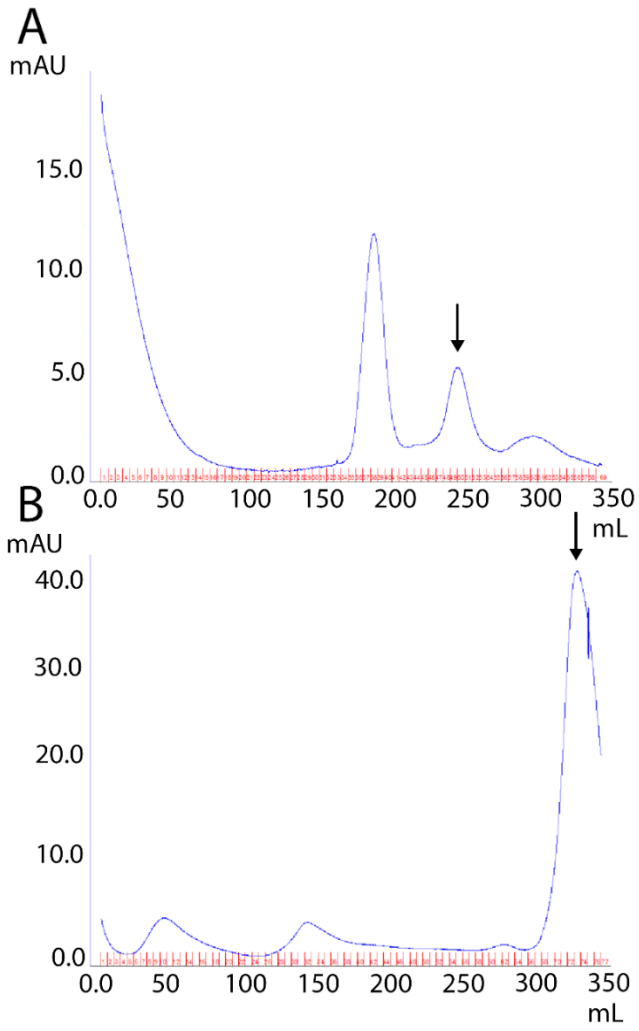

Figure Appendix C 3 Representative UV trace for truncated Tau and MAP2 on S75 and S200 columns, respectively. Representative UV (mAU) trace for A Chromatogram of K18 purified over a Superdex S75 (GE) and B truncated MAP2 (4R here) purified over a Superdex S200 (GE). Black arrow represents K18 (top) and 4R MAP2 (bottom). Chromatograms for K19 and 3R MAP2 are nearly indistinguishable from the 4R examples shown here.